

May 2023

# A Distributed Control System for Microgrids with Wide Dynamic Response Components

Hadi Akbari Haghighat  
*University of Wisconsin-Milwaukee*

Follow this and additional works at: <https://dc.uwm.edu/etd>



Part of the [Electrical and Electronics Commons](#)

---

## Recommended Citation

Akbari Haghighat, Hadi, "A Distributed Control System for Microgrids with Wide Dynamic Response Components" (2023). *Theses and Dissertations*. 3117.  
<https://dc.uwm.edu/etd/3117>

This Dissertation is brought to you for free and open access by UWM Digital Commons. It has been accepted for inclusion in Theses and Dissertations by an authorized administrator of UWM Digital Commons. For more information, please contact [scholarlycommunicationteam-group@uwm.edu](mailto:scholarlycommunicationteam-group@uwm.edu).

A DISTRIBUTED CONTROL SYSTEM FOR MICROGRIDS WITH WIDE DYNAMIC  
RESPONSE COMPONENTS

by

Hadi Akbari Haghigat

A Dissertation Submitted in  
Partial Fulfillment of the  
Requirements for the Degree of

Doctor of Philosophy  
in Engineering

at

The University of Wisconsin-Milwaukee

May 2023

## ABSTRACT

### A DISTRIBUTED CONTROL SYSTEM FOR MICROGRIDS WITH WIDE DYNAMIC RESPONSE COMPONENTS

by

Hadi Akbari Haghghat

The University of Wisconsin-Milwaukee, 2023  
Under the Supervision of Professor Adel Nasiri

Inverters play a vital part in microgrid operations and control, boosting system flexibility and efficiency. However, their limited physical inertia makes them vulnerable to network-induced oscillations. Research is primarily focused on addressing this by adding inertia to the inverter side. Earlier analysis of stand-alone microgrids utilized pure inverter-based systems with droop control for power sharing among units, and generators were responsible for voltage and frequency control. Inverter-based systems without communication latency have been studied. However, these studies don't provide a complete dynamic model of microgrids, especially for hybrid microgrids.

In this study, a systematic approach is presented to model a hybrid microgrid consisting of one synchronous generator and two inverters operating in two modes. The master inverter is responsible for voltage and frequency control during islanded mode, and setting power values for the generator and slave inverter. It also supports the grid as a voltage source in grid-connected mode.

The proposed MG differs from previous studies in its control approach, dynamics, and role of the master inverter for supporting pulse load and communication delay compensation. Power sharing is done via communication, not by droop control, so there's no need to add inertia to the inverter side. The synchronous generator will use an outer droop loop to adjust power based on values

from the master inverter, while the slave inverter contributes power based on values received from the master inverter.

The dissertation presents a state-space model for analyzing hybrid microgrids (MG) with various dynamic components, including a detailed model of generator, two inverters. The model captures the details of the control loops of the generator and inverters, but not the switching action. The energy storage-based inverter controls voltage and frequency, while the generator and slave inverter receive active and reactive power commands from the master inverter. The model also takes into account the effect of communication delay on the control of the hybrid MG. Each sub model is linearized around an operating point and the resulting system matrix is used to derive the eigenvalues. This dissertation focuses on the study of the transient response of a hybrid MG using eigenvalues to indicate the frequency and damping of oscillatory components in both islanded and grid-connected modes

Electrical vehicle charger can serve as an example of a hybrid system based on the mentioned topology. This study can generate a platform to analyze such applications and increase the stability and resilience of the system.

© Copyright by Hadi Akbari Highlight, 2023  
All Rights Reserved

To  
My parents,  
My wife Ghoncheh  
To my sons Elmir & Elshan  
My Brothers  
My nephew Shayan

# TABLE OF CONTENTS

LIST OF FIGURES .....	viii
LIST OF TABLES .....	x
LIST OF ABBREVIATIONS.....	xi
ACKNOWLEDGEMENTS.....	xii
1. Chapter 1 Introduction .....	1
1.1 Background.....	1
1.2 Microgrid Concept.....	3
1.3 MG Control Review.....	4
1.3.1 Microgrid Control Hierarchy .....	4
1.3.2 Intelligent Control Methods.....	5
1.4 Primary Control Techniques.....	5
1.5 Stability of Microgrids.....	6
1.6 Problem Statement.....	7
2 Chapter 2 Microgrid Configuration and Component Modeling.....	10
2.1 The Hybrid System Configuration.....	10
2.2 Natural Gas Generator (Synchronous generator).....	11
2.2.1 Exciter Modeling .....	12
2.2.2 Natural Gas Governor Model.....	13
2.3 2.3 Voltage Source Converter System.....	14
2.3.1 Grid-Forming Concept.....	15
2.3.2 Grid-Following Concept.....	16
2.4 LCL Filter .....	17
3 Chapter 3 State Space Modeling and Stability Analysis of the proposed MG.....	19
3.1 Dynamic Model of the Proposed MG.....	21
3.2 Dynamic Model of Natural Gas Generator (Synchronous Generator) .....	22
3.2.1 Mechanical model.....	23
3.2.2 Electrical Model of SG .....	26
3.2.3 Exciter state space modeling.....	38

3.3	State space modelling of grid forming Inverter (Islanding mode).....	45
3.3.1	The effect of load to the dynamic model of the master inverter.....	52
3.3.2	Dynamic Analysis of Grid Forming inverter.....	53
3.3.3	Dynamic model of the grid forming inviter in grid connected mode.....	55
3.4	Dynamic model of grid following inviter (Slave inviter).....	57
3.4.1	Dynamic Analysis of Grid Following inverter.....	63
4	Chapter 4 The Control Architecture of the proposed MG and Simulation Results.....	67
4.1	The Master Controller.....	67
4.1.1	Simulation results of primary controllers.....	69
4.1.2	The Grid Forming inviter.....	72
4.1.3	The Slave Inverter.....	72
4.2	Simulation Results of the Proposed Microgrid with the Master Controller.....	73
5	Chapter 3 Fault Classification based on Data Model to Support MG Resiliency.....	79
5.1	Introduction.....	79
5.2	Definitions of Resiliency.....	80
5.3	Fault classification informed by data model.....	83
5.4	A novel method for classifying data model under fault scenario.....	85
6	Chapter 6 Conclusions.....	94
7	References.....	96
8	Appendix: System parameters for simulation.....	101

## LIST OF FIGURES

FIGURE 1-1 THE MICROGRID CONCEPT.....	3
FIGURE 1-2 CONCEPTUAL FRAMEWORK OF HIERARCHICAL CONTROL.....	4
FIGURE 1-3 HYBRID MICRO GRID UNDER STUDY.....	9
FIGURE 2-1 THE BLOCK DIAGRAM OF SYSTEM UNDER STUDY.....	11
FIGURE 2-2 BLOCK DIAGRAM OF A NATURAL GAS GENERATOR.....	12
FIGURE 2-3 BASIC BLOCK DIAGRAM OF AN EXCITATION CONTROL SYSTEM.....	13
FIGURE 2-4 THE DETAILED CONTROL SYSTEM OF GOVERNOR.....	13
FIGURE 2-5 INVERTER BLOCK DIAGRAM.....	14
FIGURE 2-6 A SIMPLIFIED DEPICTION OF A GRID-FORMING CONVERTER.....	15
FIGURE 2-7 THE PROPOSED CONTROL STRATEGY OF GRID FORMING INVERTER.....	15
FIGURE 2-8 A SIMPLIFIED DEPICTION OF A GRID- FOLLOWING CONVERTER.....	16
FIGURE 2-9 THE BLOCK DIAGRAM OF THE SLAVED INVERTER.....	16
FIGURE 2-10 LCL FILTER.....	17
FIGURE 3-1 DYNAMIC MODEL OF THE PROPOSED MG.....	21
FIGURE 3-2 SYSTEM BLOCK DIAGRAM OF SYNCHRONOUS GENERATOR.....	23
FIGURE 3-3 THE COMPLETE MECHANICAL SYSTEM WITH ACTIVE POWER SETTING VALUE FROM THE MASTER INVERTER.....	24
FIGURE 3-4 THE SIMPLIFIED GENERATOR MODEL.....	29
FIGURE 3-5 THE ELECTRICAL MODEL OF SG IN DQ FRAME.....	30
FIGURE 3-6 THE STATE SPACE MODEL OF GOVERNOR.....	33
FIGURE 3-7 A. THE IMPACT OF ENGINES DELAY. B. THE IMPACT OF THE FUEL VALVE DELAY.....	35
FIGURE 3-8 THIS SIMULATION DATA DEMONSTRATES THE IMPACT OF ENGINE DELAY ON SG FREQUENCY.....	35
FIGURE 3-9 EXPLORING THE EFFECTS OF CHANGING DROOP GAIN ON EIGENVALUE PLOTS IN ISLANDING MODE.....	35
FIGURE 3-10 PRESENTING SIMULATION RESULTS THAT DEMONSTRATE THE EFFECT OF DROOP GAIN ON SG FREQUENCY DURING ISLANDING MODE.....	36
FIGURE 3-11 PLOT OF EIGENVALUES WITH INCREASING COMMUNICATION DELAY BETWEEN THE MASTER CONTROLLER AND SG.....	37
FIGURE 3-12 THE TRANSFER FUNCTION OF COMMUNICATION BETWEEN TWO UNITS.....	37
FIGURE 3-13 COMPARISON OF TWO METHODS OF TIME DELAY APPROXIMATION.....	37
FIGURE 3-14 BLOCK DIAGRAM OF EXCITATION SYSTEM.....	38
FIGURE 3-15 THE STATE SPACE MODEL OF EXCITER.....	43
FIGURE 3-16 THE IMPACT OF PROPORTIONAL GAIN ON VOLTAGE STABILITY.....	44
FIGURE 3-17 SIMULATION ILLUSTRATES HOW THE VOLTAGE OF SG IS AFFECTED BY $K_p$ DURING ISLANDING MODE.....	44
FIGURE 3-18 THE IMPACT OF COMMUNICATION DELAY IN THREE CASES.....	44
FIGURE 3-19 BLOCK DIAGRAM OF GRID FORMING INVERTER.....	45
FIGURE 3-20 LCL FILTER.....	46
FIGURE 3-21 PLL CONTROL LOOP IS USED FOR MEASURING A FREQUENCY.....	48
FIGURE 3-22 STATE SPACE MODEL OF GRID-FORMING INVERTER (ISLANDING MODE).....	50
FIGURE 3-23 MG COMMON CONNECTION CIRCUIT.....	52
FIGURE 3-24 THE EIGENVALUE PLOT WITH VARIABLE C AND RC.....	54
FIGURE 3-25 VOLTAGE OF THE MASTER INVERTER WHEN $RC=1$ .....	54
FIGURE 3-26 VOLTAGE OF THE MASTER INVERTER WHEN $RC=1$ .....	54
FIGURE 3-27 THE EIGENVALUE PLOT WITH VARIABLE PLL GAINS.....	55
FIGURE 3-28 STATE SPACE EQUATIONS OF GRID-FORMING INVERTER.....	56
FIGURE 3-29 BLOCK DIAGRAM OF THE SLAVE INVERTER.....	57
FIGURE 3-30 THE GRID FORMING INVITER WITH LCL FILTER.....	58
FIGURE 3-31 STATE SPACE MODEL OF GRID FOLLOWING INVERTER.....	62
FIGURE 3-32 THE IMPACT OF FORWARD PATH COM DELAY COMPARED TO FEEDBACK PATH COM DELAY.....	63
FIGURE 3-33 THE INFLUENCE OF FILTER BANDWIDTH ON STABILITY IN THE PRESENCE OF VARIABLE FEEDBACK DELAY.....	64
FIGURE 3-34 DYNAMIC MODEL OF PROPOSED HYBRID SYSTEM.....	65
FIGURE 4-1 THE MAIN CONTROL ARCHITECTURE OF MG UNDER STUDY.....	68
FIGURE 4-2 STEP RESPONSE OF A CLOSED-LOOP EXCITATION SYSTEM.....	69

FIGURE 4-3 STEP RESPONSE OF GOVERNOR SYSTEM .....	70
FIGURE 4-4 DROOP CONTROL .....	70
FIGURE 4-5 THE OUTPUT POWER IS CONTROLLED BY UTILIZING DROOP CONTROL.....	71
FIGURE 4-6 POWER CONTROLLING IN SG IS ACHIEVED BY MAINTAINING A FREQUENCY .....	71
FIGURE 4-7 THE STEP RESPONSE OF THE MASTER INVERTER VOLTAGE IN DQ FRAME .....	72
FIGURE 4-8 THE ACTIVE AND REACTIVE POWER OF THE SLAVE INV.....	73
FIGURE 4-9 BLOCK DIAGRAM OF THE MASTER CONTROLLER .....	74
FIGURE 4-10 ACTIVE POWER PLOTS OF THE PROPOSED SYSTEM DURING GMC .....	75
FIGURE 4-11 THE FREQUENCY SIGNAL OF THE MG IN GCM WHEN CASE 1 IS APPLIED .....	75
FIGURE 4-12 MG VOLTAGE SIGNAL DURING SYNCHRONIZATION WITH GRID .....	76
FIGURE 4-13 ACTIVE POWER PLOTS OF THE PROPOSED SYSTEM DURING ISM .....	77
FIGURE 4-14 ADDING COMMUNICATION DELAY ( $T_D=10\text{ms}$ ) BETWEEN SG AND THE MASTER INVERTER IN ISLANDED MODE .....	77
FIGURE 4-15 ADDING COMMUNICATION DELAY ( $T_D=100\text{ms}$ ) BETWEEN SG AND THE MASTER INVERTER IN ISLANDED MODE .....	78
FIGURE 5-1 LOAD PRIORITY [47] .....	81
FIGURE 5-2 THE THREE MAIN RESILIENCE LAYERS [49] .....	82
FIGURE 5-3 FAULT CLASSIFICATION INFORMED BY DATA MODEL.....	84
FIGURE 5-4 KALMAN DECOMPOSITION MODEL .....	85
FIGURE 5-5 THE BLOCK DIAGRAM OF RESILIENCY CLASSIFICATION PROCESS.....	86
FIGURE 5-6 DATA MODEL OF THE SYSTEM UNDER STUDY .....	87
FIGURE 5-7 THE SIMPLIFIED DATA MODEL UNDER FAULT SCENARIO.....	89
FIGURE 5-8 MATRIX A AFTER GETTING FAULT BETWEEN REN AND GRID.....	89
FIGURE 5-9 DYNAMIC MODEL AFTER APPLYING KD .....	90
FIGURE 5-10 MAPPING BETWEEN TWO GROUPS OF STATES .....	90

## LIST OF TABLES

TABLE 3-1 SUMMARY OF THE DYNAMIC ANALYSIS OF UNITS IN THE PRESENCE OF COMMUNICATION DELAY .....	65
TABLE 4-1 MG CASE STUDY SPECIFICATION .....	74
TABLE 5-1 TABLE FOR RESILIENCE CLASSIFICATION .....	91
TABLE 5-2 THE CLASSIFICATION OF RESILIENCE LEVELS FOR SUPPORTING CRITICAL LOADS .....	92

## LIST OF ABBREVIATIONS

DG	Distributed Generation
DOE	Department of Energy
MG	Microgrid
AVR	Automatic Voltage Regulator
VSI	Voltage Source Inverter
PLL	Phase locked loop
SOC	State of Charge
SG	Synchronous Generator
NG	Natural Gas
COM	Communication
MInv	Master Inverter
SInv	Slave Inverter
GC	Grid Connected Mode
ISM	Islanded Mode
ReC	Resiliency classification
KD	Kalman Decomposition
UC	UnObservability
UO	Uncontrollability
EV	Electrical Vehicle
HIL	Hardware In the Loop
DER	Distributed Energy Resources
ESS	Energy Storage System

## ACKNOWLEDGEMENTS

I am grateful to express my appreciation to Professor Adel Nasiri, who has been my advisor, guide, and supporter throughout my academic journey. The unwavering support and expert guidance provided by Professor Adel Nasiri have been the key factors that have contributed to my success. I hope that I have met his expectations, and I am eager to continue working with him.

I would also like to express my appreciation to Professor Armstrong and Professor Rob Cuzner for his valuable suggestions and engaging discussions that have greatly contributed to the success of my work. Furthermore, I am deeply grateful to Professor Jun Zhang, Dr. Tian Zhao, and Dr. Necmi Altin for their insightful suggestions and direction towards my research. Their time and dedication as members of my committee have been greatly appreciated.

I would like to express my sincere gratitude to my parents and brothers for their endless love, support, and guidance.

Finally, my dear Ghoncheh, you have been my rock through both good and bad times, and your unwavering presence has brought me immense comfort. With you by my side, I have always found solace in the belief that after every difficulty, there is relief. I am truly grateful for your boundless patience and unwavering love, which have been essential to my personal growth and happiness. Above all, I thank God for bringing you into my life and blessing me with a partner as remarkable as you.

# Chapter 1 Introduction

## 1.1 Background

One of the main drivers for the development of distributed energy resources (DERs) is the increasing concerns regarding grid reliability and resiliency, both under physical disturbances and cyber-attacks. To address these concerns, there is a growing need for the capacity to island portions of distribution systems with interconnected DERs and loads, forming what are known as "Micro-Grids." These micro-grids can provide a reliable source of electricity during emergencies and support the overall stability of the power grid [1]

There is a consensus that micro-grids will play a significant role in improving the performance of modern distribution systems by enhancing the quality and reliability of the electric energy supply. As such, there is a growing focus on developing micro-grid technologies that can operate efficiently and effectively in a range of different scenarios, including during emergencies and under changing grid conditions.

Overall, the deregulation of the electric utility industry and the need for a more sustainable and efficient future power system have driven significant technological advancements in the sector, including the development of micro-grids. These advancements are expected to play a crucial role in improving the reliability and resilience of the power grid, while also supporting the transition to a more sustainable energy future [2].

Renewable energy is critical due to dwindling fossil fuels and the environmental impact of traditional energy sources. To meet this challenge, we must transition to renewables like solar and wind. Inverters play a key role in supplying power from these sources and energy storage to the grid.

The recent occurrences of power outages have highlighted the susceptibility of the power grid and the pressing need for a significant revamp to enhance its dependability. Additionally, the escalating use of non-linear loads in electric power networks has resulted in a grave concern in recent times - power quality distortion. Variations in power quality such as power cuts, voltage drops and surges, voltage spikes, and voltage harmonics can lead to severe repercussions on the electrical systems' loads. Consistent challenges with generation, transmission, and distribution permissions, along with unpredictable weather events like Hurricane Sandy and Katrina, and insufficient maintenance practices have all contributed to a rising number of malfunctions and power outages [3].

Incorporating renewable energy and distributed generation (DG) into the electrical distribution system can facilitate optimal usage of the current infrastructure and yield numerous advantages, provided they are appropriately managed [4]. DG has the potential to reduce consumption of fossil based fuels, reduce transmission and distribution losses, reduce the effects of electricity price fluctuations, improve system efficiency, and improve voltage quality [5].

A microgrid concept provides a solution to manage DG and renewable energy and it has the ability to maximize the overall system efficiency, power quality and power surety to critical loads [6, 7]. Renewable energy sources face a particular challenge in supporting the grid power balance, making them globally less acceptable as a direct and reliable source [8]. However, energy storage is recognized as a feasible solution to dissociate fluctuating power supply from load demand. The following research proposes utilizing storage units as a supplement to renewable energy generation to address the system demand for uninterrupted transmittable power. It is essential to accelerate the deployment of renewable power to bring about a sustainable energy system in remote places

and small hybrid systems. Electricity storage is found to be the only economic solution that can increase the fraction of renewable energy in the system to as high as 100% [9].

## 1.2 Microgrid Concept

The U.S. Department of Energy (DOE) defines a microgrid as a group of interconnected loads and DG within clearly defined electrical boundaries that act as a single controllable entity with respect to the grid [10]. There are many other definitions of microgrid, but all of them involve a collection of DG and loads connected with the utility grid. Figure 1-1 [11] shows a definition of the microgrid concept.

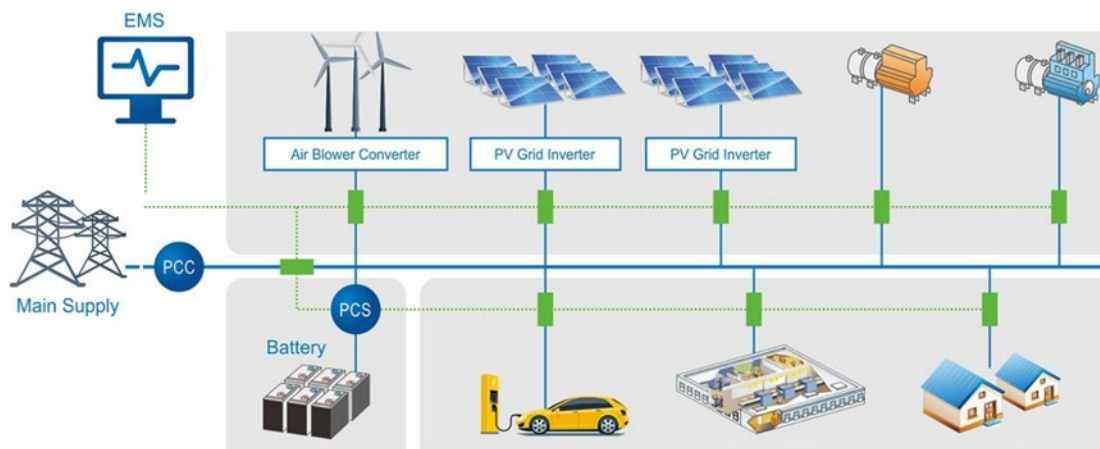


Figure 1-1 The microgrid concept

A microgrid has the capability to operate in two different forms: parallel mode or island mode. One of the most significant features of a microgrid is its ability to unintentionally separate and isolate itself from the utility's distribution system during events such as faults, voltage collapses, or blackouts. Additionally, a microgrid may intentionally disconnect from the grid during maintenance or when the quality of power from the grid falls below certain standards. When a microgrid is in island mode, it is essential to ensure the reliability of critical loads, while non-critical loads may need to disconnect unless sufficient generation capacity is available within the

microgrid. Once the utility grid is recovered, microgrids can be seamlessly reconnected without any interruption to critical loads [12].

### 1.3 MG Control Review

#### 1.3.1 Microgrid Control Hierarchy

The hierarchical control architecture is organized into three categories as primary, secondary, and tertiary levels based on the control bandwidth specification. Figure 1-2 presents the hierarchical control structure [13].

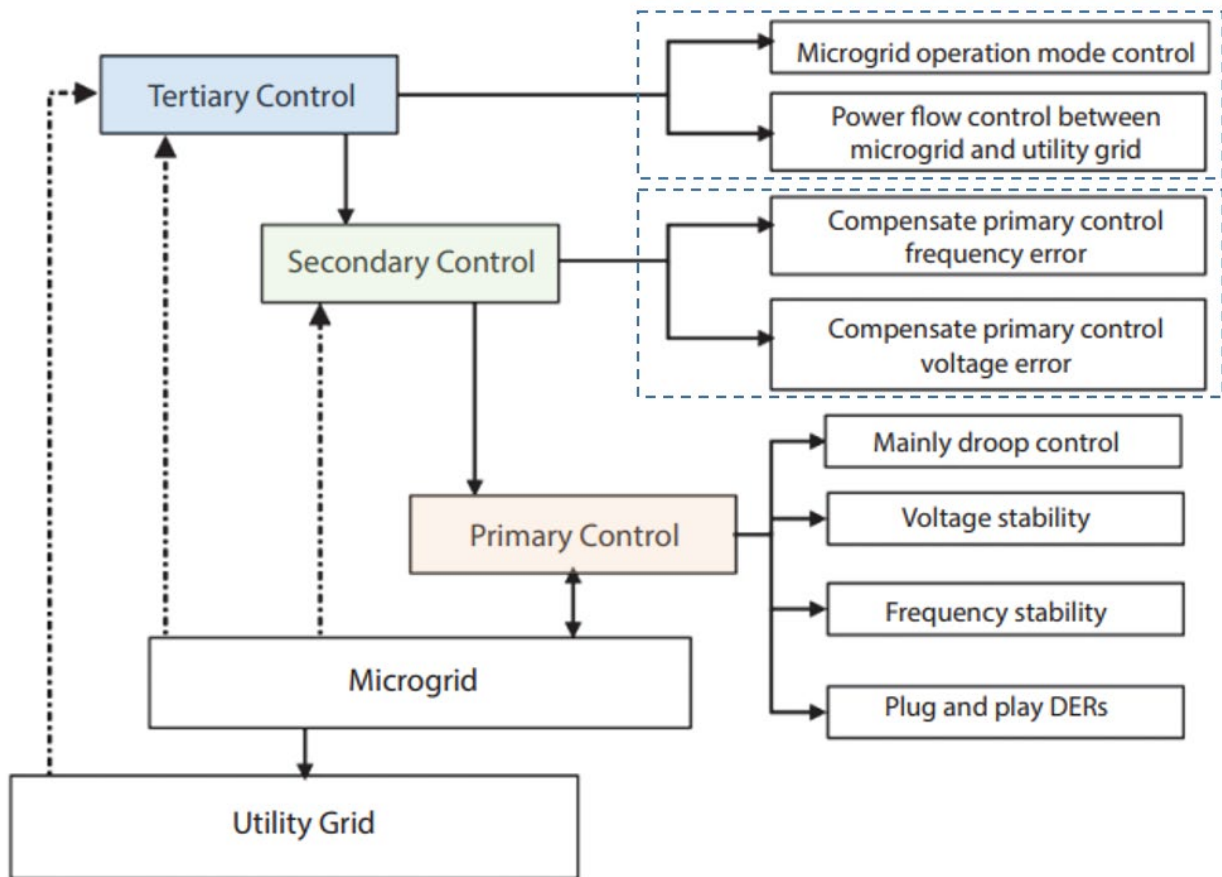


Figure 1-2 Conceptual framework of hierarchical control

The primary control is the most profound level and pertains to the actions of a local controller with the control functions related to DGs, ESS, and loads. The primary controller maintains the microgrid frequency and voltages within the acceptable limits as specified by IEEE

1547 standards. Additionally, it ensures proper power sharing among the parallel DGs. It supports the plug-and-play operation of the DERs maintaining voltage and frequency during the transition from grid-connected mode to islanding mode. The primary controller is the fastest acting controller. In the primary control, there is a trade off in selecting the value of droop coefficient. For better power sharing higher droop coefficient is required but at the cost of frequency and voltage fluctuations. Therefore, the steady state deviations in the voltage and frequency are further controlled by the secondary control. The secondary control involves the control at MG level and also includes the ancillary services of MG. The tertiary control level is the global control that provides an interface to the upstream network.

### 1.3.2 Intelligent Control Methods

Intelligent control methods in power systems, such as fuzzy logic and artificial neural networks, have extensive research scope for power electronic converters-based functions. Fuzzy logic consists of fuzzifier, rule evaluator, and defuzzifier, while artificial neural networks are used for parameter evaluation, islanding detection, and load forecasting. Adaptive neuro-fuzzy inference system (ANFIS) is another droop control strategy that offers benefits like independence from line impedances and model configuration, but may increase computational burden and require high-speed processors [14].

### 1.4 Primary Control Techniques

Primary control techniques in microgrids (MGs) are categorized as communication-based control and droop-based control, with communication-based control further divided into centralized and decentralized control. Droop-based control is typically decentralized, and factors such as overall cost, complexity, implementation ease, system expandability, and redundancy often make droop-based control strategies preferred [15, 16]

A centralized controller enables bidirectional communication among system components for status and set point information, eliminating the need for a secondary controller. This control allows for system-wide information, accurate power sharing, and superior voltage regulation. However, it has drawbacks such as higher costs due to communication requirements, potential interferences, and limited system expandability. Master-slave control is an example of centralized control where one DG unit acts as the master, and the slave units follow its current reference for uniform current distribution. In master-slave control, the master operates in voltage-controlled mode as VSC, whereas the slave units operate in PQ mode as current source converters.

The conventional droop control approach bears resemblance to synchronous generator droop control, with active power tied to frequency and reactive power correlated with voltage. Specifically, as active power escalates, system frequency diminishes, and as reactive power rises, system voltage declines [17, 18]. To address the limitations of conventional droop control methods, modified droop control strategies have been developed. These strategies are categorized based on the variations in control approaches they employ [19].

## 1.5 Stability of Microgrids

Microgrids (MGs) differ from conventional power systems due to their small size and operation at low to medium voltage levels. MGs primarily rely on renewable energy sources (RESs), resulting in rapid changes in power generation and reduced inertia. This lack of inertia is due to distributed energy resources (DERs) and smaller synchronous generators. MGs have a higher power coupling due to smaller reactance to resistance ratio. Additionally, islanded MGs may experience voltage and frequency fluctuations during load switching due to their smaller short circuit capacity. Bidirectional power flow between the utility and consumers further complicates stability, as does unbalanced loading within the MG.

Stability in MG is classified based on the time span of instability, cause of instability, nature of disturbance, equipment's involved and methodology used to analyze the instability. In a conventional power system, stability analysis is well established and for the different frequency ranges of possible concern there are models that include the appropriate features. However, detailed generalized dynamic models for a microgrid are not available [20, 21]. Previous dynamic analysis of microgrid system considered inverters as an ideal source, which are not appropriate to study the stability of the microgrid and are not useful to analyze the robustness of microgrid controls [22].

## 1.6 Problem Statement

The increasing adoption of energy storage systems and renewable sources coupled to the MG through inverters has introduced new challenges due to their distinct dynamic behavior compared to traditional synchronous generators. These differences in dynamic behavior can affect the overall stability and performance of the power grid, and need to be addressed for the effective integration and operation of inverter based systems [23]

To address the response time for sudden load changes, the inviter will provide quick responses, especially for pulse loads. In a microgrid with both synchronous generators (SGs) and inverters operating in grid forming mode, this feature may temporarily cause the inverters to supply a larger share of the load following a load step-up. However, this could also result in the State of Charge (SOC) of energy storage being insufficient due to prolonged operation in island mode. In such scenarios, the proposed controller may be vulnerable. Additionally, the master controller can cover transient conditions using the features of the inverters.

The main objective of this dissertation is to propose a novel approach for transient control of microgrids, incorporating dynamic modeling, stability analysis, and utilization of energy storage-

based inverter as a grid-forming inverter for voltage and frequency control. The proposed hybrid microgrid considered in this study includes a synchronous generator, a grid-forming inverter as a master inverter, and a grid-following inverter as a slave inverter, is shown in Figure 1-3.

The proposed system is capable of effectively managing dynamic loads, such as pulse loads, during islanded operation, optimizing the utilization of synchronous generators (SGs), and minimizing the power demand on energy storage by accommodating dynamic loads. The master inverter is responsible for transmitting power set points through a communication line. In this study, the communication delay is considered as a part of the dynamic model, and the impact of the delay on stability is analyzed

The proposed control strategy aims to mitigate the impact of communication latency through rapid response from the master inverter, thereby enhancing the system's capability to handle delays in communication.

A comprehensive dynamic modeling of each unit has been conducted in this dissertation, which is distinct compared to other existing efforts in the literature. A novel modified resiliency classification technique is proposed in this dissertation, which aims to enhance the resilience of the microgrid (MG) system by incorporating data modeling approaches. The proposed technique involves an innovative approach to classify and categorize the system's resilience levels based on various source of faults.

In order to assess the robustness of the proposed control strategy, it is necessary to conduct a thorough investigation into the stability of the microgrid system. To this end, a state space model has been developed, which incorporates the detailed dynamic characteristics of each inverter-based and machine-based distributed generator (DG) as well as load dynamics. The stability analysis of the proposed control strategy encompasses an examination of the effects of changes in microgrid

and controller parameters, as well as communication delays. This analysis is crucial in determining the system's stability and performance under varying conditions, and provides valuable insights into the effectiveness and reliability of the proposed control strategy.

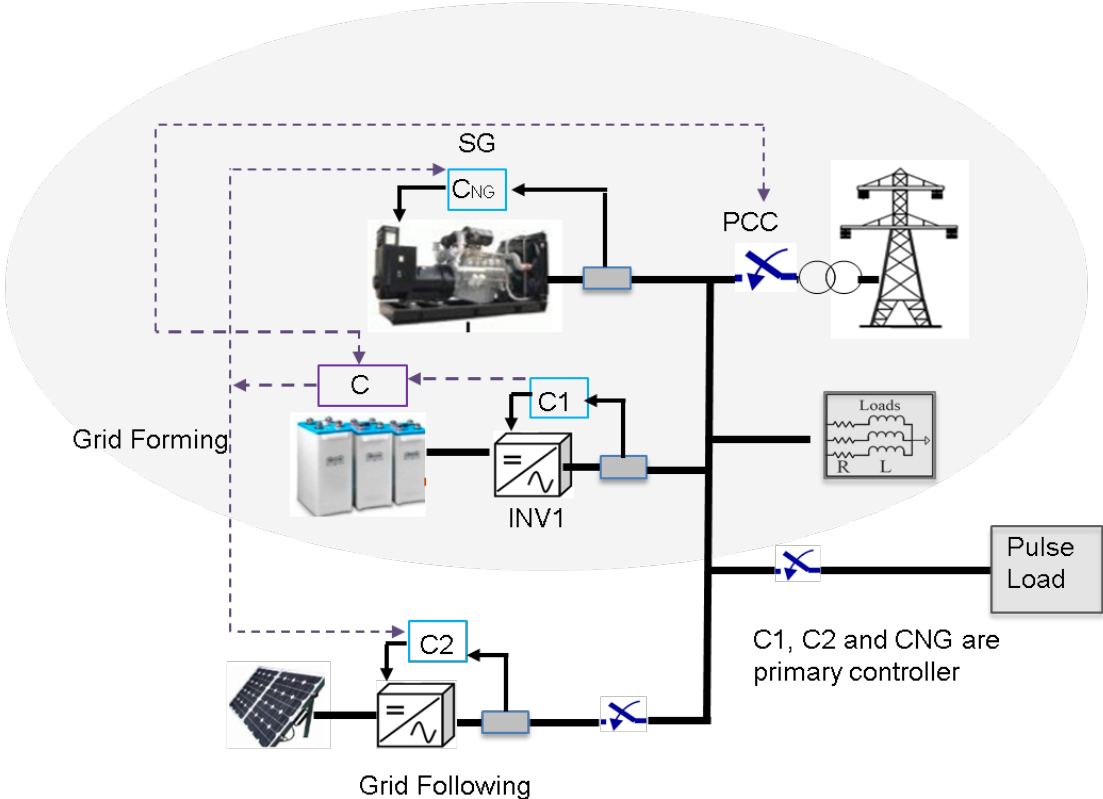


Figure 1-3 Hybrid Micro Grid under study

## Chapter 2 Microgrid Configuration and Component Modeling

### 2.1 The Hybrid System Configuration

The Hybrid System Configuration is a cutting-edge energy management solution that combines multiple components, including a synchronous generator, energy storage system, renewable energy source, and pulse load, to optimize power generation and consumption in a sustainable manner.

The synchronous generator provides stable power output, while the energy storage system stores excess energy for later use during transient change and peak demand periods. The renewable energy source, such as solar or wind, harnesses clean energy to further supplement the power generation. Additionally, the pulse load, which represents intermittent or fluctuating energy demands, is effectively managed through the Hybrid System Configuration, ensuring smooth operation and reliability. This innovative system configuration offers a flexible, efficient, and environmentally-friendly solution for sustainable power generation and utilization in various applications, including islanded mode of operation and grid connect mode.

Figure 2-1 represents the proposed configuration of the hybrid system. The master inverter is responsible for preparing the reference voltage and frequency for the microgrid (MG) in islanded mode, as well as acting as a voltage source to support the grid during grid-connected mode. Each unit within the hybrid system has its own primary controller, and the master controller is located in the master inverter, serving as a central controller. The secondary control layer is connected to the other units through a communication line, enabling coordination and synchronization among the different components of the system. This setup enables the master inverter to share active and reactive power among the other units based on the load demand and system situation.

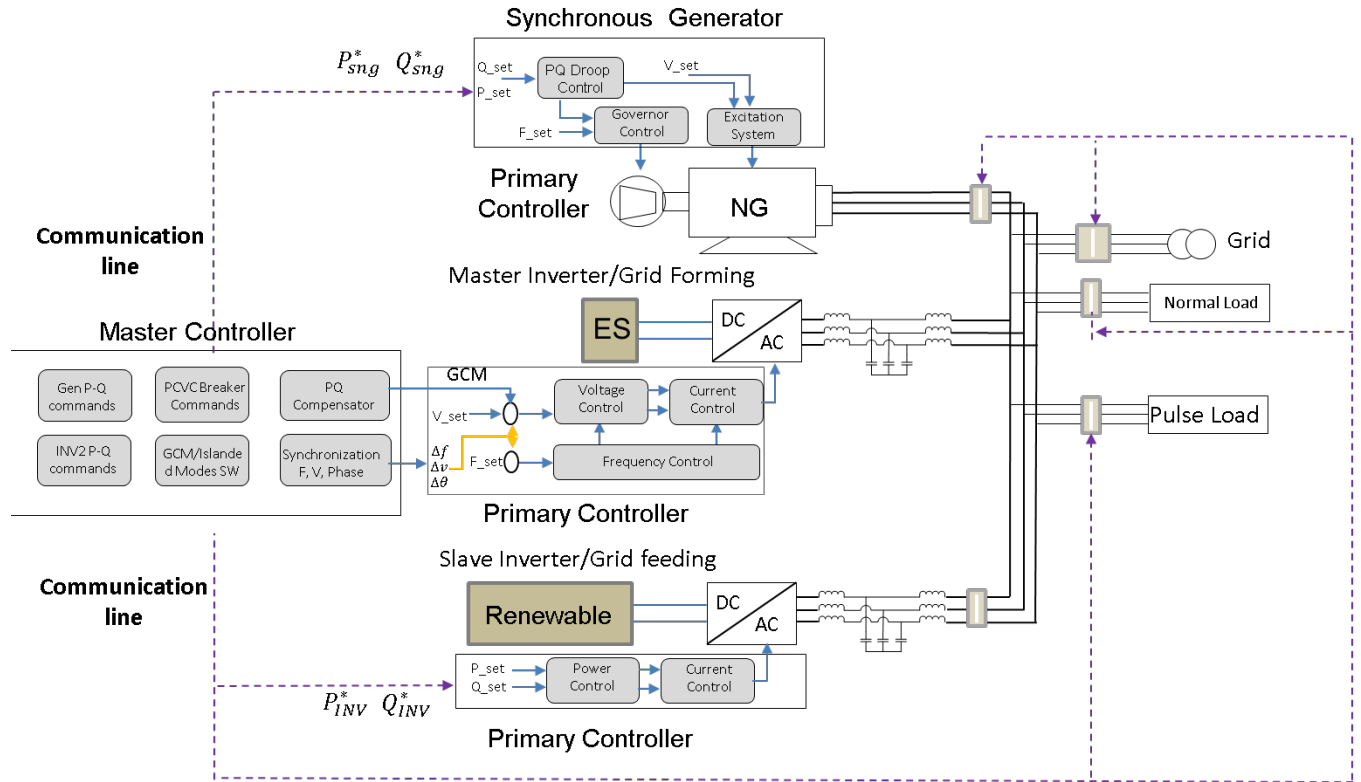


Figure 2-1 The block diagram of system under study

In relation to the varying response times between the synchronous generator and the master inverter, the inverter is capable of supporting this change by rapidly responding to new demand. However, relying on energy storage for long-term load support may not be feasible. Therefore, a crucial responsibility of the master controller is to effectively adjust the power distribution between the generator and the slave inverter during operation.

## 2.2 Natural Gas Generator (Synchronous generator)

The natural gas generator plays a pivotal role in microgrids, offering numerous advantages for power production when the utility grid fails. In comparison to coal, gasoline, and oil, natural gas is considered the cleanest fossil fuel with minimal environmental pollution. Greenhouse gas emissions, particularly CO<sub>2</sub>, are significantly reduced with the use of a natural gas generator.

Additionally, the availability of pipelines for easy transportation and the cost-effective nature of natural gas generators further drive their utilization in microgrids [24].

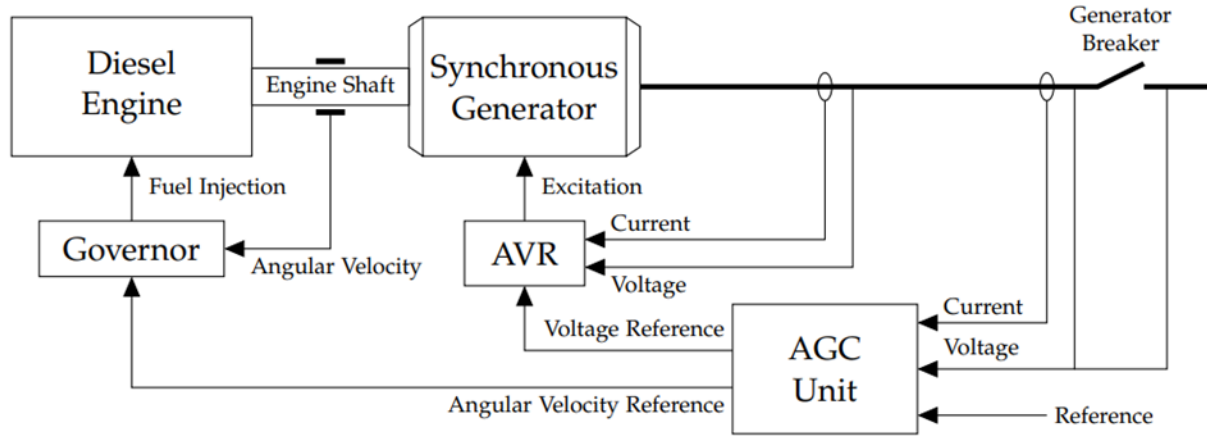


Figure 2-2 Block diagram of a natural gas generator

The excitation system of a natural gas generator is responsible for controlling reactive power, while the governor system adjusts the active power output. By supplying both active and reactive power to the system, the generator helps maintain a constant voltage and frequency within the microgrid. Figure 2-2 illustrates the basic block diagram of a natural gas generator connected to a grid or microgrid. In order to thoroughly study the behavior of a natural gas generator, it is imperative to create detailed models for the synchronous generator, excitation system, Automatic Voltage Regulator (AVR) system, gas engine, and governor system [25]. The detailed modeling of all the components of a natural gas generator is described in the next chapter.

### 2.2.1 Exciter Modeling

The fundamental purpose of an excitation system is to furnish direct current to the field winding of a synchronous machine. The excitation system must possess the capability to automatically regulate the field current to uphold the prescribed terminal voltage/reactive power. In order to conduct a comprehensive investigation into the behavior of a synchronous machine for power system stability studies, it is crucial to meticulously model the excitation system of the

machine with sufficient detail. The basic block diagram of an excitation control system is given in Figure 2-3.

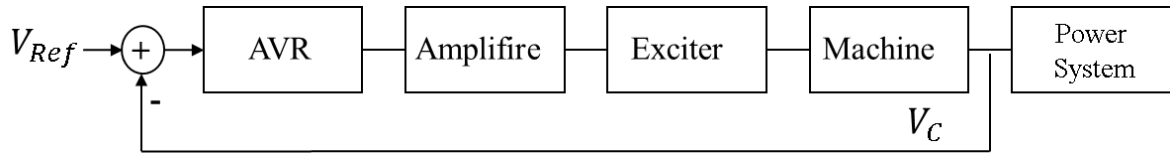


Figure 2-3 Basic block diagram of an excitation control system

### 2.2.2 Natural Gas Governor Model

The natural gas engine requires precise control to efficiently convert its power to useful work. This is achieved through the use of a governor, an essential device that regulates the engine's speed or power output. To enhance the speed response, an electronic control system is utilized in the governor control system. The governor senses the speed of the prime mover and sends an electrical signal to the actuator, which then adjusts the fuel supply to the engine to maintain the desired speed/load level. The gas engine, governor, and actuator are modeled with meticulous details, and the governor controls are fine-tuned to align with the engine's typical performance. The gain and time constant of the governor model are adjusted until a satisfactory response is achieved [26]. The basic control block diagram of a natural gas engine and the governor system is shown in Figure 2-4.

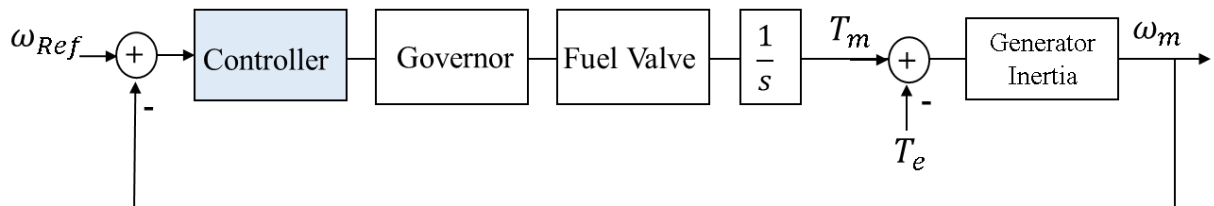


Figure 2-4 The detailed control system of Governor

### 2.3 Voltage Source Converter System

The field of power electronics has witnessed remarkable growth in recent years, driven by advancements in semiconductor fabrication technology and revolutionary breakthroughs in digital signal processors. Power converter systems play a pivotal role in enabling efficient energy exchange between two subsystems according to predefined performance criteria. These subsystems often operate with different voltage and current forms, frequencies, phase angles, and magnitudes, making direct interfacing impossible. Power electronics converter systems serve as an interface link, facilitating seamless integration between these dissimilar subsystems.

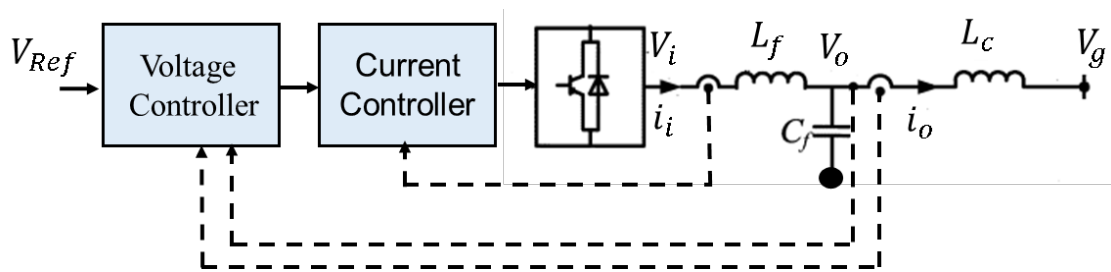


Figure 2-5 Inverter block diagram

The voltage source inverter (VSI) is a power electronic circuit that convert DC signals to AC. Typically, the renewable energy sources like photo-voltaic (PV) cells produce DC current and power which need to be converted to AC through a VSI in order to be supplied to local load or the utility grid. A VSI comprises of DC source (PV, fuel cells, batteries), switching circuit, passive filter for connecting to the grid and controller are illustrated in Figure 2-5. Any three phase set of variables that add up to zero in the stationary a-b-c frame can be represented in a complex plane by a complex vector that contains a real and an imaginary component.

### 2.3.1 Grid-Forming Concept

Grid-forming control controls the voltage and frequency of the inverter, making the voltage-sourced inverter behave approximately like a voltage source, as shown in Fig. Because the voltage and frequency remain constant, the grid forming inverters can work in the stand-alone mode and track the loads [27]

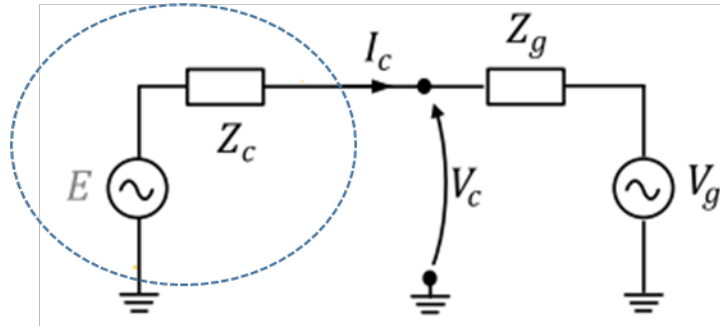


Figure 2-6 A simplified depiction of a Grid-forming converter

The master inverter functions as an advanced grid-forming inverter, equipped with the capability to regulate voltage in both islanded mode and grid-connected mode of operation. The notable improvement over the existing literature is the incorporation of a power compensator during grid-connected mode, which enables precise adjustment of reactive power during voltage regulation. This refined control system sets it apart from the previous system introduced in the literature. Figure 2-7 depicts the block diagram of grid forming inverter.

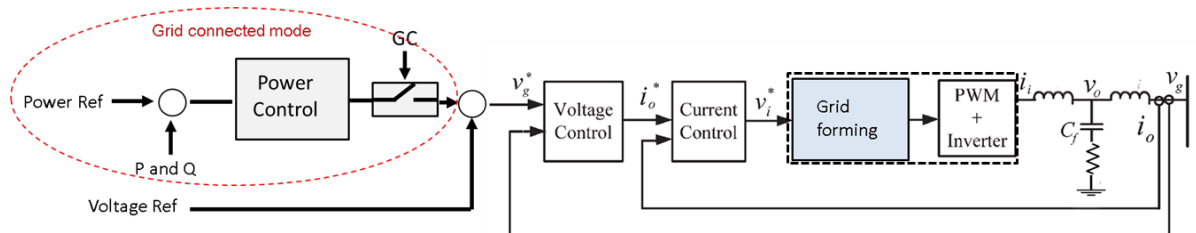


Figure 2-7 The proposed control strategy of grid forming inverter

### 2.3.2 Grid-Following Concept

Presently, grid-connected, inverter-based distributed energy resources (DERs) predominantly employ grid-following control, which utilizes a phase-lock loop (PLL) and a current control loop to achieve swift regulation of the inverter's output currents [28]. This form of control causes the voltage-sourced inverter to operate akin to a current source, as illustrated in Fig. 4(a). The advantage of grid-following control is its rapid current regulation capability. However, it lacks control over voltage and frequency, relying on an external voltage source as a reference.

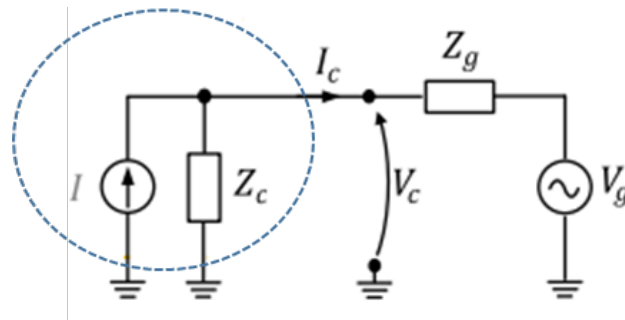


Figure 2-8 A simplified depiction of a Grid- following converter

The slave inverter in the proposed hybrid system operates as a grid-following inverter, functioning in two different modes of operation. The slave inverter is responsible for pushing power based on the reference values, which are set according to the system requirements and conditions.

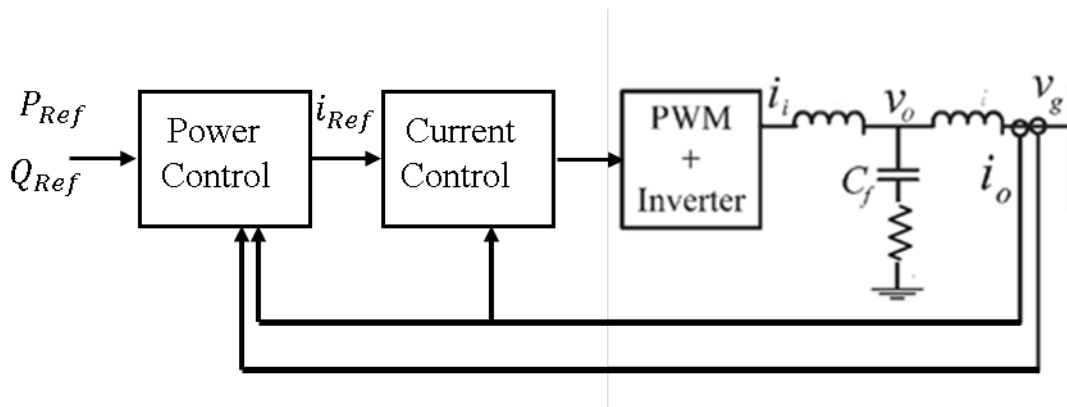


Figure 2-9 The block diagram of the slaved inverter

## 2.4 LCL Filter

Commonly, a high-order LCL filter has been used in place of the conventional L filter for smoothing the output currents from a VSI. The LCL filter achieves a higher attenuation along with cost savings, given the overall weight and size reduction of the components. LCL filters have been used in grid-connected inverters. The higher harmonic attenuation of the LCL filter allows the use of lower switching frequencies to meet harmonic constraints as defined by standards such as IEEE-519 and IEEE-1547.

The LCL filter model is shown in Figure 2-10, where  $L_1$  is the inverter side inductor,  $L_2$  is the grid-side inductor,  $C_f$  is a capacitor with a series  $R_f$  damping resistor, and voltages  $v_i$  and  $v_g$  are the input and output.

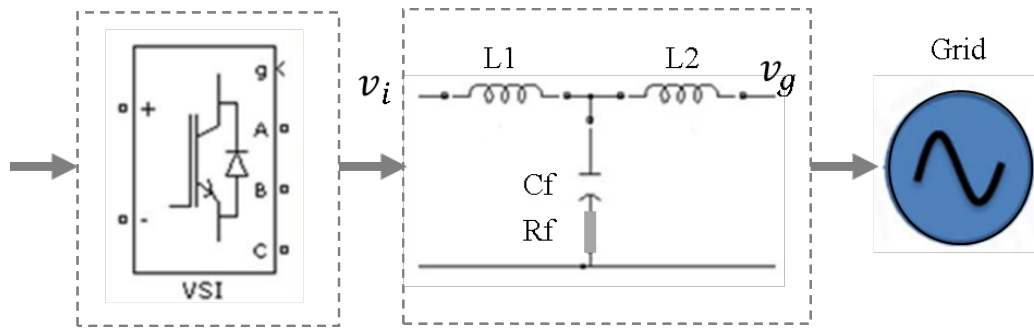


Figure 2-10 LCL filter

The transfer function of the LCL filter with damping resistance is defined by (2-1).

$$H(s) = \frac{C_f R_f s + 1}{L_1 C_f L_2 s^3 + C_f (L_1 + L_2) R_f s^2 + (L_1 + L_2) s} \quad (2-1)$$

Several characteristics must be considered in designing an LCL filter, such as current ripple, filter size, and switching ripple attenuation. The reactive power requirements may cause a resonance of the capacitor interacting with the grid. Therefore, passive or active damping must be added by including a resistor in series with the capacitor [29].

The resonate frequency is derived in the following equation.

$$\omega_{res} = \sqrt{\frac{L_1 + L_2}{L_1 L_2 C_f}} \quad (2-2)$$

The resonant frequency range must be considered to satisfy (2-3).

$$10f_g < f_{res} < 0.5f_{sw} \quad (2-3)$$

Where  $f_{res}$  is resonant frequency,  $f_g$  is grid frequency and  $f_{sw}$  is switching frequency.

## Chapter 3 State Space Modeling and Stability Analysis of the proposed MG

Frequency stability in a traditional large power system is maintained through the inertia of large synchronous generators, while voltage stability is maintained by controlling reactive power. Reactive power sources in a traditional system include synchronous generators, synchronous condensers, and capacitor banks, with regulating transformers also contributing to voltage regulation.

However, in a microgrid, which integrates a large number of inverters with renewables and energy storage, the situation is different. During island mode of operation, when the microgrid operates independently from the main grid, it may have limited inertia or no inertia at all if no synchronous generator is connected. The stability aspect of a microgrid depends on its structure and the sources connected to it, and can vary significantly.

A microgrid (MG) is a small-scale power system that can operate independently or in coordination with the main power grid. A state-space model is a mathematical representation of a dynamic system that describes how its variables change over time. In the context of microgrids, a state-space model can be used to represent the behavior of the system and predict its future behavior.

The state-space model of a microgrid includes a set of equations that describe the relationships between the system's inputs, outputs, and state variables. Inputs to the system include external disturbances such as changes in demand, renewable energy sources, or grid faults. Outputs of the system include measurements of the system's behavior, such as voltage or frequency. State variables are the internal variables of the system that change over time, such as the energy stored in batteries or capacitors.

Stability analysis is an important aspect of microgrid operation as it ensures the system remains in a safe operating condition. Stability analysis of a microgrid can be carried out using the state-space model by determining the eigenvalues of the system's matrix. The eigenvalues indicate the stability of the system, and if all eigenvalues have negative real parts, then the system is stable. If any eigenvalue has a positive real part, then the system is unstable, and corrective actions must be taken to ensure the system remains safe and reliable.

In this chapter, the state space model of voltage mode inverter, current mode inverter, natural gas generator, and transmission line has been derived. The detailed state space model of each unit in the hybrid microgrid has been developed. The stability analysis of the microgrid can be performed in various scenarios using this model. It can also be used to design controllers for the microgrid, such as governor and excitation systems for synchronous generators, active and reactive power controllers for current mode inverters, as well as voltage and frequency controllers for voltage mode inverters. Additionally, the developed state space model can be utilized for analyzing the stability and sensitivity of controller parameters.

In power electronics, inverters are commonly modeled using a space-state formulation, where the power devices within the inverter are idealized as switches. While this approximation sacrifices some accuracy, it allows for faster simulation times by reducing the time required for analysts to set up simulations and for computers to produce results [30]. By neglecting the switching behavior of the power devices, the inverter can be modeled as a linear time-invariant system. This simplification allows for the use of well-established control theory techniques and linear system analysis tools. Additionally, it reduces the complexity of the model and the simulation time, making it easier to analyze and design control strategies for the system.

### 3.1 Dynamic Model of the Proposed MG

The dynamic model of the proposed microgrid incorporates the interactions and behaviors of various components, including generators, inverters, storage systems, and loads, to accurately capture the system's dynamic response and behavior.

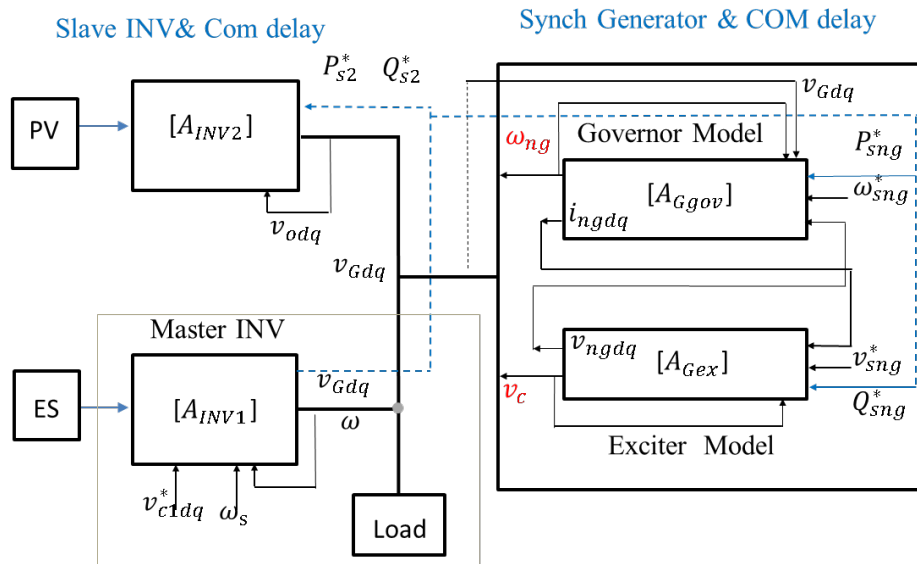


Figure 3-1 Dynamic model of the proposed MG

Figure 3-1 illustrates the detailed dynamic model of the proposed microgrid, which includes the independent modeling of each unit. This comprehensive model encompasses the dynamic interactions and behaviors of various components, such as generators, inverters, storage systems, and loads, taking into account their individual characteristics and operational modes. This detailed model enables a thorough analysis of the microgrid's dynamic behavior and performance under different operating conditions, facilitating the design and optimization of control strategies for efficient and reliable microgrid operation. Additionally, a communication line has been added as a part of the MG dynamic system, which distinguishes it from previous studies and makes it a more advanced model.

### 3.2 Dynamic Model of Natural Gas Generator (Synchronous Generator)

A natural gas (NG) generator plays a critical role in a microgrid when the state of charge (SOC) of the energy storage system is insufficient, and the renewable resources are unable to generate enough power to meet the energy demand of the microgrid. The natural gas generator serves as a reliable backup power source, ensuring uninterrupted power supply to the microgrid during periods when the energy storage system's SOC is low, or when renewable resources such as solar or wind are unable to generate sufficient power to meet the load requirements of the microgrid. This ensures the stability and resilience of the microgrid, enabling it to continue providing power to critical loads even in challenging conditions. The natural gas generator acts as a reliable and flexible source of energy, complementing the intermittent nature of renewable energy sources and enhancing the overall performance and reliability of the microgrid system.

A natural gas generator helps maintain stability due to the varied time responses of generators and energy storage systems. It is essential to consider the natural gas generator in stability studies. In this section, the state space model of the natural gas generator will be derived.

Synchronous machines have complex dynamics and control mechanisms that cannot be fully addressed in a short lecture. Therefore, several topics such as the accurate prime mover dynamics or the structure of excitation systems are not fully explained. Additional information may be found in [31, 32].

The delivered state space model of a synchronous generator covers the mechanical model to illustrate the model of the governor and engine, as well as the excitation model with communication delay between the generator and the master inverter. The details of the synchronous generator block diagram are illustrated in Figure 3-2.

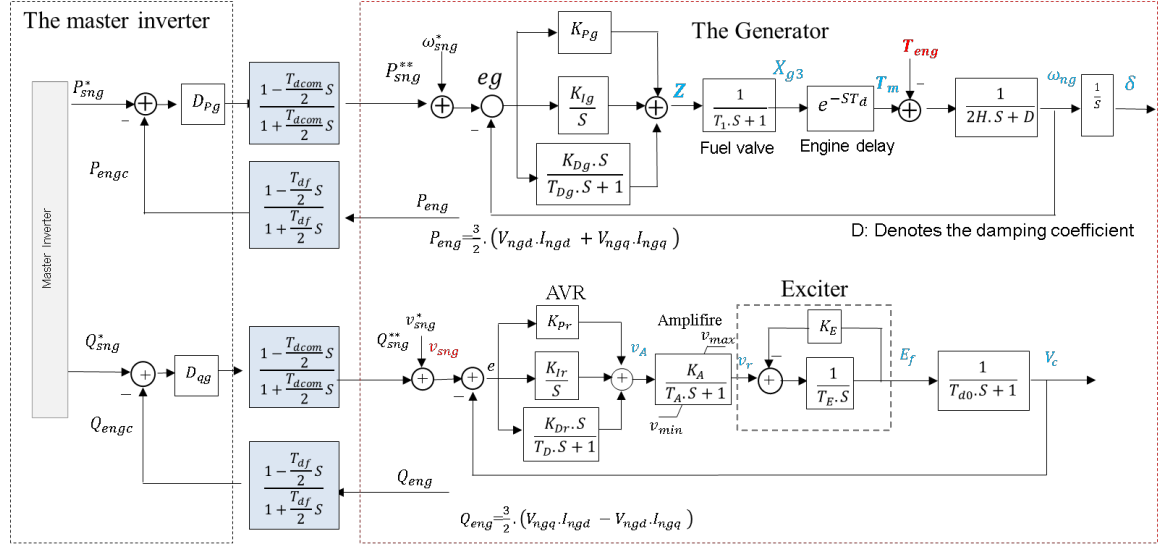


Figure 3-2 System block diagram of synchronous generator

### 3.2.1 Mechanical model

The rotational inertia equations are important in stability analysis describing the effect of unbalance between the electromagnetic torque and the mechanical torque of synchronous machine.

These equations are called swing equations, which are given by

$$2H \cdot \frac{d\omega_r}{dt} = T_m - T_e \quad (3-1)$$

Where  $T_m$  is mechanical torque in N-m,  $T_e$  is electrical torque and  $\omega_r$  is angular velocity of the rotor radian per second.  $H$  is inertia constant.

In order to accurately study the behavior of a natural gas generator, it is necessary to incorporate the dynamics of the natural gas engine, governor, fuel valve, communication delay and control system into the mathematical model. The complete mechanical system is shown in Figure 3-3.

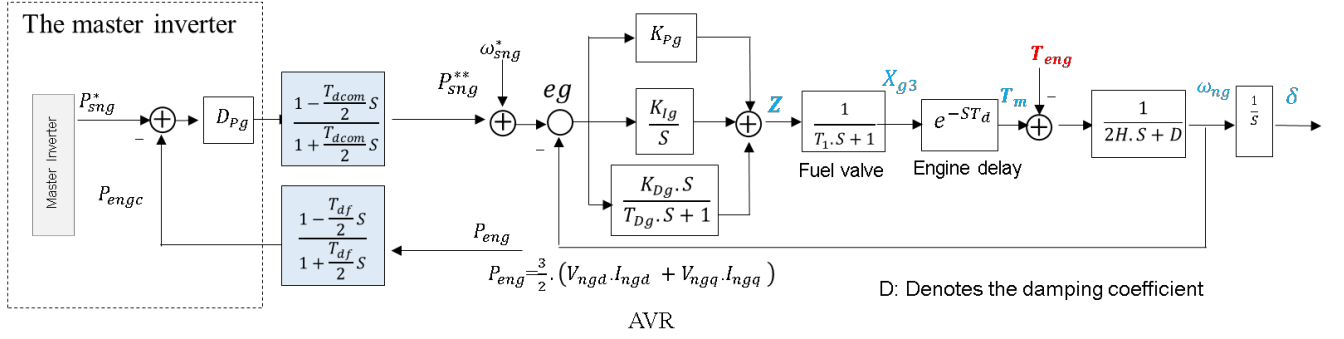


Figure 3-3 The complete mechanical system with active power setting value from the master inverter

The NG operates in power control mode. In order to increase the power output, the mechanical torque has to be increased. The speed reference for governor system is  $\omega_{sng}^* + P_{sng}^{**}$ . Where  $\omega_{sng}^*$  is reference speed and  $P_{sng}^{**}$  is the output of the droop control is derived from the master inverter. The differential equation of internal state can be represented by following equation.

$$\frac{Z}{E_g} = \left( K_{Pg} + \frac{K_{Ig}}{S} + \frac{K_{Dg} \cdot S}{T_{Dg} \cdot S + 1} \right) \cdot \frac{X_{g1}}{X_{g1}} \quad (3-2)$$

$$\dot{x}_{g1} = x_{g2} \quad (3-3)$$

$$z = (K_{Pg} T_{Dg} + K_{Dg}) x_{g2} + (K_{Ig} \cdot T_{Dg} + K_{Pg}) x_{g2} + K_{Ig} \cdot x_{g1} \quad (3-4)$$

$$e_g = S \cdot (T_{Dg} \cdot S + 1) X_{g1} = \omega_{sng}^* - \omega_{ng} + P_{sng}^{**} \quad (3-5)$$

$$P_{sng}^{**} = D_{Pg} \frac{1 - \frac{T_{dcomi} S}{2}}{1 + \frac{T_{dcomi} S}{2}} \cdot (P_{sng}^* - P_{engc}) \quad (3-6)$$

Where  $x_{g1}$ ,  $x_{g2}$  are internal state of PID controller,  $D_{Pg}$  is droop coefficient,  $P_{sng}^*$  is the active power reference value generated from the master controller before applying COM delay,  $P_{engc}$  is the feedback value of the active power coming from the generator.

$$X_{gp1} = \frac{1}{1 + \frac{T_{dcomi} S}{2}} \cdot (P_{sng}^* - P_{engc}) \quad (3-7)$$

By applying the inverse Laplace transform on equation (3-7), the state space equations for control system can be written as follows.

$$\dot{x}_{gp1} = -\frac{2}{T_{dcomi}} \cdot x_{gp1} + \frac{2}{T_{dcomi}} \cdot (P_{sng}^* - P_{engc}) \quad (3-8)$$

$x_{gp1}$  is internal state and  $T_{dcomi}$  is COM delay

According to the block diagram and the equation (3-8), can be written as follows.

$$P_{sng}^{**} = D_{Pg} \left( 1 - \frac{T_{dcomi}}{2} S \right) \cdot x_{gp1} = 2 \cdot D_{Pg} x_{gp1} - D_{Pg} \cdot (P_{sng}^* - P_{engc}) \quad (3-9)$$

From power feedback through communication delay, the following equation can be written

$$P_{engc} = \frac{1 - \frac{T_{df}}{2} S}{1 + \frac{T_{df}}{2} S} P_{eng} \quad (3-10)$$

$$X_{gp2} = \frac{1}{1 + \frac{T_{df}}{2} S} \cdot P_{eng} \quad (3-11)$$

Where  $T_{df}$  is feedback line delay from the NG to the master controller,  $X_{gp2}$  is an internal state used to describe the state-space equation for the COM delay transfer function.

$$\dot{x}_{gp2} = -\frac{2}{T_{df}} \cdot x_{gp2} + \frac{2}{T_{df}} \cdot P_{eng} \quad (3-12)$$

And,

$$P_{engc} = 2 \cdot x_{gp2} - P_{eng} \quad (3-13)$$

The transfer function of the fuel valve is given by following equations.

$$X_{g3} = \frac{1}{T_{1g} \cdot S + 1} Z \quad (3-14)$$

The states of the control system is  $X_{g3}$ . The state space equations for fuel valve can be written as follows.

$$\dot{x}_{g3} = -\frac{1}{T_{1g}}x_{g3} + \frac{1}{T_{1g}}z \quad (3-15)$$

The transfer function of engine delay is given by following equations.

$$T_m = \frac{1 - \frac{T_d}{2}S}{1 + \frac{T_d}{2}S} X_{g3} \quad (3-16)$$

Where  $T_m$  is mechanical torque,  $T_d$  is engine delay. The state-space equations for the engine delay can be written as follows.

$$X_{Tm} = \frac{1}{1 + \frac{T_d}{2}S} \cdot X_{g3}, \quad \dot{x}_{Tm} = -\frac{2}{T_d} \cdot x_{Tm} + \frac{2}{T_d} x_{g3} \quad (3-17)$$

$x_{Tm}$  is an internal state used to extract the state-space representations of engine delay questions.

$$T_m = 2 \cdot x_{Tm} - x_{g3} \quad (3-18)$$

The equation of motion of the rotor of synchronous generator, which is driven by prime mover is given by [33].

$$2H \frac{d\omega_r}{dt} + D\omega_r = T_m - T_{eng} \quad (3-19)$$

Where  $J=2H$  is the total moment of inertia and  $D$  is the damping torque coefficient. From the transfer function the state space equation can be written as follows.

$$\omega_{ng} = \frac{1}{2H \cdot S + D} (T_m - T_{eng}) \quad , \quad (3-20)$$

$$\dot{\omega}_{ng} = -\frac{D}{2H} \omega_{ng} + \frac{1}{2H} T_m - \frac{1}{2H} T_{eng}$$

### 3.2.2 Electrical Model of SG

This section presents an electrical model of the machine which is based on dq0 quantities. The machine is described as a system of coupled inductors.

$$\begin{aligned}
v_a &= -R_a i_a + \frac{d}{dt} \lambda_a \\
v_b &= -R_b i_b + \frac{d}{dt} \lambda_b \\
v_c &= -R_c i_c + \frac{d}{dt} \lambda_c \\
v_f &= -R_f i_f + \frac{d}{dt} \lambda_f
\end{aligned}
\tag{3-21}$$

Where  $\lambda_{a,b,c}$  denote the stator flux linkages,  $i_{a,b,c}$  denote the stator currents (generator output currents). The negative signs have been included since currents are positive when flowing out of the generator,  $\lambda_f$  denotes the field winding flux linkage, and  $i_f$  denotes the field winding flux link. In addition,  $v_{a,b,c}$  denote the stator terminal voltages (generator output voltages),  $v_f$  denotes the field winding voltage,  $R_{a,b,c}$  denotes the resistance of each winding on the stator;  $R_f$  denotes the field winding resistance.

The model defined by the above equations typically does not have an equilibrium point since the inductances depend on the rotor angle  $\theta$ , and thus vary with time. For this reason, we will now develop an equivalent model which is based on dq0 quantities. Such a model may be obtained by applying the dq0 transformation to the equations above. Omitting the algebraic details, the resulting dq0-based model is given by.

$$\begin{aligned}
v_d &= -R_a i_d + \frac{d}{dt} \lambda_d - \omega \lambda_q \\
v_q &= -R_a i_q + \frac{d}{dt} \lambda_q + \omega \lambda_d \\
v_f &= -R_f i_f + \frac{d}{dt} \lambda_f
\end{aligned}
\tag{3-22}$$

$$\lambda_d = -L_d i_d + L_{af} i_f$$

$$\lambda_q = -L_q i_q \quad (3-23)$$

$$\lambda_f = -\frac{3}{2} L_{af} i_d + L_{ff} i_f$$

Where  $L_d$  is the direct-axis synchronous inductance,  $L_q$  is the quadrature-axis synchronous inductance and  $L_{ff}$  is the field winding self-inductance with constant value.

For a perfectly round rotor with (no saliency effects)  $L_d = L_q$ , the synchronous inductances are equal equation (3-24).

$$L_s = \frac{1}{2}(L_d + L_q), \quad L_s = L_d = L_q \quad (3-24)$$

Where  $L_s$  is the synchronous inductance of the machine. This section presents a simplified dynamic model of the machine. The model is based on the following assumption  $v = L_d = L_q$ ,  $i_f = \text{Constant}$ , by replacing equation (3-23) into equation (3-22), the new state space can be written as follows.

$$v_d = -R_a i_d - L_s \frac{d}{dt} i_d + \omega L_s i_q$$

$$v_q = -R_a i_q - L_s \frac{d}{dt} i_q - \omega L_s i_d + \omega L_{af} I_f \quad (3-25)$$

$I_f$  is constant value. Using the definition.

$$V_E = \omega_s L_{af} I_f = \text{Constant} \quad (3-26)$$

These equations may be written as (3-27)

$$v_d = 0 - R_a i_d - (L_s \frac{d}{dt} i_d - \omega L_s i_q)$$

$$v_q = \frac{\omega}{\omega_s} V_E - R_a i_q - (L_s \frac{d}{dt} i_q + \omega L_s i_d) \quad (3-27)$$

Where  $\omega$  denotes the rotor electrical frequency and  $\omega_s$  denotes the nominal grid frequency,

Based on these expressions the machine's simplified model may be compactly described as an internal voltage source (induced EMF) behind a series impedance, as shown in Figure 3-4

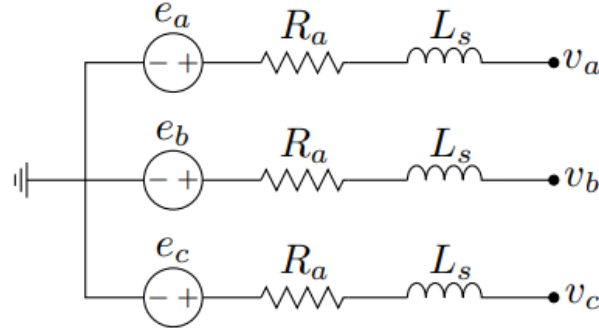


Figure 3-4 The simplified generator model

In this equivalent circuit the internal voltage source is given by equation (3-28)

$$\begin{bmatrix} e_a \\ e_b \\ e_c \end{bmatrix} = \begin{bmatrix} 0 \\ \omega \\ \omega_s \\ 0 \end{bmatrix} V_E \quad (3-28)$$

The power equation of the machine can be summarized as follows.

$$P_e = \frac{3}{2} (e_d i_d + e_q i_q) = T_e \omega_m \quad (3-29)$$

According to Figure 3-3 and equation 3-29, the active power output of natural gas generator is given by following equation.

$$P_{eng} = \frac{3}{2} \cdot (v_{ngd} \cdot i_{ngd} + v_{ngq} \cdot i_{ngq}) \quad (3-30)$$

After linearizing the above equation, linearized equation can be written as follows

$$\Delta P_{eng} = \frac{3}{2} \cdot (V_{ngd} \cdot \Delta i_{ngd} + I_{ngd} \cdot \Delta v_{ngd} + V_{ngq} \Delta i_{ngq} + I_{ngq} \cdot \Delta v_{ngq}) \quad (3-31)$$

The differential stator voltage equations in the d-q reference frame, as shown in Figure 3-5, can be written as follows.

$$L_{ng} \frac{di_{ngd}}{dt} = v_{ngd} - v_{Gd} - R_{ng}i_{ngd} + \omega_{ng}L_{ng}i_{ngq}$$

$$L_{ng} \frac{di_{ngq}}{dt} = v_{ngq} - v_{Gq} - R_{ng}i_{ngq} - \omega_{ng}L_{ng}i_{ngd}$$
( 3-32 )

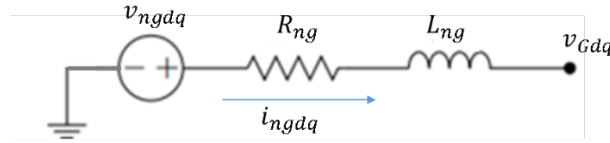


Figure 3-5 The electrical model of SG in dq frame

After linearizing the above equations, linearized equation can be expressed as follows.

$$\Delta \dot{i}_{ngd} = \frac{1}{L_{ng}} \cdot v_{ngd} - \frac{1}{L_{ng}} \cdot v_{Gd} + \omega_{ngs} \cdot i_{ngq} - \frac{R_{ng}}{L_{ng}} i_{ngd} + I_{ngq} \cdot \omega_{ng}$$

$$\Delta \dot{i}_{ngq} = \frac{1}{L_{ng}} \cdot v_{ngq} - \frac{1}{L_{ng}} \cdot v_{Gq} - \omega_{ngs} \cdot i_{ngd} - \frac{R_{ng}}{L_{ng}} i_{ngq} - I_{ngd} \cdot \omega_{ng}$$
( 3-33 )

By assuming the speed constant, the electrical power is equal to electromagnetic torque in per unit. Regarding equations (3-29) and (3-30), the electromagnetic torque can be expressed by the following equations.

$$T_{eng} = \frac{3}{2 \cdot \omega_{ngs}} \cdot (V_{ngd} \cdot i_{ngd} + I_{ngd} \cdot v_{ngd} + V_{ngq} \cdot i_{ngq} + I_{ngq} \cdot v_{ngq})$$

$$- \frac{1}{\omega_{ngs}^2} \cdot \frac{3}{2} \cdot (V_{ngd} \cdot I_{ngd} + V_{ngq} \cdot I_{ngq}) \cdot \omega_{ng}$$
( 3-34 )

By replacing equations (3-34) into equation (3-20).

$$\begin{aligned}
\dot{\omega}_{ng} &= -\frac{D}{2H}\omega_{ng} + \frac{1}{H}\cdot x_{Tm} - \frac{1}{2H}x_{g3} - \frac{1}{2H}V_{ngd}\cdot i_{ngd} - \frac{1}{4H}\frac{3}{\omega_{ngs}} \\
&I_{ngd}\cdot v_{ngd} - \frac{1}{4H}\frac{3}{\omega_{ngs}}V_{ngq}\cdot i_{ngq} - \frac{1}{4H}\frac{3}{\omega_{ngs}}I_{ngq}\cdot v_{ngq} + \\
&\frac{1}{4H}\frac{3}{\omega_{ngs}^2}(V_{ngd}\cdot I_{ngd} + V_{ngq}\cdot I_{ngq})\cdot \omega_{ng} , \\
F &= \frac{1}{4H}\frac{3}{\omega_{ngs}^2}(V_{ngd}\cdot I_{ngd} + V_{ngq}\cdot I_{ngq})
\end{aligned} \tag{3-35}$$

By replacing equations (3-4), (3-5), (3-9), (30-31) and (3-34) into equation (3-3), the equation can be written as follows.

$$\begin{aligned}
eg &= \omega_{sng}^* - \omega_{ng} + 2\cdot D_{Pg}x_{gp1} - D_{Pg}P_{sng}^* + D_{Pg}2\cdot x_{gp2} \\
&- D_{Pg}\frac{3}{2}\cdot V_{ngd}\cdot i_{ngd} - D_{Pg}\frac{3}{2}I_{ngd}\cdot v_{ngd} - D_{Pg}\frac{3}{2}V_{ngq}\cdot i_{ngq} \\
&- D_{Pg}\frac{3}{2}I_{ngq}\cdot v_{ngq}
\end{aligned} \tag{3-36}$$

$$\begin{aligned}
Z &= K_{G1}\omega_{sng}^* - K_{G1}\omega_{ng} + 2\cdot K_{G1}D_{Pg}x_{gp1} - K_{G1}D_{Pg}P_{sng}^* + K_{G1}D_{Pg}2\cdot x_{gp2} \\
&- K_{G1}D_{Pg}\frac{3}{2}\cdot V_{ngd}\cdot i_{ngd} - K_{G1}D_{Pg}\frac{3}{2}I_{ngd}\cdot v_{ngd} \\
&- K_{G1}D_{Pg}\frac{3}{2}V_{ngq}\cdot i_{ngq} - K_{G1}D_{Pg}\frac{3}{2}I_{ngq}\cdot v_{ngq} \\
&+ ((K_{Ig}\cdot T_{Dg} + K_{Pg}) - K_{G1})x_{g2} + K_{Ig}\cdot x_{g1}
\end{aligned} \tag{3-37}$$

$$K_{G1} = \frac{K_{Pg}T_{Dg} + K_{Dg}}{T_{Dg}} \tag{3-38}$$

By replacing equations (3-37) into equation (3-14) the equation can be expressed as follows.

$$\begin{aligned}
\dot{x}_{g3} = & -\frac{1}{T_{1g}}x_{g3} + \frac{1}{T_{1g}}(K_{G1}\omega_{sng}^* - K_{G1}\omega_{ng} + 2.K_{G1}D_{Pg}x_{gp1} \\
& - K_{G1}D_{Pg}P_{sng}^* + K_{G1}D_{Pg}2.x_{gp2} \\
& - K_{G1}D_{Pg}\frac{3}{2}.V_{ngd}.i_{ngd} - K_{G1}D_{Pg}\frac{3}{2}I_{ngd}.v_{ngd} \\
& - K_{G1}D_{Pg}\frac{3}{2}V_{ngq}.i_{ngq} - K_{G1}D_{Pg}\frac{3}{2}I_{ngq}.v_{ngq} \\
& + ((K_{I_g}.T_{Dg} + K_{Pg}) - K_{G1})x_{g2} + K_{I_g}.x_{g1})
\end{aligned} \tag{3-39}$$

From above discussion and above differential equations, the state space equations for mechanical system is given (3-40).

- $\dot{x}_{gp1} = -\frac{2}{T_{dcom}}.x_{gp1} + \frac{2}{T_{dcom}}P_{sng}^* - \frac{4}{T_{dcom}}x_{gp2} + \frac{3}{T_{dcom}}(V_{ngd}.i_{ngd} + I_{ngd}.v_{ngd} + V_{ngq}.i_{ngq} + I_{ngq}.v_{ngq})$
- $\dot{x}_{gp2} = -\frac{2}{T_{df}}.x_{gp2} + \frac{3}{T_{df}}.(V_{ngd}.i_{ngd} + I_{ngd}.v_{ngd} + V_{ngq}.i_{ngq} + I_{ngq}.v_{ngq})$
- $\dot{x}_{g1} = x_{g2}$  ,
- $\dot{x}_{g2} = \frac{1}{T_{Dg}}(\omega_{sng}^* - \omega_{ng} + 2.D_{Pg}x_{gp1} - D_{Pg}P_{sng}^* + D_{Pg}2.x_{gp2} - D_{Pg}\frac{3}{2}.V_{ngd}.i_{ngd} - D_{Pg}\frac{3}{2}I_{ngd}.v_{ngd} - D_{Pg}\frac{3}{2}V_{ngq}.i_{ngq} - D_{Pg}\frac{3}{2}I_{ngq}.v_{ngq}) - \frac{1}{T_{Dg}}x_{g2}$
- $\dot{x}_{g3} = -\frac{1}{T_{1g}}x_{g3} + \frac{1}{T_{1g}}(K_{G1}\omega_{sng}^* - K_{G1}\omega_{ng} + 2.K_{G1}D_{Pg}x_{gp1} - K_{G1}D_{Pg}P_{sng}^* + K_{G1}D_{Pg}2.x_{gp2} - K_{G1}D_{Pg}\frac{3}{2}.V_{ngd}.i_{ngd} - K_{G1}D_{Pg}\frac{3}{2}I_{ngd}.v_{ngd} - K_{G1}D_{Pg}\frac{3}{2}V_{ngq}.i_{ngq} - K_{G1}D_{Pg}\frac{3}{2}I_{ngq}.v_{ngq} + ((K_{I_g}.T_{Dg} + K_{Pg}) - K_{G1})x_{g2} + K_{I_g}.x_{g1})$  (3-40)
- $\dot{x}_{Tm} = -\frac{2}{T_d}.x_{Tm} + \frac{2}{T_d}x_{g3}$
- $\dot{\omega}_{ng} = -\frac{D}{2H}\omega_{ng} + \frac{1}{H}.x_{Tm} - \frac{1}{2H}x_{g3} - \frac{1}{4H}\frac{3}{\omega_{ngs}}V_{ngd}.i_{ngd} - \frac{1}{4H}\frac{3}{\omega_{ngs}}I_{ngd}.v_{ngd} - \frac{1}{4H}\frac{3}{\omega_{ngs}}V_{ngq}.i_{ngq} - \frac{1}{4H}\frac{3}{\omega_{ngs}}I_{ngq}.v_{ngq} + \frac{1}{4H}\frac{3}{\omega_{ngs}^2}(V_{ngd}.I_{ngd} + V_{ngq}.I_{ngq}).\omega_{ng}$
- $\dot{\delta} = \omega_{ng}$
- $\dot{i}_{ngd} = \frac{1}{L_{ng}}.v_{ngd} - \frac{1}{L_{ng}}.v_{Gd} + \omega_{ngs}.i_{ngq} - \frac{R_{ng}}{L_{ng}}i_{ngd} + I_{ngq}.\omega_{ng}$

$$\bullet \quad \dot{i}_{ngq} = \frac{1}{L_{ng}} \cdot v_{ngq} - \frac{1}{L_{ng}} \cdot v_{Gq} - \omega_{ngs} \cdot i_{ngd} - \frac{R_{ng}}{L_{ng}} i_{ngq} - I_{ngd} \cdot \omega_{ng}$$

Figure 3-6 shows a state space model of a governor. The mechanical system has three inputs, which consist of the MG reference voltage, frequency reference value, active power setting value from the master controller, and terminal voltage coming from the exciter side. The mechanical model states cover internal states to describe the controller, COM delay, and mechanical parameters.

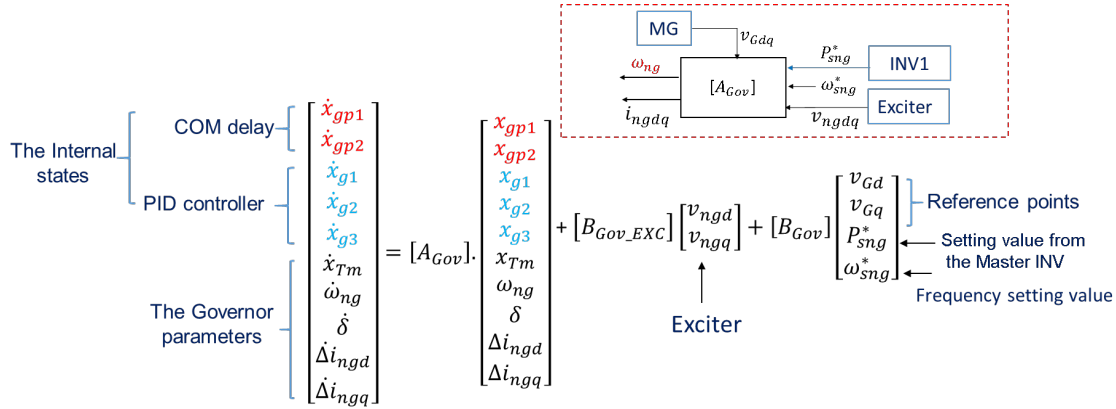


Figure 3-6 The state space model of governor

According to Figure 3-6, state space matrixes are defined as follows.

$$A_{Gov} =$$

$$\begin{bmatrix} -\frac{2}{T_{dcomi}} & -\frac{4}{T_{dcom}} & 0 & 0 & 0 & 0 & 0 & 0 & \frac{3V_{ngd}}{T_{dcom}} & \frac{3V_{ngq}}{T_{dcom}} \\ 0 & -\frac{2}{T_{df}} & 0 & 0 & 0 & 0 & 0 & 0 & \frac{3V_{ngd}}{T_{df}} & \frac{3V_{ngq}}{T_{df}} \\ 0 & 0 & 0 & 1 & 0 & 0 & 0 & 0 & 0 & 0 \\ \frac{2}{T_{Dg}} \cdot D_{Pg} & \frac{2}{T_{Dg}} \cdot D_{Pg} & 0 & -\frac{1}{T_{Dg}} & 0 & 0 & -\frac{1}{T_{Dg}} & 0 & -\frac{3}{2} \frac{1}{T_{Dg}} \cdot D_{Pg} \cdot V_{ngd} & -\frac{3}{2} \frac{1}{T_{Dg}} \cdot D_{Pg} \cdot V_{ngq} \\ \frac{2 \cdot K_{G1} D_{Pg}}{T_{1g}} & \frac{2 \cdot K_{G1} D_{Pg}}{T_{1g}} & \frac{1}{T_{1g}} K_{Ig} & -\frac{1}{T_{1g}} K_{G1} + \frac{1}{T_{1g}} (K_{Ig} \cdot T_{Dg} + K_{Pg}) & -\frac{1}{T_{1g}} & 0 & -\frac{K_{G1}}{T_{1g}} & 0 & -\frac{3K_{G1} D_{Pg}}{2T_{1g}} \cdot V_{ngd} & -\frac{3K_{G1} D_{Pg}}{2T_{1g}} \cdot V_{ngq} \\ 0 & 0 & 0 & 0 & \frac{2}{T_{dg}} & -\frac{2}{T_{dg}} & 0 & 0 & 0 & 0 \\ 0 & 0 & 0 & 0 & -\frac{1}{2H} & \frac{1}{H} & -\frac{D}{2H} + F & 0 & -\frac{3}{4H \cdot \omega_{ngs}} V_{ngd} & -\frac{3}{4H \cdot \omega_{ngs}} V_{ngq} \\ 0 & 0 & 0 & 0 & 0 & 0 & 1 & 0 & 0 & 0 \\ 0 & 0 & 0 & 0 & 0 & 0 & I_{ngq} & 0 & -\frac{R_{ng}}{L_{ng}} & \omega_{ngs} \\ 0 & 0 & 0 & 0 & 0 & 0 & -I_{ngd} & 0 & -\omega_{ngs} & -\frac{R_{ng}}{L_{ng}} \end{bmatrix}$$

$$B_{Gov\_EXC} = \begin{bmatrix} \frac{3I_{ngd}}{T_{dcom}} & \frac{3I_{ngq}}{T_{dcom}} \\ \frac{3I_{ngd}}{T_{df}} & \frac{3I_{ngq}}{T_{df}} \\ 0 & 0 \\ -\frac{3}{2} \frac{1}{T_{Dg}} \cdot D_{Pg} \cdot I_{ngd} & -\frac{3}{2} \frac{1}{T_{Dg}} \cdot D_{Pg} \cdot I_{ngq} \\ -\frac{3K_{G1} D_{Pg}}{2T_{1g}} \cdot I_{ngd} & -\frac{3K_{G1} D_{Pg}}{2T_{1g}} \cdot I_{ngq} \\ 0 & 0 \\ -\frac{1}{4H} \cdot \frac{3}{\omega_{ngs}} \cdot I_{ngd} & -\frac{1}{4H} \cdot \frac{3}{\omega_{ngs}} \cdot I_{ngq} \\ 0 & 0 \\ \frac{1}{L_{ng}} & 0 \\ 0 & \frac{1}{L_{ng}} \end{bmatrix}$$

$$B_{Gov} = \begin{bmatrix} 0 & 0 & \frac{2}{T_{dcom}} & 0 \\ 0 & 0 & 0 & 0 \\ 0 & 0 & 0 & 0 \\ 0 & 0 & -\frac{1}{T_{Dg}} \cdot D_{Pg} & \frac{1}{T_{Dg}} \\ 0 & 0 & -\frac{K_{G1}}{T_{1g}} \cdot D_{Pg} & \frac{K_{G1}}{T_{1g}} \\ 0 & 0 & 0 & 0 \\ 0 & 0 & 0 & 0 \\ 0 & 0 & 0 & 0 \\ -\frac{1}{L_{ng}} & 0 & 0 & 0 \\ 0 & -\frac{1}{L_{ng}} & 0 & 0 \end{bmatrix}$$

### 3.2.2.1 Dynamic Analysis of Governor System

To analyze the stability of the mechanical system, a state space model is utilized. From this model, eigenvalues are derived, and the impact of communication delay and mechanical delay on the system is assessed. Figure 3-7(a) shows that the eigenvalues move to the right side as more delay is added to the engine transfer function. The simulation results in Figure 3-8 confirm this analysis. The same concept as in Figure 3-7(a) applies to the fuel valve, as shown in Figure 3-7(b).

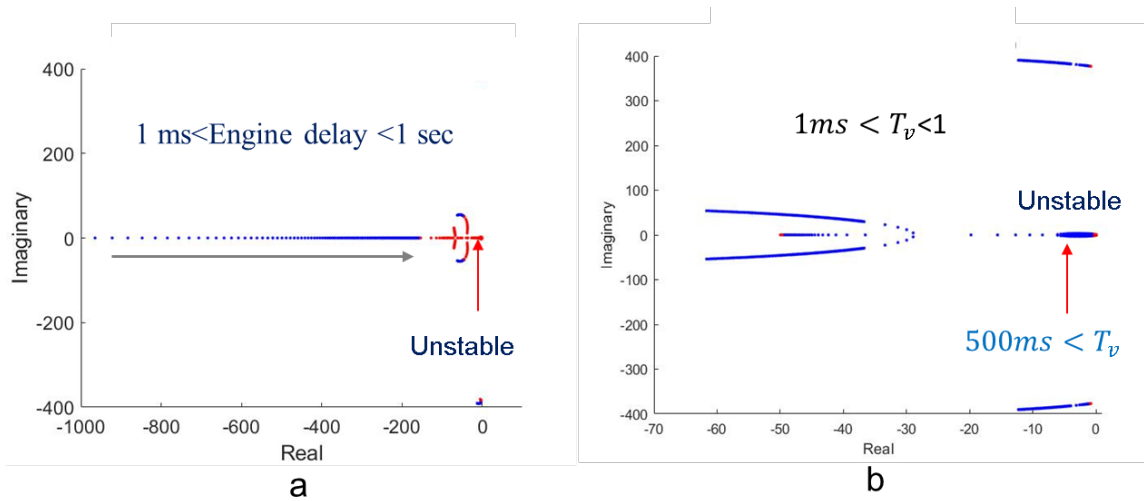


Figure 3-7 a. The impact of engines delay. b. The impact of the fuel valve delay

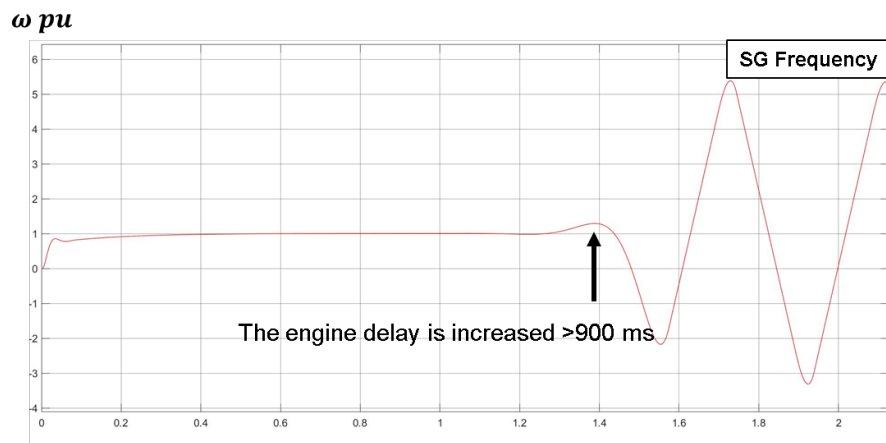


Figure 3-8 This simulation data demonstrates the impact of engine delay on SG frequency

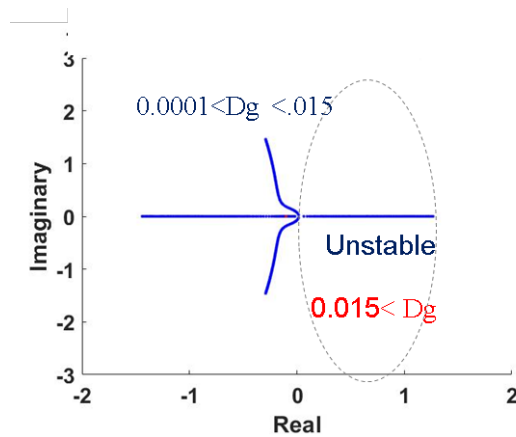


Figure 3-9 Exploring the effects of changing droop gain on eigenvalue plots in islanding mode

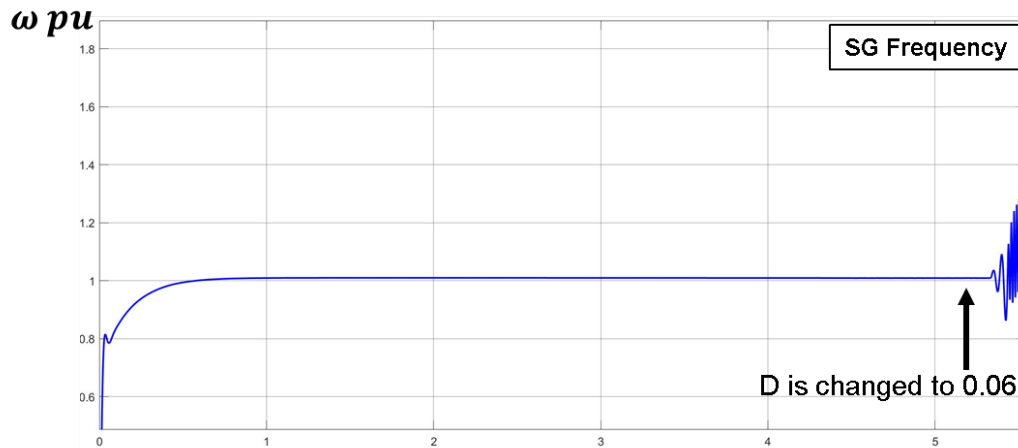


Figure 3-10 Presenting simulation results that demonstrate the effect of droop gain on SG frequency during islanding mode

The droop coefficient is another parameter that is analyzed. While it does not have a significant effect during standalone operation, the droop gain becomes highly sensitive when the generator is connected to the MG, leading to instability in the system. Figure 3-9 displays eigenvalue plots for varying values of droop gain, and Figure 3-10 illustrates the system's instability during islanding mode as the droop value increases.

The communication delay was the last parameter that was studied. Two scenarios were proposed: In the first one, there is the same amount of delay in the forward and backward paths, while in the second scenario, we have two different delays in each path. Before proceeding, it is essential to obtain an accurate estimation for the time delay. Latency refers to the duration it takes for a signal to travel from its source to its destination, typically from a transmitter through a network to a receiver. In the context of a distributed control system, latency is measured as the time it takes for a message to be transmitted from the sender and received by the receiver.

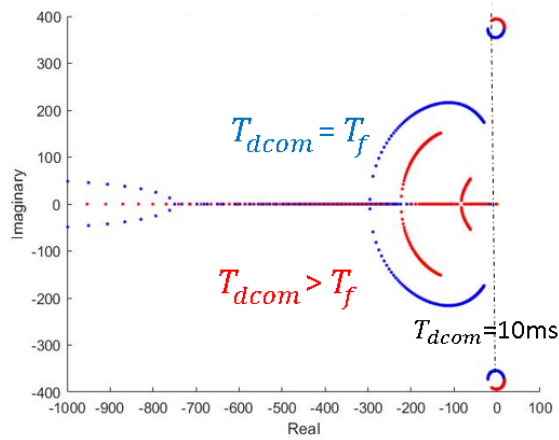


Figure 3-11 Plot of Eigenvalues with increasing communication delay between the master controller and SG

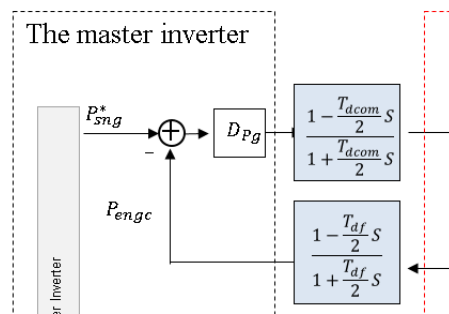


Figure 3-12 The transfer function of communication between two units



Figure 3-13 Comparison of two methods of time delay approximation

One of the methods commonly used for the rational approximation of the time delay transfer function is the application of Padé approximants. As illustrated in Figure 3-13, the

results obtained from Padé approximants are superior to those of Taylor series. In this study, we have utilized a first-order approximation for the time delay transfer function.

$$e^{-T_d s} = \frac{1 - \frac{T_d}{2} s}{1 + \frac{T_d}{2} s} \quad (3-41)$$

Regarding Figure 3-11, it can be observed that in the second scenario, the output power will start to fluctuate earlier than in scenario number one, when the delay in both paths is increased. This highlights the significance of considering the delays in forward paths more carefully than in the first case.

### 3.2.3 Exciter state space modeling

The excitation system's comprehensive block diagram is presented in Figure 3-14. By examining the block diagram, it can be deduced that the voltage reference for the Automatic Voltage Regulator (AVR) system is composed of two parts:  $v_{sng}^* + Q_{sng}^{**}$ . The voltage reference, denoted by  $v_{sng}^*$ , is generated internally within the system, whereas  $Q_{sng}^{**}$  is received from the droop controller to control the reference reactive power. Together, these two components determine the output voltage of the generator.

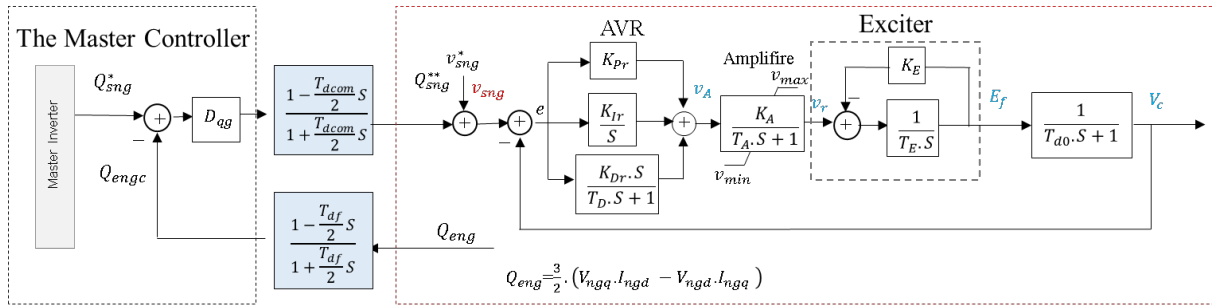


Figure 3-14 Block diagram of excitation system

Reactive power output of natural gas generator is given by following equation.

$$Q_{eng} = \frac{3}{2} \cdot (V_{ngq} \cdot I_{ngd} - V_{ngd} \cdot I_{ngq}) \quad (3-42)$$

After linearizing the above equation, linearized equation can be written as follows.

$$\Delta Q_{eng} = \frac{3}{2} \cdot (V_{ngq} \cdot \Delta i_{ngd} + I_{ngd} \cdot \Delta v_{ngq} - V_{ngd} \cdot \Delta i_{ngq} - I_{ngq} \cdot \Delta v_{ngd}) \quad (3-43)$$

According to the block diagram depicted in Figure 3-14 and equation 3-43 we can write equation

(3-44)

$$e = v_{sng}^* + D_{qg} \cdot Q_{sng} - \frac{3}{2} \cdot D_{qg} (V_{ngq} \cdot \Delta i_{ngd} + I_{ngd} \cdot \Delta v_{ngq} - V_{ngd} \cdot \Delta i_{ngq} - I_{ngq} \cdot \Delta v_{ngd}) - v_c \quad (3-44)$$

$$Q_{sng}^{**} = D_{Qg} \frac{1 - \frac{T_{dcomi} S}{2}}{1 + \frac{T_{dcomi} S}{2}} \cdot (Q_{sng}^* - Q_{engc}), \quad X_{gq1} = \frac{1}{1 + \frac{T_{dcomi} S}{2}} \cdot (Q_{sng}^* - Q_{engc}) \quad (3-45)$$

$$\dot{x}_{gq1} = -\frac{2}{T_{dcomi}} \cdot x_{gq1} + \frac{2}{T_{dcomi}} \cdot (Q_{sng}^* - Q_{engc}) \quad (3-46)$$

$$Q_{sng}^{**} = D_{Qg} \left(1 - \frac{T_{dcomi} S}{2}\right) \cdot x_{gq1} = 2 \cdot D_{Qg} x_{gq1} - D_{Qg} \cdot (Q_{sng}^* - Q_{engc}) \quad (3-47)$$

Equations (3-48) and (3-49) can be used to model the feedback delay.

$$Q_{engc} = \frac{1 - \frac{T_{df} S}{2}}{1 + \frac{T_{df} S}{2}} Q_{eng} \quad (3-48)$$

$$X_{gq2} = \frac{1}{1 + \frac{T_{df}}{2}S} \cdot Q_{eng} \quad (3-49)$$

Where  $X_{gq2}$  is internal state, the state space equation for feedback line can be written as follows.

$$\dot{x}_{gq2} = -\frac{2}{T_{df}} \cdot x_{gq2} + \frac{2}{T_{df}} \cdot Q_{eng} \quad (3-50)$$

$$Q_{engc} = 2 \cdot x_{gq2} - Q_{eng} \quad (3-51)$$

The transfer function of AVR system is given by following equation.

$$\frac{V_A}{E} = (K_{Pr} + \frac{K_{Ir}}{S} + \frac{K_{Dr} \cdot S}{T_D \cdot S + 1}) \cdot \frac{X_{v1}}{X_{v1}} \quad (3-52)$$

Where  $x_{v1}$  and  $x_{v2}$  are internal state.

$$\dot{x}_{v1} = x_{v2} \quad (3-53)$$

$$\dot{x}_{v2} = \frac{1}{T_D} e - \frac{1}{T_D} x_{v2} \quad (3-54)$$

From equation (3-52)

$$v_A = K_{E1}e + [-K_{E1} + (K_{Ir} \cdot T_D + K_{pr})]x_{v2} + K_{Ir} \cdot x_{v1} \quad (3-55)$$

Where  $K_{E1} = \frac{(K_{Pr}T_D + K_{Dr})}{T_D}$

By using equation (3-47), the new equation can be written as follows

$$e = v_{sng}^* - v_c + Q_{sng}^{**} \quad (3-56)$$

$$= v_{sng}^* - v_c + 2 \cdot D_{Qg}x_{gq1} - D_{Qg}Q_{sng}^* + D_{Qg}2 \cdot x_{gq2} - D_{Qg}Q_{eng}$$

By replacing equation (3-56) into (3-55), the new equation can be expressed as follows.

$$\begin{aligned}
v_A = & K_{E1}v_{sng}^* - K_{E1}v_c + 2K_{E1} \cdot D_{Qg}x_{gq1} - K_{E1}D_{Qg}Q_{sng}^* + K_{E1}D_{Qg}2 \cdot x_{gq2} \\
& - K_{E1}D_{Qg}\frac{3}{2}V_{ngq} \cdot \Delta i_{ngd} - K_{E1}D_{Qg}\frac{3}{2}I_{ngd} \cdot \Delta v_{ngq} \\
& + K_{E1}D_{Qg}\frac{3}{2}V_{ngd} \Delta i_{ngq} + K_{E1}D_{Qg}\frac{3}{2}I_{ngq} \cdot \Delta v_{ngd} + [-K_{E1} \\
& + (K_{Ir} \cdot T_D + K_{pr})]x_{v2} + K_{Ir} \cdot x_{v1}
\end{aligned} \tag{3-57}$$

The transfer function of the amplifier is given by following equation.

$$V_r = \frac{K_A}{T_A \cdot S + 1} V_A \tag{3-58}$$

By replacing equation (3-57) into equation (3-58), the first order differential and output equations can be written as follows.

$$\begin{aligned}
\dot{v}_r = & \frac{K_A}{T_A} K_{E1}v_{sng}^* - \frac{K_A}{T_A} K_{E1}v_c + 2\frac{K_A}{T_A} K_{E1} \cdot D_{Qg}x_{gq1} - \frac{K_A}{T_A} K_{E1}D_{Qg}Q_{sng}^* \\
& + \frac{K_A}{T_A} K_{E1}D_{Qg}2 \cdot x_{gq2} - \frac{K_A}{T_A} K_{E1}D_{Qg}\frac{3}{2}V_{ngq} \cdot \Delta i_{ngd} \\
& - \frac{K_A}{T_A} K_{E1}D_{Qg}\frac{3}{2}I_{ngd} \cdot \Delta v_{ngq} + \frac{K_A}{T_A} K_{E1}D_{Qg}\frac{3}{2}V_{ngd} \Delta i_{ngq} \\
& + \frac{K_A}{T_A} K_{E1}D_{Qg}\frac{3}{2}I_{ngq} \cdot \Delta v_{ngd} + \frac{K_A}{T_A} [-K_{E1} \\
& + (K_{Ir} \cdot T_D + K_{pr})]x_{v2} + \frac{K_A}{T_A} K_{Ir} \cdot x_{v1} - \frac{1}{T_A} \cdot v_r
\end{aligned} \tag{3-59}$$

The transfer function of the exciter is given by following equation.

$$E_f = \frac{1}{T_E \cdot S + K_E} V_r \tag{3-60}$$

The process of obtaining the first order differential equation can be explained as follows.

$$E \cdot \dot{f} = \frac{-K_E}{T_E} E_f + \frac{1}{T_E} \cdot v_r \tag{3-61}$$

The open circuit transfer function of the generator field is expressed by the following equation.

$$V_c = \frac{1}{T_{do} \cdot S + 1} E_f \quad (3-62)$$

Where  $T_{do}$  is a time constant of field, the first order differential equation can be given as follows.

$$\dot{v}_c = \frac{-1}{T_{do}} v_c + \frac{1}{T_{do}} \cdot E_f \quad (3-63)$$

Where  $v_{ngd} = v_c$ ,  $F$  and  $v_{ngq} = 0$ , from above small perturbation equations, the state space equation for exciter system can be written as follows.

- $\dot{x}_{gq1} = -\frac{2}{T_{dcomi}} \cdot x_{gq1} + \frac{2}{T_{dcomi}} Q_{sng}^* - \frac{4}{T_{dcomi}} \cdot x_{gq2} + \frac{3}{T_{dcomi}} (V_{ngq} \cdot \Delta i_{ngd} - V_{ngd} \Delta i_{ngq} - I_{ngq} \cdot v_c)$
- $\dot{x}_{gq2} = -\frac{2}{T_{df}} \cdot x_{gq2} + \frac{3}{T_{df}} (V_{ngq} \cdot \Delta i_{ngd} - V_{ngd} \Delta i_{ngq} - I_{ngq} \cdot c)$
- $\dot{x}_{v1} = x_{v2}$  ,
- $\dot{x}_{v2} = \frac{1}{T_D} (v_{sng}^* - v_c + 2 \cdot D_{Qg} x_{gq1} - D_{Qg} Q_{sng}^* + D_{Qg} 2 \cdot x_{gq2} - D_{Qg} \frac{3}{2} V_{ngq} \cdot \Delta i_{ngd} + D_{Qg} \frac{3}{2} V_{ngd} \Delta i_{ngq} + D_{Qg} \frac{3}{2} I_{ngq} \cdot v_c) - \frac{1}{T_D} x_{v2}$
- $\dot{v}_r = \frac{K_A}{T_A} K_{E1} v_{sng}^* + (\frac{K_A}{T_A} K_{E1} D_{Qg} \frac{3}{2} I_{ngq} - \frac{K_A}{T_A} K_{E1}) v_c + 2 \frac{K_A}{T_A} K_{E1} \cdot D_{Qg} x_{gq1} - \frac{K_A}{T_A} K_{E1} D_{Qg} Q_{sng}^* + \frac{K_A}{T_A} K_{E1} D_{Qg} 2 \cdot x_{gq2} - \frac{K_A}{T_A} K_{E1} D_{Qg} \frac{3}{2} V_{ngq} \cdot \Delta i_{ngd} + \frac{K_A}{T_A} K_{E1} D_{Qg} \frac{3}{2} V_{ngd} \Delta i_{ngq} + \frac{K_A}{T_A} K_{E1} D_{Qg} \frac{3}{2} I_{ngq} \cdot v_c + \frac{K_A}{T_A} [-K_{E1} + (K_{Ir} \cdot T_D + K_{pr})] x_{v2} + \frac{K_A}{T_A} K_{Ir} \cdot x_{v1} - \frac{1}{T_A} \cdot v_r$
- $\dot{E}_f = \frac{-K_E}{T_E} E_f + \frac{1}{T_E} \cdot v_r$
- $\dot{v}_c = \frac{-1}{T_{do}} v_c + \frac{1}{T_{do}} \cdot E_f$

Where,

$$K_{E1} = \frac{(K_{pr} T_D + K_{Dr})}{T_D} \quad (3-65)$$

Figure 3-15 shows a state space model of an exciter system. The exciter system has three inputs, which consist of the MG reference voltage, reactive power setting value from the master

controller, and terminal current coming from the exciter side. The model states cover internal states to describe the controller, COM delay, and field parameters.

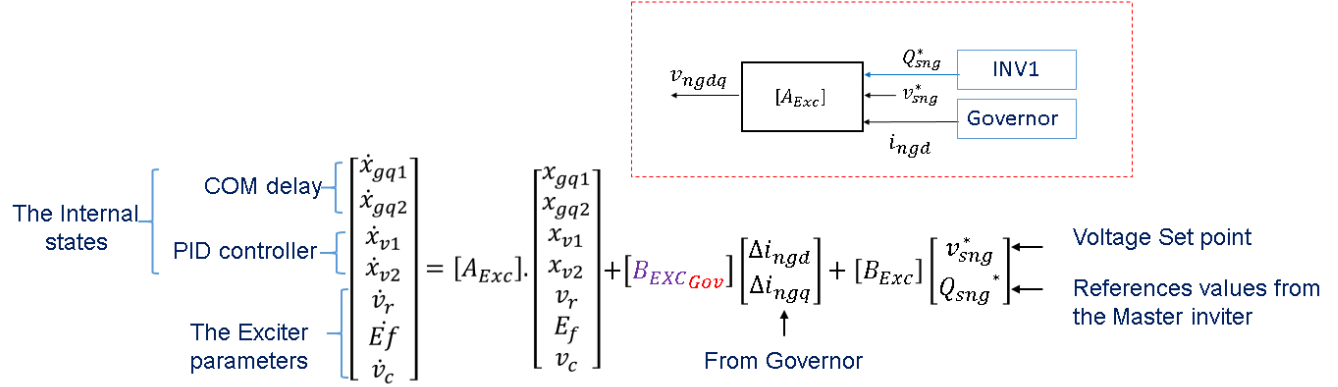


Figure 3-15 The state space model of exciter

According to the model shown in Figure 3-15, state space matrixes are defined as follows.

$$\begin{aligned}
 & \quad \quad \quad [A_{Exc}] \quad \quad \quad \quad \quad \quad [B_{ExcGov}] \quad \quad \quad [B_{Exc}] \\
 & \begin{pmatrix} -\frac{2}{T_{dcom}} & -\frac{4}{T_{dcom}} & 0 & 0 & 0 & 0 & -\frac{3}{T_{dcom}} I_{ngq} \\ 0 & -\frac{2}{T_{dcom}} & 0 & 0 & 0 & 0 & -\frac{3}{T_{df}} I_{ngq} \\ 0 & 0 & 0 & 1 & 0 & 0 & 0 \\ \frac{2 \cdot D_{Qg}}{T_D} & \frac{2 \cdot D_{Qg}}{T_D} & 0 & -\frac{1}{T_D} & 0 & 0 & \left( \frac{1 \cdot 3}{T_D} \cdot D_{Qg} \cdot I_{ngd} \right) \cdot -\frac{1}{T_D} \\ 2 \frac{K_A}{T_A} K_{E1} \cdot D_{Qg} & \frac{2 K_A}{T_A} K_{E1} D_{Qg} & \frac{K_A}{T_A} K_{Ir} & \frac{K_A}{T_A} [-K_{E1} + (K_{Ir} \cdot T_D + K_{pr})] & -\frac{1}{T_A} & 0 & \frac{K_A}{T_A} K_{E1} D_{Qg} \frac{3}{2} I_{ngq} - \frac{K_A}{T_A} K_{E1} \\ 0 & 0 & 0 & 0 & \frac{1}{T_E} & -\frac{K_E}{T_E} & 0 \\ 0 & 0 & 0 & 0 & 0 & \frac{1}{T_{do}} & -\frac{1}{T_{do}} \\ 0 & 0 & 0 & 0 & 0 & 0 & \frac{-1}{T_{do}} \end{pmatrix} \begin{pmatrix} \frac{3}{T_{dcom}} I_{ngd} & -\frac{3}{T_{dcom}} V_{ngd} \\ \frac{3}{T_{df}} I_{ngd} & -\frac{3}{T_{df}} V_{ngd} \\ 0 & 0 \\ -\frac{1 \cdot 3}{T_D} D_{Qg} V_{ngq} & \frac{1 \cdot 3}{T_D} D_{Qg} V_{ngd} \\ -\frac{K_A}{T_A} K_{E1} D_{Qg} \frac{3}{2} V_{ngq} & \frac{K_A}{T_A} K_{E1} D_{Qg} \frac{3}{2} V_{ngd} \\ 0 & 0 \\ 0 & 0 \end{pmatrix} \begin{pmatrix} 0 & \frac{2}{T_{dcom}} \\ 0 & \frac{2}{T_{dcom}} \\ 0 & \frac{1}{T_{dcom}} \\ \frac{1}{T_D} & -\frac{1}{T_D} D_{Qg} \\ \frac{K_A}{T_A} K_{E1} & -\frac{K_A}{T_A} K_{E1} D_{Qg} \\ 0 & 0 \\ 0 & 0 \end{pmatrix}
 \end{aligned}$$

### 3.2.3.1 Dynamic Analysis of exciter system

To analyze the stability of the excitation system, a state space model is utilized, as shown in Figure 3-16. Without any changes in parameters, all eigenvalues are located on the left side, ensuring the stability of the excitation system. In order to assess the impact of communication delay and controller gains on the system, eigenvalues are derived from the state space model.

Figure 3-16(a) demonstrates that the eigenvalues shift towards the right side as the proportional

gain is increased. These results are confirmed through simulation, as shown in Figure 3-17.

Additionally, Figure 3-16(b) illustrates the impact of proportional gain on communication delay across three different values.

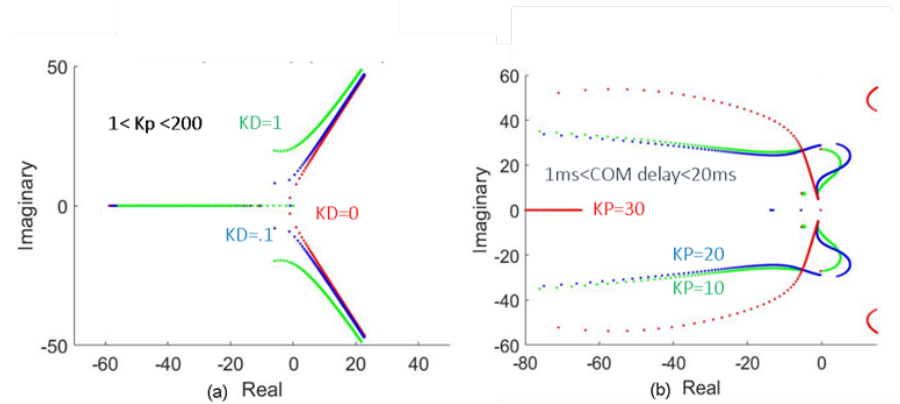


Figure 3-16 The impact of proportional gain on voltage stability

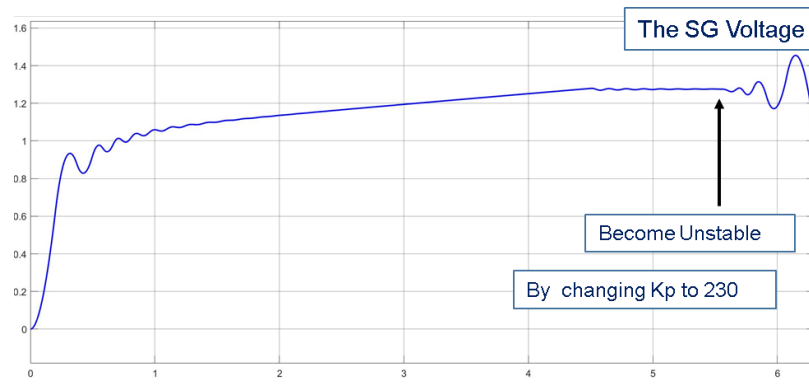


Figure 3-17 Simulation illustrates how the voltage of SG is affected by  $K_p$  during islanding mode

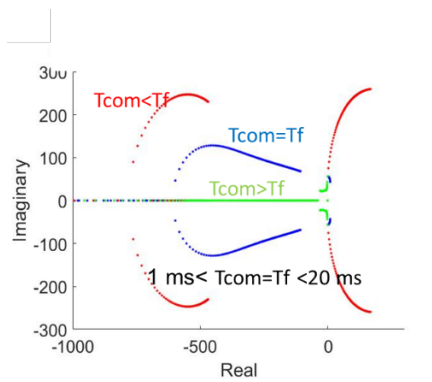


Figure 3-18 The impact of communication delay in three cases

### 3.3 State space modelling of grid forming Inverter (Islanding mode)

In the studied microgrid model, the energy storage system operates in voltage mode. Additionally, with regards to the reliability of the source, the inverter is defined as a master inverter. Figure 3-19 shows the schematic diagram of the grid forming inverter, which is connected to the microgrid (MG) through an LCL filter. During islanded mode, a power compensation is not a part of controller. This diagram is utilized to derive the state space model of the voltage mode inverter.

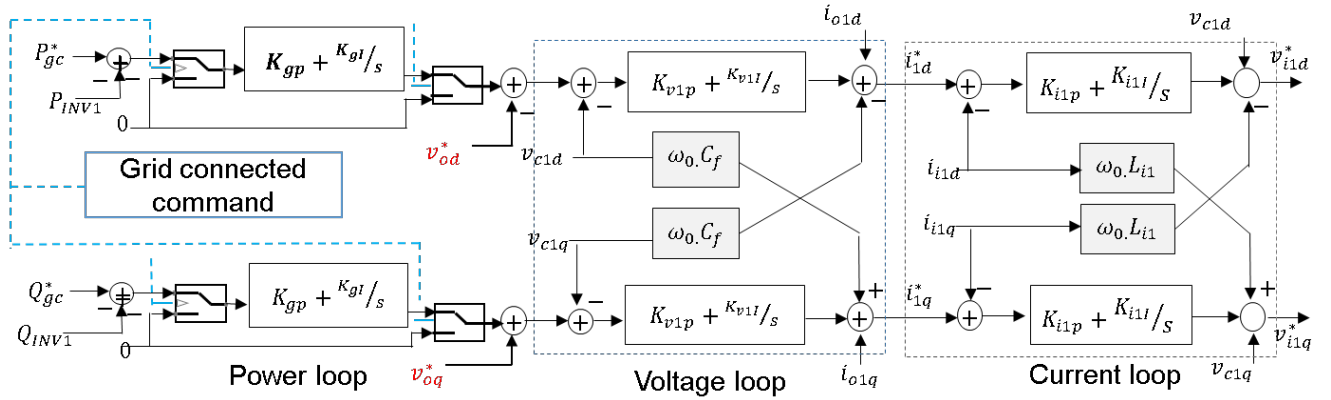


Figure 3-19 block diagram of grid forming inverter

The equations that describe the dynamics of the three-phase LCL filter can be expressed into d-q reference frame as follows. All equations are linearized around equilibrium.

$$\begin{aligned} \dot{i}_{i1d} &= \frac{1}{L_{i1}} \cdot v_{i1d} - \frac{1}{L_{i1}} \cdot v_{c1od} + \omega_0 \cdot i_{i1q} - \frac{R_{l1}}{L_{i1}} i_{i1d} + I_{i1q} \cdot \Delta\omega \\ \dot{i}_{i1q} &= \frac{1}{L_{i1}} \cdot v_{i1q} - \frac{1}{L_{i1}} \cdot v_{c1oq} - \omega_0 \cdot i_{i1d} - \frac{R_{l1}}{L_{i1}} i_{i1q} - I_{i1d} \cdot \Delta\omega \end{aligned} \quad (3-66)$$

Where,

$$\begin{aligned} & i_{i1dq} + I_{i1dq} \\ & i_{o1dq} + I_{o1dq} \\ & i v_{c1dq} + V_{c1dq} \\ & \Delta\omega + \omega_0 \end{aligned} \quad (3-67)$$

Figure 3-20 shows the LCL filter with passive damping resistor

$$\begin{aligned} v_{c1od} &= v_{c1d} + R_{c1} \cdot (i_{i1d} - i_{o1d}) = v_{c1d} + R_{c1} \cdot i_{i1d} - R_{c1} i_{o1d} \\ v_{c1oq} &= v_{c1q} + R_{c1} \cdot (i_{i1q} - i_{o1q}) = v_{c1q} + R_{c1} \cdot i_{i1q} - R_{c1} i_{o1q} \end{aligned} \quad (3-68)$$

Where  $v_{c1odq}$  is output voltage and  $R_{c1}$  is damping resistor shown in figure 3-20

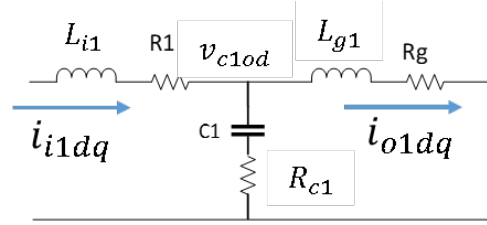


Figure 3-20 LCL filter

The system stability would be threatened, especially in high power systems where switching frequency and internal loss are relatively low. In this study, an active damping method equivalent to the implementation of resistors in series to the filter capacitors is suggested and it is shown that the bandwidth of the LCL filter with the proposed damping method can be extended further than that with a conventional capacitor current feedback type damping method.

$$\begin{aligned} v_{c1d} &= \frac{1}{C_1} \cdot i_{i1d} - \frac{1}{C_1} \cdot i_{o1d} + \omega_0 \cdot v_{c1q} + V_{c1q} \cdot \Delta\omega \\ v_{c1q} &= \frac{1}{C_1} \cdot i_{i1q} - \frac{1}{C_1} \cdot i_{o1q} - \omega_0 \cdot v_{c1d} - V_{c1d} \cdot \Delta\omega \end{aligned} \quad (3-69)$$

Where  $v_{c1dq}$  is capacitor voltage

$$\begin{aligned} i_{o1d} &= \frac{1}{L_{g1}} \cdot v_{c1od} - \frac{1}{L_{g1}} \cdot v_{g1d} + \omega_0 \cdot i_{o1q} - \frac{R_{g1}}{L_{g1}} i_{o1d} + I_{o1q} \cdot \Delta\omega \\ i_{o1q} &= \frac{1}{L_{g1}} \cdot v_{c1oq} - \frac{1}{L_{g1}} \cdot v_{g1q} - \omega_0 \cdot i_{o1d} - \frac{R_{g1}}{L_{g1}} i_{o1q} - I_{o1d} \cdot \Delta\omega \end{aligned} \quad (3-70)$$

The current references are derived from the voltage loop controller as follows.

$$\begin{aligned}\dot{\beta}_{1d} &= v_{c1d}^* - v_{c1od} = v_{O1d}^* - v_{c1d} - R_{c1} \cdot i_{i1d} + R_{c1} i_{o1d} \\ \dot{\beta}_{1q} &= v_{c1q}^* - v_{c1oq} = v_{O1q}^* - v_{c1q} - R_{c1} \cdot i_{i1q} + R_{c1} i_{o1q}\end{aligned}\quad (3-71)$$

Where,

$$\beta_{dq} = \int (v_{c1dq}^* - v_{c1odq}) dt \quad (3-72)$$

The following procedure can be used to derive reference values for the current loop.

$$\begin{aligned}i_{i1d}^* &= i_{o1d} + k_{v1P} \cdot \dot{\beta}_{1d} + k_{v1I} \cdot \beta_{1d} - C_1 \cdot \omega_0 \cdot v_{c1oq} - C_1 \cdot V_{c1q} \cdot \Delta\omega \\ i_{i1q}^* &= i_{o1q} + k_{v1P} \cdot \dot{\beta}_{1q} + k_{v1I} \cdot \beta_{1q} + C_1 \cdot \omega_0 \cdot v_{c1od} + C_1 \cdot V_{c1d} \cdot \Delta\omega\end{aligned}\quad (3-73)$$

The equation (3-74) for the inner loop controller can be defined.

$$\begin{aligned}\dot{\alpha}_{1d} &= i_{i1d}^* - i_{i1d} \\ \dot{\alpha}_{1q} &= i_{i1q}^* - i_{i1q}\end{aligned}\quad (3-74)$$

$$\begin{aligned}v_{i1d}^* &= v_{c1od} + k_{i1P} \cdot \dot{\alpha}_{1d} + k_{i1I} \cdot \alpha_{1d} - L_1 \cdot \omega_0 \cdot i_{i1q} - L_1 \cdot I_{1q} \cdot \Delta\omega \\ v_{i1q}^* &= v_{c1oq} + k_{i1P} \cdot \dot{\alpha}_{1q} + k_{i1I} \cdot \alpha_{1q} + L_1 \cdot \omega_0 \cdot i_{i1d} + L_1 \cdot I_{1d} \cdot \Delta\omega\end{aligned}\quad (3-75)$$

By replacing equation (3-73) into (3-74), equation (3-75) can be written.

$$\begin{aligned}\dot{\alpha}_{1d} &= i_{o1d} + k_{v1P} \cdot (v_{O1d}^* - v_{c1od}) + k_{v1I} \cdot \beta_{1d} - C_1 \cdot \omega_0 \cdot v_{c1oq} - V_{c1q} \Delta\omega \\ &\quad - i_{i1d} \\ \dot{\alpha}_{1q} &= i_{o1q} + k_{v1P} \cdot (v_{O1q}^* - v_{c1oq}) + k_{v1I} \cdot \beta_{1q} + C_1 \cdot \omega_0 \cdot v_{c1od} \\ &\quad + V_{c1d} \cdot \Delta\omega - i_{i1q}\end{aligned}\quad (3-76)$$

A PLL is required to measure the actual frequency of the system. A dq based PLL was chosen [34]. The PLL input is the q axis component of the voltage measured across the filter capacitor.

Therefore, the phase is locked such that  $v_{c1oq} = 0$ , shown in Figure 3-21.

$$\omega = K_{P-PLL} \cdot v_{c1oq} + K_{I-PLL} \cdot \int v_{c1oq} \cdot dt + \omega_0 \quad (3-77)$$

$$\dot{\gamma} = v_{c1oq} = v_{c1q} + R_{c1} \cdot i_{i1q} - R_{c1} i_{o1q} \quad (3-78)$$

$$\Delta\omega = K_{P-PLL} \cdot \dot{\gamma} + K_{I-PLL} \cdot \gamma \quad (3-79)$$

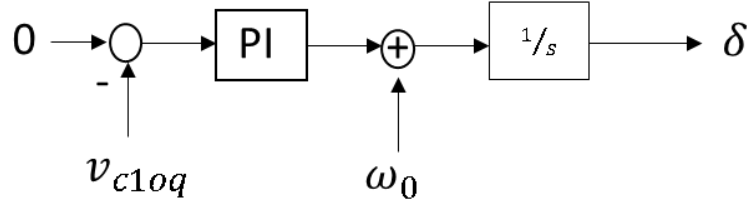


Figure 3-21 PLL control loop is used for measuring a frequency

Regarding equations (3-66) to (3-79), the complete state-space model of the grid-forming inverter, considering the LCL filter, can be written as follows.

- $\dot{\beta}_{1d} = v_{o1d}^* - v_{c1d} - R_{c1} \cdot i_{i1d} + R_{c1} i_{o1d}$
- $\dot{\beta}_{1q} = v_{o1q}^* - v_{c1q} - R_{c1} \cdot i_{i1q} + R_{c1} i_{o1q}$
- $\dot{\alpha}_{1d} = i_{o1d} + k_{v1P} v_{o1d}^* + k_{v1I} \cdot \beta_{1d} - k_{v1P} v_{c1d} - k_{v1P} R_{c1} \cdot i_{i1d} + k_{v1P} R_{c1} i_{o1d} - (C_1 \cdot \omega_0 + V_{c1q} K_{P-PLL}) v_{c1q} + Aq(-R_{c1} \cdot i_{i1q} + R_{c1} i_{o1q}) - V_{c1q} K_{I-PLL} \cdot \gamma - i_{i1d}$
- $\dot{\alpha}_{1q} = i_{o1q} + k_{v1P} \cdot v_{o1q}^* - k_{v1P} v_{c1q} - k_{v1P} R_{c1} \cdot i_{i1q} + k_{v1P} R_{c1} i_{o1q} + k_{v1I} \cdot \beta_{1q} + C_1 \cdot \omega_0 \cdot v_{c1d} + V_{c1d} \cdot K_{P-PLL} v_{c1q} + Ad \cdot (R_{c1} \cdot i_{i1d} - R_{c1} i_{o1d}) + V_{c1d} K_{I-PLL} \cdot \gamma - i_{i1q}$  (3-80)
- $\dot{i}_{i1d} = \frac{k_{i1P}}{L_{i1}} i_{o1d} + \frac{k_{i1P}}{L_{i1}} k_{v1P} R_{c1} i_{o1d} + \frac{k_{i1P}}{L_{i1}} k_{v1P} \cdot v_{o1d}^* - \frac{k_{i1P}}{L_{i1}} k_{v1P} v_{c1d} + \frac{k_{i1P}}{L_{i1}} k_{v1I} \cdot \beta_{1d} - Aid \cdot v_{c1q} - Aid \cdot (R_{c1} \cdot i_{i1q} - R_{c1} i_{o1q}) - \frac{k_{i1P}}{L_{i1}} C_1 \cdot V_{c1q} K_{I-PLL} \cdot \gamma - (\frac{k_{i1P} + R_{i1}}{L_{i1}}) i_{i1d} - \frac{k_{i1P}}{L_{i1}} k_{v1P} R_{c1} \cdot i_{i1d} + \frac{1}{L_{i1}} k_{i1I} \cdot \alpha_{1d}$

- $$\begin{aligned} \dot{i}_{i1q} = & \frac{k_{i1P}}{L_{i1}} i_{o1q} + \frac{k_{v1P} k_{i1P}}{L_{i1}} R_{c1} i_{o1q} - Aiq \cdot R_{c1} i_{o1q} + \\ & \frac{k_{i1P}}{L_{i1}} C_1 \cdot \omega_0 R_{c1} \cdot i_{i1d} \frac{k_{i1P}}{L_{i1}} C_1 \cdot \omega_0 R_{c1} i_{o1d} + \frac{k_{i1P}}{L_{i1}} C_1 \cdot \omega_0 \cdot v_{c1d} - \\ & \frac{k_{v1P} k_{i1P}}{L_{i1}} v_{c1q} + Aiq \cdot v_{c1q} - \frac{k_{v1P} k_{i1P}}{L_{i1}} R_{c1} \cdot i_{i1q} + Aiq R_{c1} \cdot i_{i1q} - \\ & \left( \frac{k_{i1P}}{L_{i1}} + \frac{R_{i1}}{L_{i1}} \right) i_{i1q} + \frac{k_{i1P} k_{v1I}}{L_{i1}} \cdot \beta_{1q} + \frac{1}{L_{i1}} k_{i1I} \cdot \alpha_{1q} + \\ & \frac{k_{i1P}}{L_{i1}} C_1 \cdot V_{c1d} K_{I-PLL} \cdot \gamma + \frac{k_{v1P} k_{i1P}}{L_{i1}} \cdot v_{O1q}^* \end{aligned}$$
- $$\begin{aligned} v_{c1d} = & \frac{1}{C_1} \cdot i_{i1d} - \frac{1}{C_1} \cdot i_{o1d} + (\omega_0 + V_{c1q} \cdot K_{P-PLL}) v_{c1q} + \\ & V_{c1q} \cdot K_{P-PLL} R_{c1} \cdot i_{i1q} - V_{c1q} \cdot K_{P-PLL} R_{c1} i_{o1q} + V_{c1q} K_{I-PLL} \cdot \gamma \end{aligned}$$
- $$\begin{aligned} v_{c1q} = & \frac{1}{C_1} \cdot i_{i1q} - \frac{1}{C_1} \cdot i_{o1q} - \omega_0 \cdot v_{c1d} - V_{c1d} \cdot K_{P-PLL} v_{c1q} - \\ & V_{c1d} \cdot K_{P-PLL} R_{c1} \cdot i_{i1q} + V_{c1d} \cdot K_{P-PLL} R_{c1} i_{o1q} - V_{c1d} K_{I-PLL} \cdot \gamma \end{aligned}$$
- $$\begin{aligned} \dot{i}_{o1d} = & \frac{1}{L_{g1}} \cdot v_{c1d} + \frac{1}{L_{g1}} R_{c1} \cdot i_{i1d} - \left( \frac{1}{L_{g1}} R_{c1} + \frac{R_{g1}}{L_{g1}} \right) i_{o1d} - \\ & \frac{1}{L_{g1}} \cdot v_{g1d} + (\omega_0 - I_{o1q} \cdot K_{P-PLL} R_{c1}) i_{o1q} + \\ & I_{o1q} \cdot K_{P-PLL} R_{c1} \cdot i_{i1q} + I_{o1q} K_{I-PLL} \cdot \gamma \end{aligned}$$
- $$\begin{aligned} \dot{i}_{o1q} = & \frac{1}{L_{g1}} \cdot v_{c1q} + \frac{1}{L_{g1}} R_{c1} \cdot i_{i1q} - I_{o1d} \cdot K_{P-PLL} R_{c1} \cdot i_{i1q} + \left( -\frac{R_{c1}}{L_{g1}} - \right. \\ & \left. \frac{R_{g1}}{L_{g1}} + I_{o1d} \cdot K_{P-PLL} R_{c1} \right) i_{o1q} - \frac{1}{L_{g1}} \cdot v_{g1q} - \omega_0 \cdot i_{o1d} - \\ & I_{o1d} K_{I-PLL} \cdot \gamma \end{aligned}$$
- $$\dot{\gamma} = v_{c1q} + R_{c1} \cdot i_{i1q} - R_{c1} i_{o1q}$$

$$\begin{array}{l}
\text{The Internal states} \\
\text{PI controller} \\
\text{The INV1} \\
\text{parameters}
\end{array}
\begin{bmatrix}
\beta_{1d} \\
\beta_{1q} \\
\alpha_{1d} \\
\alpha_{1q} \\
i_{i1d} \\
i_{i1q} \\
v_{c1d} \\
v_{c1q} \\
i_{o1d} \\
i_{o1q} \\
\gamma
\end{bmatrix}
= [A_{INV1}] \cdot
\begin{bmatrix}
\beta_{1d} \\
\beta_{1q} \\
\alpha_{1d} \\
\alpha_{1q} \\
i_{i1d} \\
i_{i1q} \\
v_{c1d} \\
v_{c1q} \\
i_{o1d} \\
i_{o1q} \\
\gamma
\end{bmatrix}
+ [B_{INV1}] \begin{bmatrix} v_{c1d}^* \\ v_{c1q}^* \end{bmatrix} + [B_{mg}] \begin{bmatrix} v_{g1d} \\ v_{g1q} \end{bmatrix}$$

Voltage Set point
The Load Voltage

$$Y_{INV1} = \begin{bmatrix}
0 & 0 & 0 & 0 & 1 & 0 & 0 & 0 & 0 & 0 & 0 \\
0 & 0 & 0 & 0 & 0 & 1 & 0 & 0 & 0 & 0 & 0 \\
0 & 0 & 0 & 0 & 0 & 0 & 1 & 0 & 0 & 0 & 0 \\
0 & 0 & 0 & 0 & 0 & 0 & 0 & 1 & 0 & 0 & 0 \\
0 & 0 & 0 & 0 & 0 & 0 & 0 & 0 & 1 & 0 & 0 \\
0 & 0 & 0 & 0 & 0 & 0 & 0 & 0 & 0 & 1 & 0 \\
0 & 0 & 0 & 0 & 0 & 0 & 0 & 0 & 0 & 0 & 1
\end{bmatrix} X_{INV1}$$

Figure 3-22 State Space model of Grid-Forming Inverter (Islanding Mode)

Figure 3-22 illustrates a state space model of a grid forming inverter, which takes two main inputs - the reference voltage and the common point voltage. The model includes several internal states that describe the inverter controllers and its parameters. Moreover, the matrix C represents the output of the inverter, which includes its voltage, current, and frequency. According to the model shown in Figure 3-22, state space matrixes are defined as follows.

$$A_{INV1} = \begin{bmatrix}
0 & 0 & 0 & 0 & -R_{c1} & 0 & -1 & 0 & R_{c1} & 0 & 0 \\
0 & 0 & 0 & 0 & 0 & -R_{c1} & 0 & -1 & 0 & R_{c1} & 0 \\
k_{v1P} & 0 & 0 & 0 & -1 - k_{v1P} R_{c1} & -Aq R_{c1} & -k_{v1P} & -Aq & 1 + k_{v1P} R_{c1} & Aq R_{c1} & -V_{c1q} K_{I-PLL} \\
0 & k_{v1I} & 0 & 0 & Ad. R_{c1} & -1 + k_{v1P} R_{c1} & +C_1 \cdot \omega & -k_{v1P} + V_{c1d} \cdot K_{P-PLL} & -Ad R_{c1} & 1 + k_{v1P} R_{c1} & V_{c1d} K_{I-PLL} \\
\frac{k_{i1P} \cdot k_{v1I}}{L_{i1}} & 0 & \frac{k_{i1I}}{L_{i1}} & 0 & AZ & -Ai. R_{c1} & -\frac{k_{v1P} \cdot k_{i1P}}{L_{i1}} & -Ai & \frac{k_{i1P}}{L_{i1}} + \frac{k_{i1P}}{L_{i1}} k_{v1P} R_{c1} & Ai R_{c1} & -\frac{k_{i1P}}{L_{i1}} C_1 \cdot V_{c1q} K_{I-PLL} \\
0 & \frac{k_{i1P} \cdot k_{v1I}}{L_{i1}} & 0 & \frac{k_{i1I}}{L_{i1}} & \frac{k_{i1P}}{L_{i1}} C_1 \cdot \omega_0 R_{c1} & AZ + Ai q R_{c1} & \frac{k_{i1P}}{L_{i1}} C_1 \cdot \omega_0 & -\frac{k_{v1P} \cdot k_{i1P}}{L_{i1}} + Ai q & \frac{k_{i1P}}{L_{i1}} C_1 \cdot \omega_0 R_{c1} & kq & \frac{k_{i1P}}{L_{i1}} C_1 \cdot V_{c1d} K_{I-PLL} \\
0 & 0 & 0 & 0 & \frac{1}{C_{i1}} & V_{c1q} \cdot K_{P-PLL} R_{c1} & 0 & \omega_0 + V_{c1q} \cdot K_{P-PLL} & -\frac{1}{C_{i1}} & -V_{c1q} \cdot K_{P-PLL} R_{c1} & V_{c1q} K_{I-PLL} \\
0 & 0 & 0 & 0 & 0 & \frac{1}{C_{i1}} - V_{c1d} \cdot K_{P-PLL} R_{c1} & -\omega_0 & -V_{c1d} \cdot K_{P-PLL} & 0 & -\frac{1}{C_{i1}} + V_{c1d} \cdot K_{P-PLL} R_{c1} & -V_{c1d} \cdot K_{I-PLL} \\
0 & 0 & 0 & 0 & \frac{R_{c1}}{L_{g1}} & I_{o1q} \cdot K_{P-PLL} R_{c1} & \frac{1}{L_{g1}} & I_{o1q} \cdot K_{P-PLL} & -\frac{(R_{g1} + R_{c1})}{L_{g1}} & \omega_0 - I_{o1q} \cdot K_{P-PLL} R_{c1} & I_{o1q} K_{I-PLL} \\
0 & 0 & 0 & 0 & 0 & \frac{R_{c1}}{L_{g1}} - I_{o1d} \cdot K_{P-PLL} R_{c1} & 0 & \frac{1}{L_{g1}} - I_{o1d} \cdot K_{P-PLL} & -\omega_0 & -\frac{(R_{g1} + R_{c1})}{L_{g1}} + I_{o1d} \cdot K_{P-PLL} R_{c1} & -I_{o1d} K_{I-PLL} \\
0 & 0 & 0 & 0 & 0 & R_{c1} & 0 & 1 & 0 & -R_{c1} & 0
\end{bmatrix}$$

Where,

$$\begin{aligned}
 Aq &= (C_1 \cdot \omega_0 + V_{c1q} K_{P-PLL}) \\
 Ad &= (C_1 \cdot \omega_0 + V_{c1d} \cdot K_{P-PLL}) \\
 Ai &= \left( \frac{k_{i1P}}{L_{i1}} C_1 \cdot \omega_0 + \frac{k_{i1P}}{L_{i1}} C_1 \cdot V_{c1q} \cdot K_{P-PLL} \right) \\
 A2 &= -\frac{k_{i1P} + R_{i1}}{L_{i1}} - \frac{k_{i1P}}{L_{i1}} k_{v1P} R_{c1} \\
 Aiq &= \frac{k_{i1P}}{L_{i1}} C_1 \cdot V_{c1d} \cdot K_{P-PLL} \\
 Kq &= \frac{k_{i1P}}{L_{i1}} + \frac{k_{v1P} k_{i1P}}{L_{i1}} R_{c1} - Aiq \cdot R_{c1}
 \end{aligned} \tag{3-81}$$

$$\begin{array}{cc}
 \mathbf{B}_{INV1} & \mathbf{B}_{mg} \\
 \left[ \begin{array}{cc}
 1 & 0 \\
 0 & 1 \\
 k_{v1P} & 0 \\
 0 & k_{v1P} \\
 \frac{k_{v1P} \cdot k_{i1P}}{L_{i1}} & 0 \\
 0 & \frac{k_{v1P} \cdot k_{i1P}}{L_{i1}} \\
 0 & 0 \\
 0 & 0 \\
 0 & 0 \\
 0 & 0 \\
 0 & 0
 \end{array} \right] & \left[ \begin{array}{cc}
 0 & 0 \\
 0 & 0 \\
 0 & 0 \\
 0 & 0 \\
 0 & 0 \\
 0 & 0 \\
 0 & 0 \\
 0 & 0 \\
 \frac{1}{L_{g1}} & 0 \\
 0 & -\frac{1}{L_{g1}} \\
 0 & 0
 \end{array} \right]
 \end{array}$$

### 3.3.1 The effect of load to the dynamic model of the master inverter

To provide more detail on the load voltage input shown in Figure 3-22, the Figure 3-23 illustrates the common points between the master inverter, SG, slave inverter, and RL load.

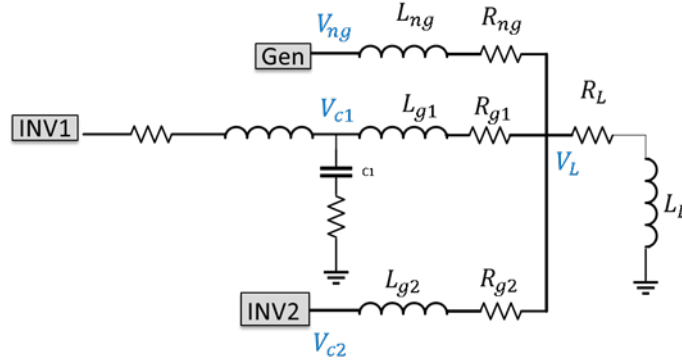


Figure 3-23 MG common connection circuit

With respect to Figure 3-23, an equation can be written for each unit and load, as follows

$$L_{ng} \frac{di_{ngd}}{dt} = v_{ngd} - v_{Ld} - R_{ng}i_{ng} + L_{ng}\omega_0 i_{ngq} \quad (3-82)$$

$$L_{g1} \frac{di_{o1d}}{dt} = v_{c1d} - v_{Ld} - R_{g1}i_{o1} + L_{g1}\omega_0 \cdot i_{o1q} \quad (3-83)$$

$$L_{g2} \frac{di_{o2d}}{dt} = v_{c2d} - v_{Ld} - R_{g2}i_{o2} + L_{g2}\omega_0 \cdot i_{o2q} \quad (3-84)$$

From load side equation (3-84) can be expressed as follows.

$$v_L = R_L(i_{ng} + i_{o1} + i_{o2}) + L_L \frac{d(i_{ng} + i_{o1} + i_{o2})}{dt} - L_L\omega_0(i_{ngq} + i_{o1q} + i_{o2q}) \quad (3-85)$$

Where  $i_{ng}$ ,  $i_{o1}$ ,  $i_{o2}$  are currents belong to SG, the master inviter and the slave inviter.

By replacing equations (3-81) to (3-83) into equation (3-84), the value of common voltage can be explained as follows.

$$\begin{aligned}
L_K v_{Ld} = & (R_L - \frac{L_L}{L_{ng}} R_{ng}) i_{ngd} + \frac{L_L}{L_{ng}} v_{ngd} + (R_L - \frac{L_L}{L_{g1}} R_{g1}) \cdot i_{o1d} + \frac{L_L}{L_{g1}} v_{c1d} \\
& + (R_L - \frac{L_L}{L_{g2}} R_{g2}) \cdot i_{o2d} + \frac{L_L}{L_{g2}} v_{c2d}
\end{aligned} \tag{3-86}$$

$$\begin{aligned}
L_K v_{Lq} = & (R_L - \frac{L_L}{L_{ng}} R_{ng}) i_{ngq} + \frac{L_L}{L_{ng}} v_{ngq} + (R_L - \frac{L_L}{L_{g1}} R_{g1}) \cdot i_{o1q} + \frac{L_L}{L_{g1}} v_{c1q} + (R_L \\
& - \frac{L_L}{L_{g2}} R_{g2}) \cdot i_{o2q} + \frac{L_L}{L_{g2}} v_{c2q}
\end{aligned} \tag{3-87}$$

$$L_K = 1 + \frac{L_L}{L_{ng}} + \frac{L_L}{L_{g1}} + \frac{L_L}{L_{g2}} \tag{3-88}$$

### 3.3.2 Dynamic Analysis of Grid Forming inverter

In order to assess the stability of the master inverter, a state space model is employed, as depicted in Figure 3-22. With no modifications to the parameters, all eigenvalues are situated on the left-hand side, which guarantees the stability of the system. In order to assess the impact of system parameters and controller gains on the system, eigenvalues are derived from the state space model. For example, Figure 3-24 demonstrates that the eigenvalues shift towards the right side as the damping resistor is equal zero. These results are confirmed through simulation, as shown in Figure 3-26. Additionally, Figure 3-27 illustrates the impact of PLL proportional gain on voltage stability.

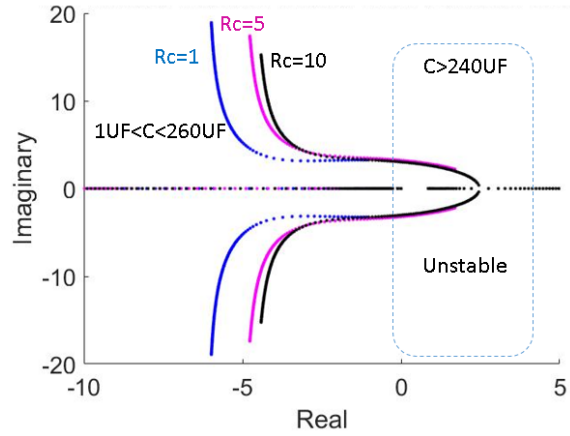


Figure 3-24 The eigenvalue plot with variable  $C$  and  $R_c$

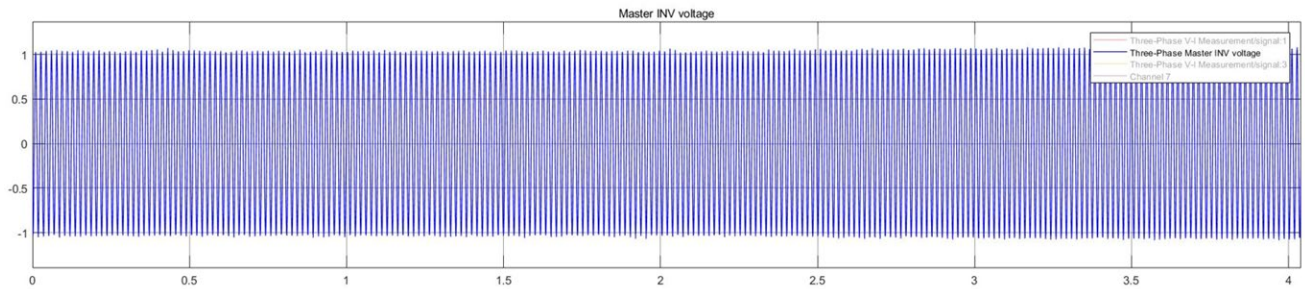


Figure 3-25 Voltage of the master Inverter when  $R_c=1$

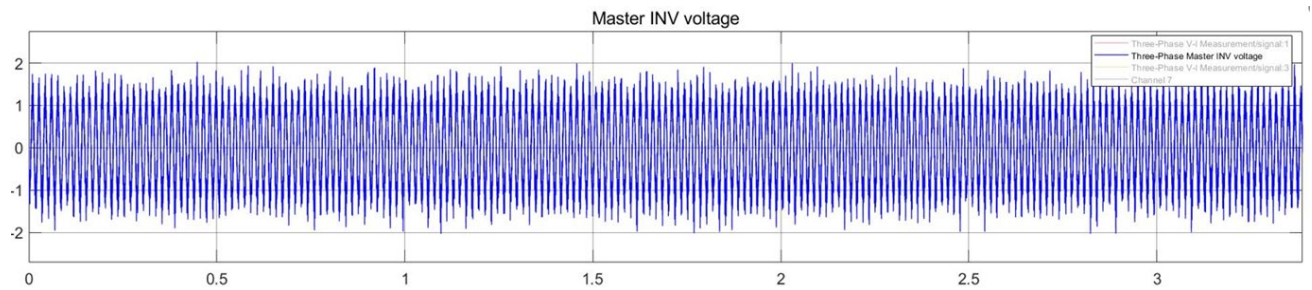


Figure 3-26 Voltage of the master Inverter when  $R_c=1$

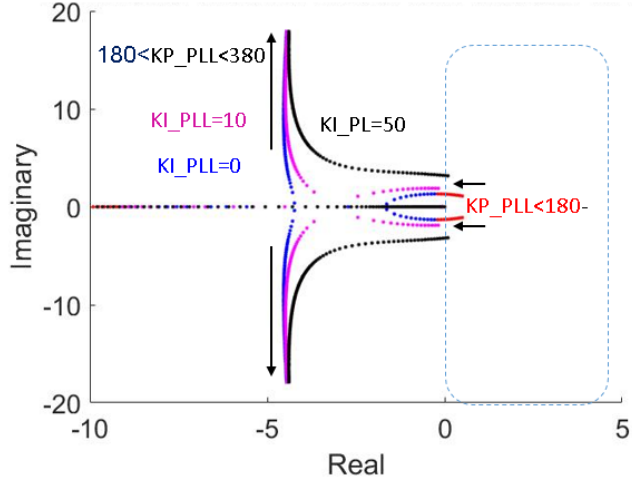


Figure 3-27 The eigenvalue plot with variable PLL gains

### 3.3.3 Dynamic model of the grid forming inverter in grid connected mode

The primary function of a grid-forming inverter is to establish and maintain the frequency and voltage of the electrical grid to which it is connected, as well as to synchronize its output with the grid. This is achieved through a sophisticated control system that ensures that the inverter's output remains stable and reliable under varying conditions, such as changes in load demand, fault conditions, and changes in the grid frequency or voltage. Power compensation is a crucial aspect of controller operation during grid-connected mode, as it enables the adjustment of reactive power to regulate voltage.

The state space equation for power compensation, as depicted in Figure 3-19, can be expressed as follows.

$$\begin{aligned}
 v_{od}^* &= v_{c1d}^* + k_{gP}(P_{gc}^* - P_{INV1}) + k_{gI} \cdot \alpha_{md} \\
 &= v_{c1d}^* + k_{gP}P_{gc}^* - \frac{3k_{gP}}{2}V_{gd} \cdot i_{od} + k_{gI} \cdot \alpha_{md}
 \end{aligned} \tag{3-89}$$

$$\begin{aligned}
 v_{oq}^* &= v_{c1q}^* + k_{gP}(Q_{gc}^* - Q_{INV1}) + k_{gI} \cdot \alpha_{mq} \\
 &= v_{c1q}^* + k_{gP}Q_{gc}^* - \frac{3k_{gP}}{2}V_{gq} \cdot i_{oq} + k_{gI} \cdot \alpha_{mq}
 \end{aligned} \tag{3-90}$$

Where,

$$\begin{aligned}\dot{\alpha}_{md} &= (P_{gc}^* - P_{INV1}) = P_{gc}^* - \frac{3}{2}V_{gd} \cdot i_{od} \\ \dot{\alpha}_{mq} &= (Q_{gc}^* - Q_{INV1}) = Q_{gc}^* - \frac{3}{2}V_{gd} \cdot i_{oq}\end{aligned}\quad (3-91)$$

The dynamic model of the system can be illustrated in Figure 3-28, as per equations (3-80) and (3-91).

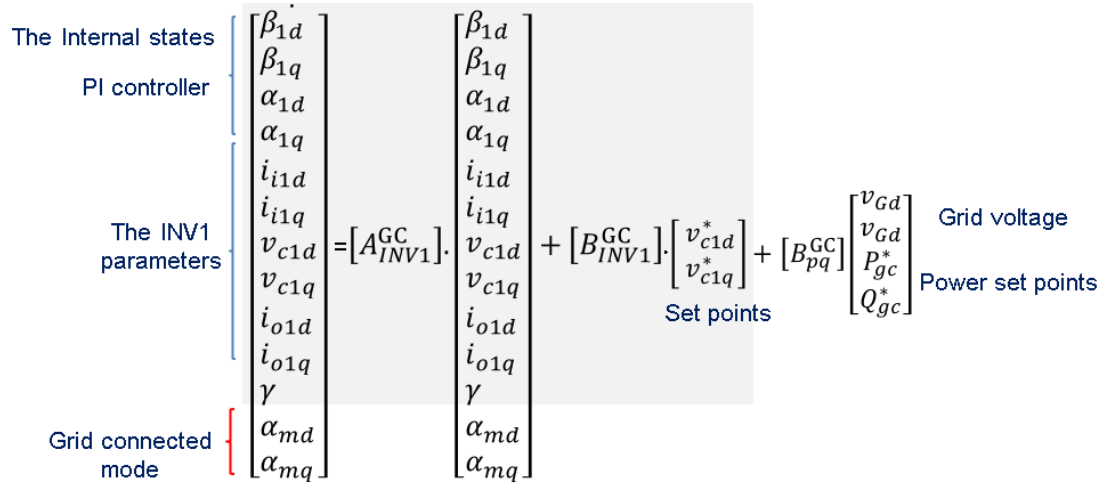


Figure 3-28 State Space Equations of Grid-Forming Inverter

During grid-connected mode, the voltage and frequency reference values are sourced from the Grid. State states matrixes are defining as follows.

$$B_{INV1}^{GC} = \begin{bmatrix} 1 & 0 \\ 0 & 1 \\ k_{v1P} & 0 \\ 0 & k_{v1P} \\ \frac{k_{v1P} \cdot k_{i1P}}{L_{i1}} & 0 \\ 0 & \frac{k_{v1P} \cdot k_{i1P}}{L_{i1}} \\ 0 & 0 \\ 0 & 0 \\ 0 & 0 \\ 0 & 0 \\ 0 & 0 \\ 0 & 0 \\ 0 & 0 \end{bmatrix} \quad B_{pq}^{GC} = \begin{bmatrix} 0 & 0 & k_{gP} & 0 \\ 0 & 0 & 0 & k_{gP} \\ 0 & 0 & k_{gP} k_{v1P} & 0 \\ 0 & 0 & 0 & k_{gP} k_{v1P} \\ 0 & 0 & \frac{k_{gP} k_{v1P} \cdot k_{i1P}}{L_{i1}} & 0 \\ 0 & 0 & 0 & \frac{k_{gP} k_{v1P} \cdot k_{i1P}}{L_{i1}} \\ 0 & 0 & 0 & 0 \\ 0 & 0 & 0 & 0 \\ -\frac{1}{L_{g1}} & 0 & 0 & 0 \\ 0 & -\frac{1}{L_{g1}} & 0 & 0 \\ 0 & 0 & 0 & 0 \\ 0 & 0 & 1 & 0 \\ 0 & 0 & 0 & 1 \end{bmatrix}$$

The matrix  $B_{pq}^{GC}$  is annotated with a blue circle and an arrow pointing to it from the text "From power compensator".

# AGC INV1

0	0	0	0	$-\frac{3k_{gp}}{2}$	0	-1	0	0	0	0	$k_{gf}$	0
0	0	0	0	0	$-\frac{3k_{gp}}{2}$	0	-1	0	0	0	0	$k_{gf}$
$k_{v1P}$	0	0	0	$\frac{3k_{v1P}k_{gp}}{2}$	0	$-k_{v1P}$	$-C_{11}\omega_0 - V_{c1q}\cdot K_{P-PLL}$	1	0	$-V_{c1q}K_{I-PLL}$	$k_{v1P}k_{gf}$	0
0	$k_{v1I}$	0	0	0	$\frac{3k_{v1P}k_{gp}}{2}$	$+C_{11}\omega$	$-k_{v1P} + V_{c1d}\cdot K_{P-PLL}$	0	1	$V_{c1d}K_{I-PLL}$	0	$k_{v1P}k_{gf}$
$\frac{k_{11P}\cdot k_{v1I}}{L_{11}}$	0	$\frac{k_{11I}}{L_{11}}$	0	$\frac{k_{v1P}\cdot k_{11P}}{L_{11}}(\frac{3k_{gp}}{2}V_{gd})$	$\frac{k_{11P}+R_{11}}{L_{11}}$	0	$-\frac{k_{v1P}\cdot C_{11}\omega}{L_{11}} - \frac{k_{11P}\cdot C_{11}\omega}{L_{11}} + (I_{11q}\cdot -V_{c1q})K_{P-PLL}$	$\frac{k_{11P}}{L_{11}}$	0	$+ (I_{11q}\cdot -V_{c1q})\cdot K_{I-PLL}$	$\frac{k_{gf}\cdot k_{v1P}\cdot k_{11P}}{L_{11}}$	0
0	$\frac{k_{11P}\cdot k_{v1I}}{L_{11}}$	0	$\frac{k_{11I}}{L_{11}}$	0	$\frac{k_{v1P}\cdot k_{11P}}{L_{11}}(\frac{3k_{gp}}{2}V_{gd})$	$\frac{k_{11P}+R_{11}}{L_{11}}$	$\frac{k_{11P}\cdot C_{11}\omega}{L_{11}} - \frac{k_{v1P}\cdot k_{11P}}{L_{11}} - (I_{11d}\cdot -V_{c1d})K_{P-PLL}$	0	$\frac{k_{11P}}{L_{11}}$	$- (I_{11d}\cdot -V_{c1d})\cdot K_{I-PLL}$	0	$\frac{k_{gf}\cdot k_{v1P}\cdot k_{11P}}{L_{11}}$
0	0	0	0	$\frac{1}{C_{11}}$	0	0	$\omega_0 + V_{c1q}\cdot K_{P-PLL}$	$-\frac{1}{C_{11}}$	0	$V_{c1q}\cdot K_{I-PLL}$	0	0
0	0	0	0	0	$\frac{1}{C_{11}}$	0	$-V_{c1d}\cdot K_{P-PLL}$	0	$-\frac{1}{C_{11}}$	$-V_{c1d}\cdot K_{I-PLL}$	0	0
0	0	0	0	0	0	$\frac{1}{L_{g1}}$	$I_{o1q}\cdot K_{P-PLL}$	$-\frac{R_{g1}}{L_{g1}}$	$\omega_0$	$I_{o1q}\cdot K_{I-PLL}$	0	0
0	0	0	0	0	0	0	$\frac{1}{L_{g1}} - I_{o1d}\cdot K_{P-PLL}$	$-\omega_0$	$-\frac{R_{g1}}{L_{g1}}$	$-I_{o1d}\cdot K_{I-PLL}$	0	0
0	0	0	0	0	0	0	0	1	0	0	0	0
0	0	0	0	$-\frac{3}{2}V_{gd}$	0	0	0	0	0	0	0	0
0	0	0	0	0	$-\frac{3}{2}V_{gd}$	0	0	0	0	0	0	0

### 3.4 Dynamic model of grid following inverter (Slave inverter)

The slave inverter has primarily been utilized in renewable energy applications, particularly in conjunction with solar PV, in the proposed MG system. All blocks of the system are shown in Figure 3-29, and includes current loop control, power loop control, and communication delay. By using Figure 3-30, the dynamics of the inverter LCL filter (resister damping is included) are represented by the following equations [35] . The state space equations are expressed based on small perturbation.

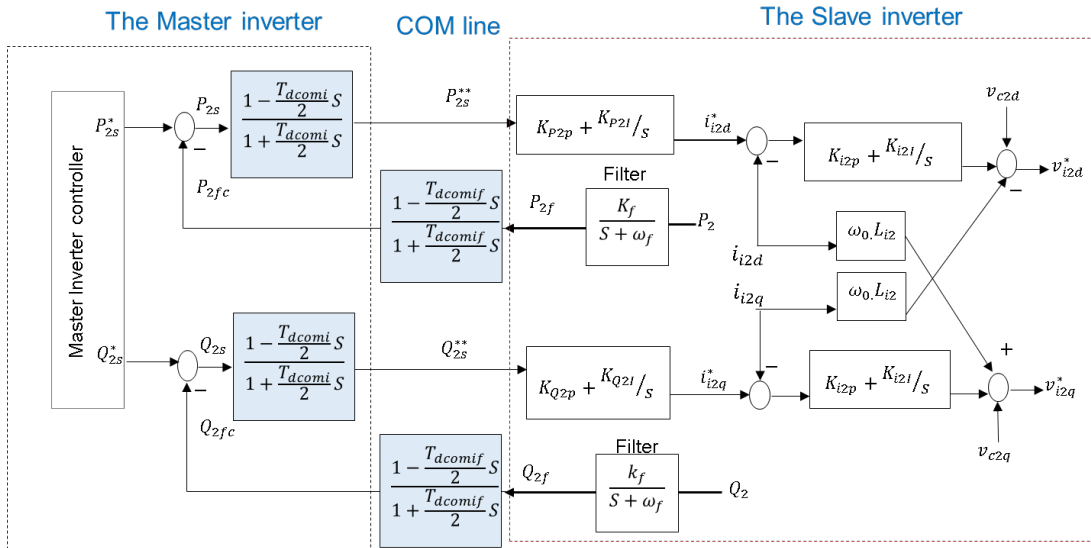


Figure 3-29 Block diagram of the slave inverter

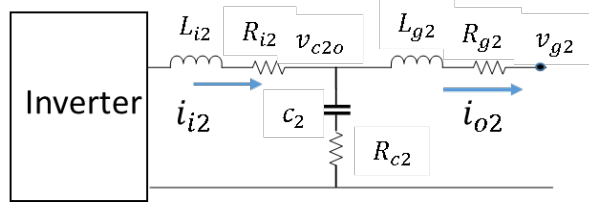


Figure 3-30 The grid forming inviter with LCL filter

$$\begin{aligned} \dot{i}_{i2d} &= \frac{1}{L_{i2}} \cdot v_{i2d} - \frac{1}{L_{i2}} \cdot v_{c2o} + \omega_0 \cdot i_{i2q} - \frac{R_{i2}}{L_{i2}} i_{i2d} + I_{i2q} \cdot \Delta\omega \\ \dot{i}_{i2q} &= \frac{1}{L_{i2}} \cdot v_{i2q} - \frac{1}{L_{i2}} \cdot v_{c2o} - \omega_0 \cdot i_{i2d} - \frac{R_{i2}}{L_{i2}} i_{i2q} - I_{i2d} \cdot \Delta\omega \end{aligned} \quad (3-92)$$

$$\begin{aligned} \dot{v}_{c2d} &= \frac{1}{C_2} \cdot i_{i2d} - \frac{1}{C_2} \cdot i_{o2d} + \omega_0 \cdot v_{c2q} + V_{c2q} \cdot \Delta\omega \\ \dot{v}_{c2q} &= \frac{1}{C_2} \cdot i_{i2q} - \frac{1}{C_2} \cdot i_{o2q} - \omega_0 \cdot v_{c2d} - V_{c2d} \cdot \Delta\omega \end{aligned} \quad (3-93)$$

$$\begin{aligned} \dot{i}_{o2d} &= \frac{1}{L_{g2}} \cdot v_{c2o} - \frac{1}{L_{g2}} \cdot v_{g2d} + \omega_0 \cdot i_{o2q} - \frac{R_{g2}}{L_{g2}} i_{o2d} + I_{o2q} \cdot \Delta\omega \\ \dot{i}_{o2q} &= \frac{1}{L_{g2}} \cdot v_{c2o} - \frac{1}{L_{g2}} \cdot v_{g2q} - \omega_0 \cdot i_{o2d} - \frac{R_{g2}}{L_{g2}} i_{o2q} - I_{o2d} \cdot \Delta\omega \end{aligned} \quad (3-94)$$

Where,

$$\begin{aligned} v_{cod} &= v_{c2d} + R_{c2} \cdot (i_{i2d} - i_{o2d}) \\ v_{coq} &= v_{c2q} + R_{c2} \cdot (i_{i2q} - i_{o2q}) \end{aligned} \quad (3-95)$$

The equations describing the dynamics of a delay transfer function in the d-q reference frame can be expressed as follows.

$$P_{2s}^{**} = \frac{1 - \frac{T_{dcomi} S}{2}}{1 + \frac{T_{dcomi} S}{2}} P_{2s}, \quad X_{sd1} = \frac{1}{1 + \frac{T_{dcomi} S}{2}} P_{2s} \quad (3-96)$$

$$P_{2s}^{**} = \left(1 - \frac{T_{dcomi} S}{2}\right) \cdot x_{sd1}, \quad P_{2s}^{**} = 2 \cdot x_{sd1} - P_{2s} \quad (3-97)$$

$$Q_{2s}^{**} = \frac{1 - \frac{T_{dcomi} S}{2}}{1 + \frac{T_{dcomi} S}{2}} Q_{2s}, \quad X_{sq1} = \frac{1}{1 + \frac{T_{dcomi} S}{2}} Q_{2s} \quad (3-98)$$

$$Q_{2s}^{**} = \left(1 - \frac{T_{dcomi} S}{2}\right) \cdot x_{sq1}, \quad Q_{2s}^{**} = 2 \cdot x_{sq1} - Q_{2s} \quad (3-99)$$

Where  $P_{2s}^{**}$  and  $Q_{2s}^{**}$  are power reference values are coming from the master controller,  $x_{sd1}$  and  $x_{sq1}$  are internal states to model the delay transfer function,  $P_{2s}$  and  $Q_{2s}$  are error values and  $T_{dcomi}$  in COM delay in forward path.

By utilizing equations (3-97) and (3-99), state space equations can be driven as follows.

$$\begin{aligned} \dot{x}_{sd1} &= -\frac{2}{T_{dcomi}} \cdot x_{sd1} + \frac{2}{T_{dcomi}} P_{2s} \\ \dot{x}_{sq1} &= -\frac{2}{T_{dcomi}} \cdot x_{sq1} + \frac{2}{T_{dcomi}} Q_{2s} \end{aligned} \quad (3-100)$$

And error values for active and reactive power is expressed in equation (3-101)

$$\begin{aligned} P_{2s} &= P_{2s}^* - P_{2fc} \\ Q_{2s} &= Q_{2s}^* - Q_{2fc} \end{aligned} \quad (3-101)$$

In the above equations,  $P_{2s}^*$  and  $Q_{2s}^*$  represent the desired power set values on the master side, while,  $P_{2fc}$  and  $Q_{2fc}$  are filtered feedback values coming through communication line.

By applying the same approach for the feedback path between the master controller and the slave inverter, the following equations can be driven.

$$P_{2fc} = \frac{1 - \frac{T_{dcomif_S}}{2}}{1 + \frac{T_{dcomif_S}}{2}} P_{2f} \quad , \quad X_{sd2} = \frac{1}{1 + \frac{T_{dcomif_S}}{2}} \cdot P_{2f} \quad (3-102)$$

$$P_{2fc} = 2 \cdot X_{sd2} - P_{2f} \quad (3-103)$$

The equations for reactive power can be expressed as follows.

$$Q_{2fc} = \frac{1 - \frac{T_{dcomif_S}}{2}}{1 + \frac{T_{dcomif_S}}{2}} Q_{2f} \quad , \quad X_{sq2} = \frac{1}{1 + \frac{T_{dcomif_S}}{2}} \cdot Q_{2f} \quad (3-104)$$

$$Q_{2fc} = 2 \cdot x_{sq2} - Q_{2f} \quad (3-105)$$

The measured power values are obtained by applying a low-pass filter,

$$\begin{aligned} P_{2f} \dot{\phantom{P}} &= -\omega_f \cdot P_{2f} + k_f \cdot P_2 \\ Q_{2f} \dot{\phantom{Q}} &= -\omega_f \cdot Q_{2f} + k_f \cdot Q_2 \end{aligned} \quad (3-106)$$

Equation (3-107) represents the output power values

$$\begin{aligned} P_2 &= \frac{3}{2} \cdot V_{2gd} \cdot i_{o2d} \\ Q_2 &= -\frac{3}{2} \cdot V_{2gd} \cdot i_{o2q} \end{aligned} \quad (3-107)$$

The current reference values are generated by the power PI controller using the following equations.

$$\begin{aligned} \dot{\beta}_{2d} &= P_{2s}^{**} = 2 \cdot x_{sd1} - P_{2s}^* + 2 \cdot x_{sd2} - P_{2f} \\ \dot{\beta}_{2q} &= Q_{2s}^{**} = 2 \cdot x_{sq1} - Q_{2s}^* + 2 \cdot x_{sq2} - Q_{2f} \end{aligned} \quad (3-108)$$

Where,

$$\begin{aligned} i_{i2d}^* &= k_{P2P} \cdot \dot{\beta}_{2d} + k_{P2I} \cdot \beta_{2d} \\ i_{i2q}^* &= k_{Q2P} \cdot \dot{\beta}_{2q} + k_{Q2I} \cdot \beta_{2q} \end{aligned} \quad (3-109)$$

The current PI controller (Inner loop) produces the voltage reference values for PWM using the following equations.

$$\begin{aligned} \dot{\alpha}_{2d} &= i_{i2d}^* - i_{i2d} \\ \dot{\alpha}_{2q} &= i_{i2q}^* - i_{i2q} \end{aligned} \quad (3-110)$$

$$\begin{aligned} v_{i2d}^* &= v_{c2d} + R_{c2} \cdot (i_{i2d} - i_{o2d}) + k_{i2P} \cdot \dot{\alpha}_{2d} + k_{i2I} \cdot \alpha_{2d} - L_2 \cdot \omega_0 \cdot i_{i2q} - L_2 I_{i2q} \cdot \Delta\omega \\ v_{i2q}^* &= v_{c2q} + R_{c2} \cdot (i_{i2q} - i_{o2q}) + k_{i2P} \cdot \dot{\alpha}_{2q} + k_{i2I} \cdot \alpha_{2q} + L_2 \cdot \omega_0 \cdot i_{i2d} + L_2 I_{i2d} \cdot \Delta\omega \end{aligned} \quad (3-111)$$

Equations (3-92) to (3-111) are used to extract the state space equation of the grid-following inverter.

- $\dot{\beta}_{2d} = 2 \cdot x_{sd1} - P_{2s}^* + 2 \cdot x_{sd2} - P_{2f}$
- $\dot{\beta}_{2q} = 2 \cdot x_{sq1} - Q_{2s}^* + 2 \cdot x_{sq2} - Q_{2f}$
- $\dot{\alpha}_{2d} = k_{P2P} 2 \cdot x_{ds1} - k_{P2P} P_{2s}^* + 2 \cdot k_{P2P} x_{sd2} - k_{P2P} P_{2f} + k_{P2I} \cdot \beta_{2d} - i_{i2d}$
- $\dot{\alpha}_{2q} = k_{Q2P} 2 \cdot x_{qs1} - k_{Q2P} Q_{2s}^* + 2 \cdot k_{Q2P} x_{sq2} - k_{Q2P} Q_{2f} + k_{Q2I} \cdot \beta_{2q} - i_{i2q}$
- $\dot{i}_{i2d} = -\frac{1}{L_{i2}} k_{i2P} i_{i2d} - \frac{(R_{i2})}{L_{i2}} i_{i2d} + 2 \frac{1}{L_{i2}} k_{i2P} \cdot x_{ds1} - \frac{1}{L_{i2}} k_{i2P} k_{P2P} P_{2s}^* +$   
 $2 \cdot \frac{1}{L_{i2}} k_{i2P} k_{P2P} x_{sd2} - \frac{1}{L_{i2}} k_{i2P} k_{P2P} P_{2f} + \frac{1}{L_{i2}} k_{i2P} k_{P2I} \beta_{2d} + \frac{1}{L_{i2}} k_{i2I} \cdot \alpha_{2d}$
- $\dot{i}_{i2q} = -\frac{1}{L_{i2}} k_{i2P} i_{i2q} - \frac{(R_{i2})}{L_{i2}} i_{i2q} + 2 \frac{1}{L_{i2}} k_{i2P} \cdot x_{qs1} - \frac{1}{L_{i2}} k_{i2P} k_{Q2P} Q_{2s}^* +$   
 $2 \cdot \frac{1}{L_{i2}} k_{i2P} k_{Q2P} x_{sq2} - \frac{1}{L_{i2}} k_{i2P} k_{Q2P} Q_{2f} + \frac{1}{L_{i2}} k_{i2P} k_{Q2I} \cdot \beta_{2q} + \frac{1}{L_{i2}} k_{i2I} \cdot \alpha_{2q}$
- $v_{c2d} = \frac{1}{C_2} \cdot i_{i2d} - \frac{1}{C_2} \cdot i_{o2d} + \omega_0 \cdot v_{c2q} + V_{c2q} \cdot \Delta\omega$
- $v_{c2q} = \frac{1}{C_2} \cdot i_{i2q} - \frac{1}{C_2} \cdot i_{o2q} - \omega_0 \cdot v_{c2d} - V_{c2d} \cdot \Delta\omega$  ( 3-112 )
- $\dot{i}_{o2d} = \frac{1}{L_{g2}} \cdot v_{c2d} + \frac{R_{c2}}{L_{g2}} \cdot i_{i2d} - \frac{1}{L_{g2}} \cdot v_{g2d} + \omega_0 \cdot i_{o2q} - \frac{(R_{c2} + R_{g2})}{L_{g2}} i_{o2d} + I_{o2q} \cdot \Delta\omega$
- $\dot{i}_{o2q} = \frac{1}{L_{g2}} \cdot v_{c2q} + \frac{R_{c2}}{L_{g2}} \cdot i_{i2q} - \frac{1}{L_{g2}} \cdot v_{g2q} - \omega_0 \cdot i_{o2d} - \frac{(R_{c2} + R_{g2})}{L_{g2}} i_{o2q} - I_{o2d} \cdot \Delta\omega$
- $P_{2f} = -\omega_f \cdot P_{2f} + \frac{3}{2} k_f \cdot V_{2gd} \cdot i_{o2d}$
- $Q_{2f} = -\omega_f \cdot Q_{2f} - \frac{3}{2} k_f \cdot V_{2gd} \cdot i_{o2q}$
- $\dot{x}_{sd1} = -\frac{2}{T_{dcomi}} \cdot x_{sd1} + \frac{2}{T_{dcomi}} P_{2s}^* - \frac{2}{T_{dcomi}} 2 \cdot x_{sd2} + \frac{2}{T_{dcomi}} P_{2f}$
- $\dot{x}_{sq1} = -\frac{2}{T_{dcomi}} \cdot x_{sq1} + \frac{2}{T_{dcomi}} (Q_{2s}^* - 2 \cdot x_{sq2} + Q_{2f})$
- $\dot{x}_{sd2} = -\frac{2}{T_{dcomif}} \cdot x_{sd2} + \frac{2}{T_{dcomif}} \cdot P_{2f}$
- $\dot{x}_{sq2} = -\frac{2}{T_{dcomif}} \cdot x_{sq2} + \frac{2}{T_{dcomif}} \cdot Q_{2f}$

The dynamic model of the grid-forming inverter, including all details, is illustrated in

Figure 3-31.

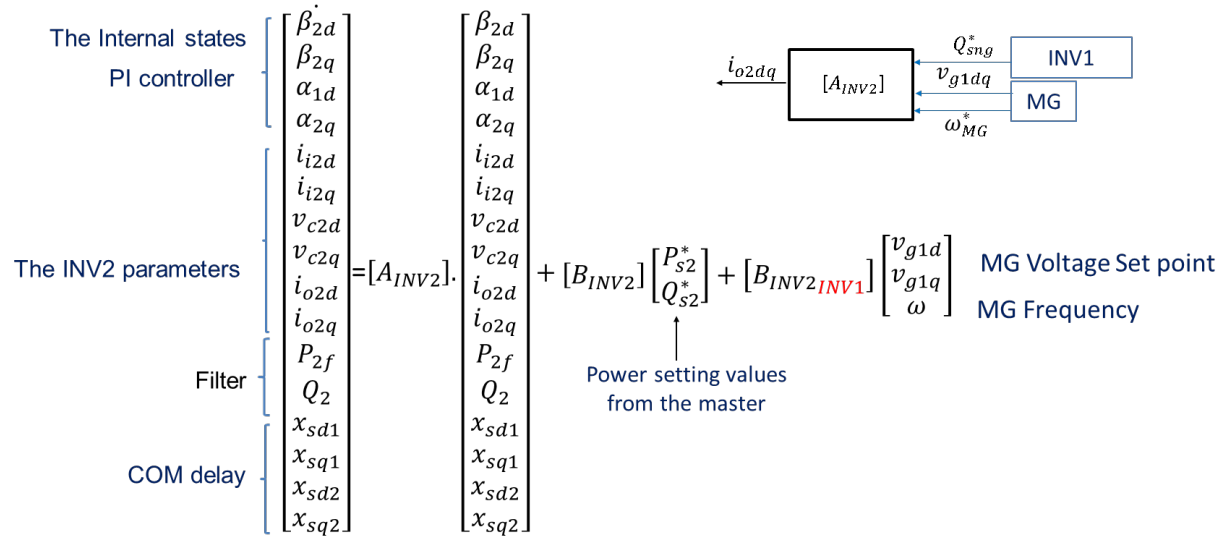


Figure 3-31 State space model of grid following inverter

The dynamic model consists of three groups of inputs. The voltage and frequency reference values come from the microgrid, and the power setting values are set by the master controller. The state matrices are defined as follows.

$$B_{INV2} = \begin{bmatrix} 1 & 0 \\ 0 & 1 \\ -k_{P2P} & 0 \\ 0 & -k_{Q2P} \\ -\frac{1}{L_{i2}} \cdot k_{i2P} \cdot k_{P2P} & 0 \\ 0 & -\frac{1}{L_{i2}} \cdot k_{i2P} \cdot k_{Q2P} \\ 0 & 0 \\ 0 & 0 \\ 0 & 0 \\ 0 & 0 \\ 0 & 0 \\ 0 & 0 \\ \frac{2}{T_{dcomi}} & 0 \\ 0 & \frac{2}{T_{dcomi}} \\ 0 & 0 \\ 0 & 0 \end{bmatrix}$$

$$B_{INV2\_INV1} = \begin{bmatrix} 0 & 0 & 0 \\ 0 & 0 & 0 \\ 0 & 0 & 0 \\ 0 & 0 & 0 \\ 0 & 0 & 0 \\ 0 & 0 & 0 \\ 0 & 0 & V_{c2q} \\ 0 & 0 & -V_{c2d} \\ -\frac{1}{L_{g1}} & 0 & I_{o2q} \\ 0 & -\frac{1}{L_{g1}} & -I_{o2d} \\ 0 & 0 & 0 \\ 0 & 0 & 0 \\ 0 & 0 & 0 \\ 0 & 0 & 0 \\ 0 & 0 & 0 \\ 0 & 0 & 0 \end{bmatrix}$$

### 3.4.1 Dynamic Analysis of Grid Following inverter

Employing a state space model illustrated in Figure 3-31, the stability of the slave inverter is evaluated. During normal operation, all eigenvalues are located on the left-hand side, indicating a stable system [36, 37]. In order to analyze the impact of system parameters and communication delay, eigenvalues are derived from the state space model. Three different communication delay scenarios were tested, including equal delay for both forward and backward lines, more delay on the command line, and more delay on the feedback line. The results in Figure 3-32 indicate that when the feedback line delay is less than the forward line delay, the system is more stable.

Another aspect analyzed in this study is the impact of filter bandwidth on stability in the presence of variable feedback delay. The results, as shown in Figure 3-33, indicate that decreasing the filter bandwidth increases the effect of delay.

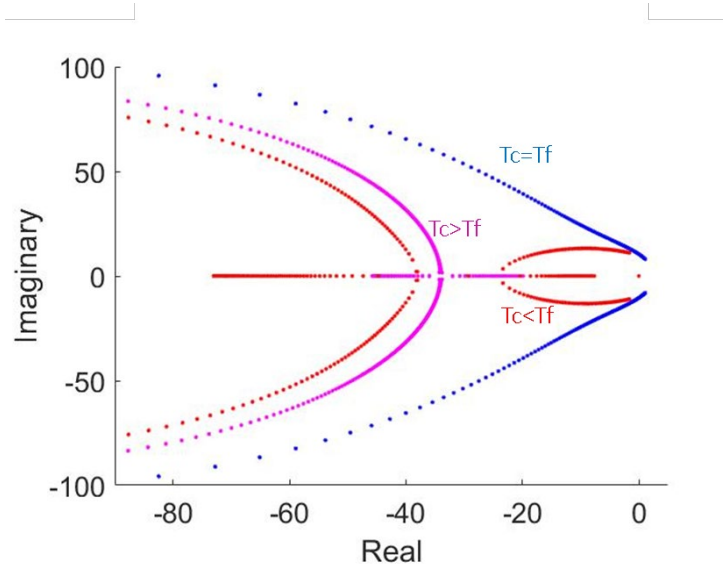


Figure 3-32 The impact of forward path COM delay compared to feedback path COM delay

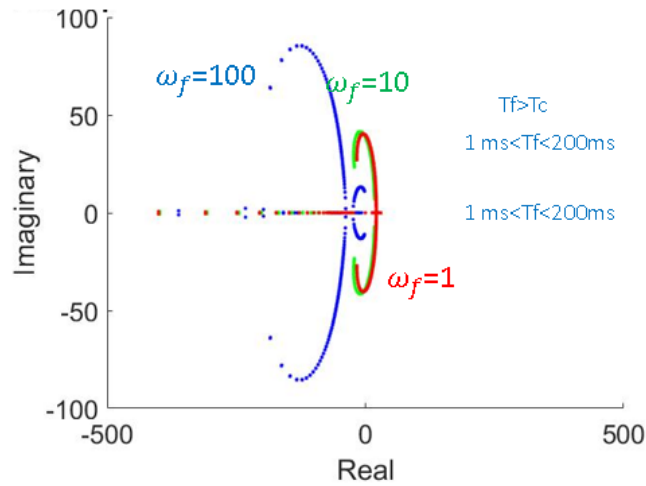


Figure 3-33 The influence of filter bandwidth on stability in the presence of variable feedback delay

The summary of the dynamic analysis of units in the presence of communication delay is presented in Table 3-1, providing an overview of research findings related to the impact of communication delays on the dynamic behavior of units. The table highlights how communication delays can result in stability issues in power systems, and it explores various methods for mitigating the impact of communication delays on system stability.

Table 3-1 Summary of the dynamic analysis of units in the presence of communication delay.

Units		Stability analysis is performed by varying the communication delay			Sensitivity of system parameters is analyzed by varying the communication delay.		Two different delays are considered for the sending and receiving side
Governor	Command delay Tc	1 msec	5 msec	Delay >5 msec	Delay<10 msec	Delay>10 msec	Tc=1 msec
	Feedback delay Tf	1 msec	5 msec	Delay >5 msec	Delay <10 msec	Delay >10 msec	1<TF<10
		Tc=Tf	Tc=Tf	Tc=Tf	Tc=Tf	Tc=Tf	Tc=Tf
	Droop gain	0.01	0.01	0.01	0.00025	0.00025	0.01
	System mode	Stable	Stable	Unstable	Stable	Unstable	Unstable
	Figure	3-11			3-11		3-11
Exciter	Command delay	1 msec	5 msec	Delay >5 msec	Delay<10 msec	Delay>10 msec	Tc=1 msec
	Feedback delay	1 msec	5 msec	Delay >5 msec	Delay <10 msec	Delay >10 msec	1<TF<10
		Tc=Tf	Tc=Tf	Tc=Tf	Tc=Tf	Tc=Tf	Tc<Tf
	Droop gain	0.01	0.01	0.01	0.0025	0.0025	0.01
	System mode	Stable	Stable	Unstable	Stable	Unstable	Unstable
	Figure	3-18			3-18		3-18
Inverter	Command delay	1 msec	3 msec	Delay >3 msec	1 msec	10 msec	Tc=1 msec
	Feedback delay	1 msec	3 msec	Delay >3 msec	1 msec	10 msec	1<TF<10
		Tc=Tf	Tc=Tf	Tc=Tf	Tc=Tf	Tc=Tf	Tc<Tf
	Power measuring Filter bandwidth	F	F	F	F -10F	Ff -10F	F
	System mode	Stable	Stable	Unstable	Stable	Unstable	Unstable
	Figure	3-32			3-32		3-32

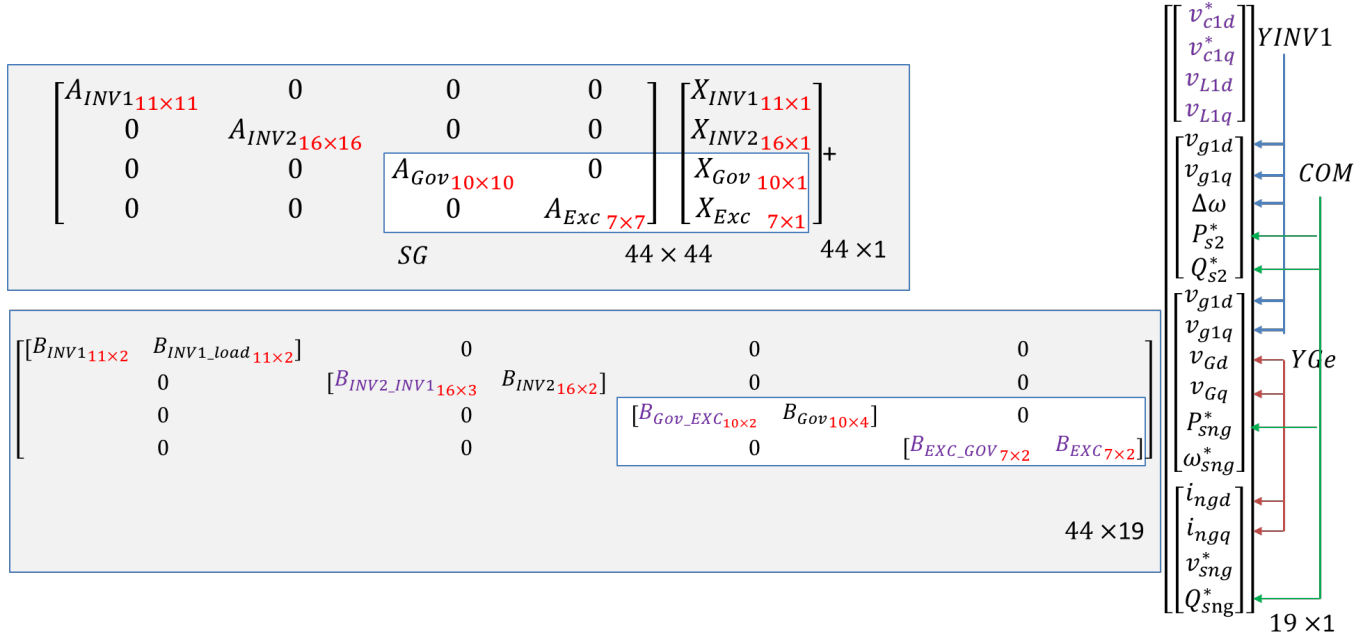


Figure 3-34 Dynamic model of proposed hybrid system

After deriving the dynamic equations for each unit, the hybrid system's state space model is represented in Figure 3-34, which encompasses all the system's states. From an input

perspective, all inputs are categorized based on the source of the signal. Ultimately, the system has 44 states and 19 inputs.

## Chapter 4 The Control Architecture of the proposed MG and Simulation Results

This chapter is dedicated to describing the main architecture of the master controller that coordinates other units with different time responses when we have sudden changes in the load side, such as pulse loads. As an interface between the DG and the power grid or local loads, a grid forming inverter is the most common topology which can operate either in grid-connected or islanded mode to provide a controlled and high-quality power exchange with the grid or local loads [38, 39, 40]. In islanded mode, it is necessary for the local loads to be supplied by the DG units, which operate as controlled voltage sources according to reference [41]. However, to ensure stable and efficient operation and prevent circulating currents between the DG units, appropriate control measures must be implemented for the MGs

### 4.1 The Master Controller

There are various methods available to regulate the voltage and frequency of a microgrid. Most studies indicate that voltage control is typically performed by synchronous generators, while other units are synchronized by the SG when the microgrid has generator and inverter-based power sources [42, 43].

The proposed system is responsible for adjusting the power setting values of the SG and the slave inverter (SINV) in response to the current situation of the master inverter (MINV). The master inverter supports transient demand from the load side by utilizing its fast response dynamics. Once the transient step is completed, the MINV reduces its own power preparation share and the master controller increases the contribution of other units.

Figure 1-4 illustrates all the blocks of the controller. The controller is located on the MINV side and communicates with the SG and SInv via a dedicated communication line.

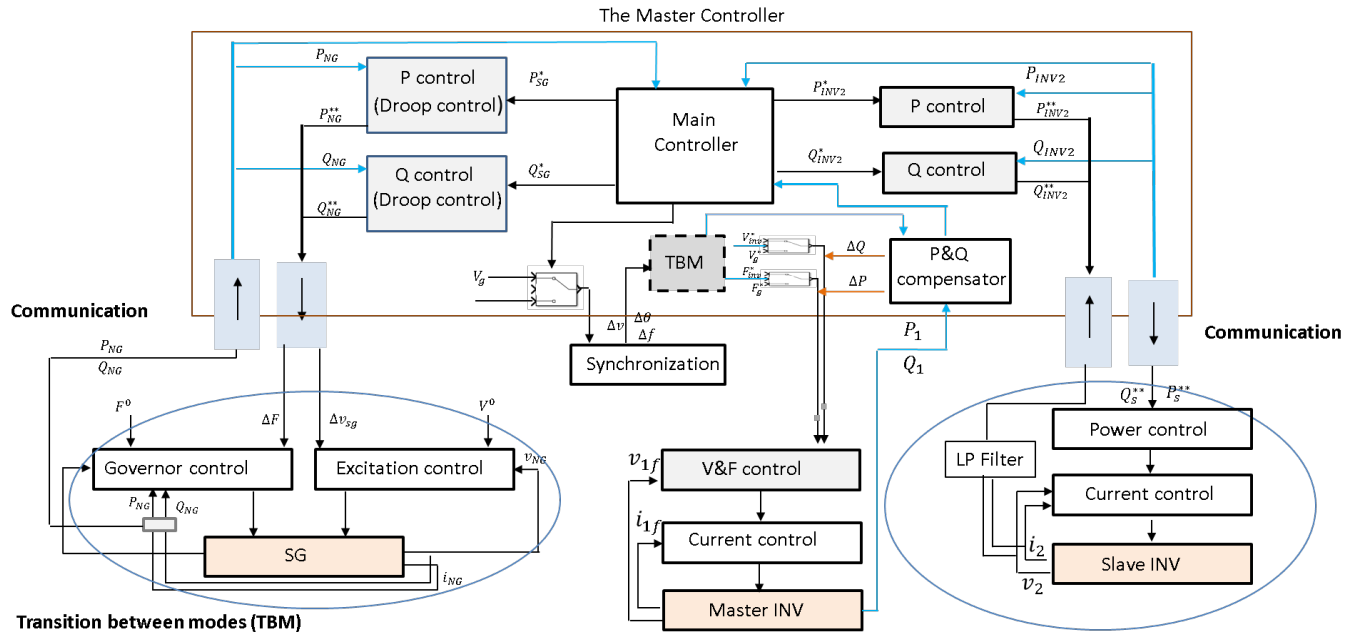


Figure 4-1 The main control architecture of MG under study

As discussed in the previous chapter, communication delay is an important concept to consider in this study. Previous research has already been conducted on mitigating the impact of communication delay [44], and the main focus of this study is to analyze its effects on the system's dynamics.

The controller comprises three main blocks. The first block is the local control, which is responsible for regulating the voltage and frequency of the MInv in islanded mode, as well as power compensation, voltage control, and frequency control in grid-connected mode (GM). The second block is the synchronization block, which synchronizes the MInv with the grid during grid connection and synchronizes with the SG in islanded mode (IsM). This block also controls the transition from one mode to the other. The last block is responsible for generating power reference values for SG and SInv.

The MG model introduced in the previous discussion is simulated, in Matlab Simulink and primary controllers are designed and simulated for each unit.

4.1.1 Simulation results of primary controllers

Each unit is equipped with its own primary controller, allowing it to operate independently and control its own output signals.

4.1.1.1 Synchronous generator

The SG (synchronous generator) is capable of independent operation for controlling both voltage and frequency. Voltage control is achieved through the use of a PI controller and reactive droop controller as an outer loop in the excitation system. Simulation results of the excitation system, as shown in Figure 4-2, demonstrate that by adjusting the voltage set point, the output signal can accurately track the command with minimal fluctuation.

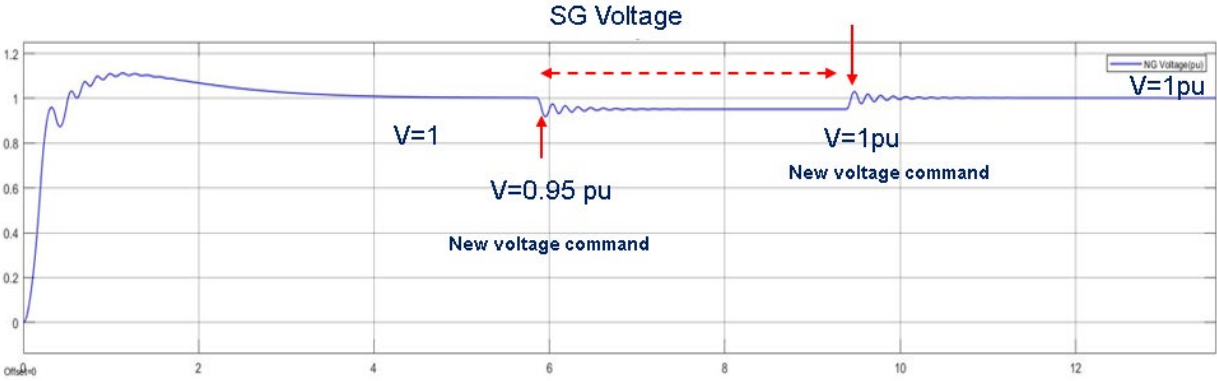


Figure 4-2 Step response of a closed-loop excitation system

Furthermore, the frequency of the SG is controlled by the Governor using a PID controller and active power droop control. Figure 4-3 illustrates how the frequency of the system is able to

accurately follow different commands.

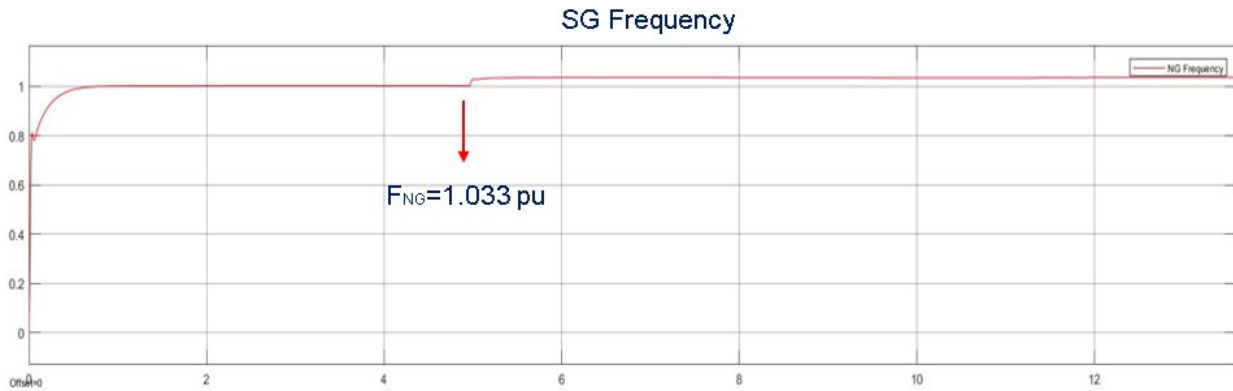


Figure 4-3 Step response of governor system

Proper power sharing among multiple DGs (distributed generators) is achieved through a control strategy known as droop control. Typically, both active power frequency ( $P-\omega$ ) and reactive power-voltage ( $Q-V$ ) droop control methods are used to regulate frequency and voltage by adjusting the droop gain. This droop control strategy enables the synchronous generator control to participate more effectively by increasing the droop gain, as shown in Figure 4-4. By adjusting the slope of the plot in Figure 4-4 while keeping reference values constant, the power sharing of the SG can be controlled. In this study, a different method was used for controlling power instead of changing droop gain.

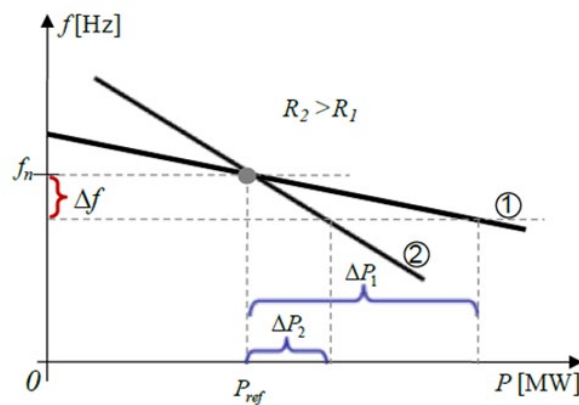


Figure 4-4 Droop control

The proposed system's methodology is presented in Figure 4-5, where the power output of SG is regulated using a master controller.

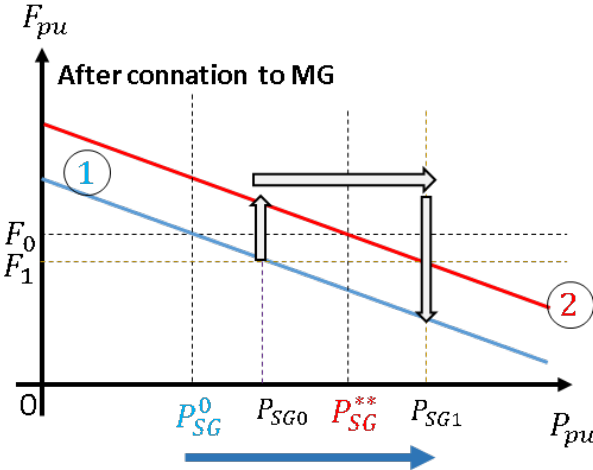


Figure 4-5 The output power is controlled by utilizing droop control

The simulation results, depicted in Figure 4-6, show that the proposed method successfully maintains a consistent frequency during active power changes.

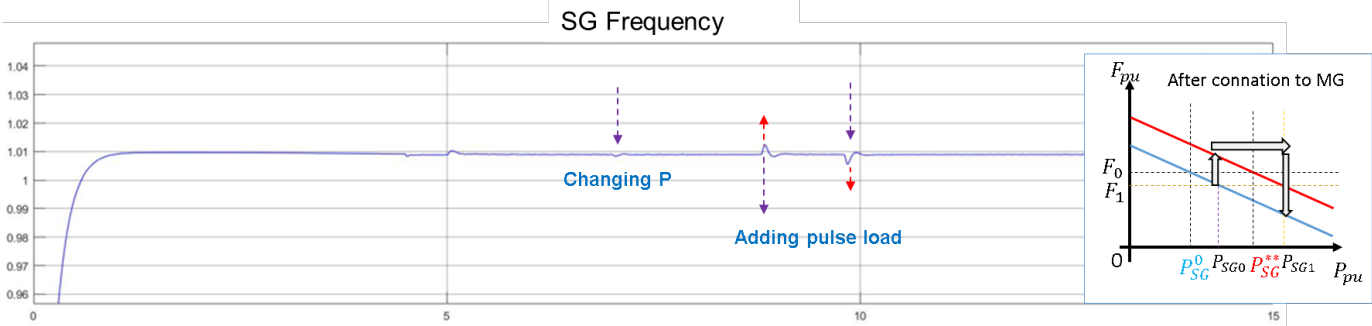


Figure 4-6 Power controlling in SG is achieved by maintaining a frequency

### 4.1.2 The Grid Forming inverter

The master inverter is equipped with a voltage regulator that generates a voltage reference for the microgrid during islanded mode. In addition, a power compensator is incorporated during grid-connected mode to adjust the reactive power while regulating the voltage for the grid. The voltage signal of the master inverter during islanded mode is depicted in Figure 4-7. The results demonstrate the successful operation of the controllers.

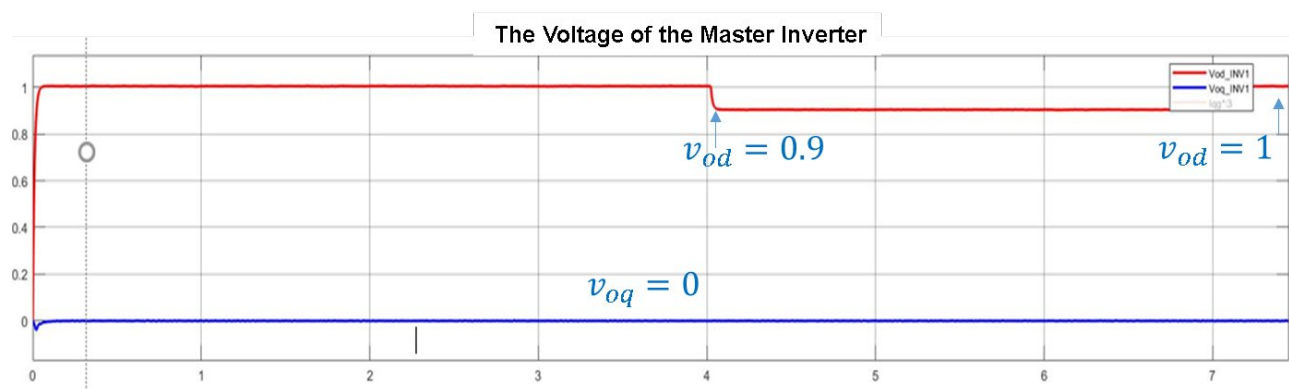


Figure 4-7 The step response of the master inverter voltage in dq frame

### 4.1.3 The Slave Inverter

The controllers of the slave generator are responsible for generating active and reactive power in accordance with the set points. The system was simulated with various command values for active and reactive power, and the results, as depicted in Figure 4-8, confirmed the effectiveness of the controller concept.

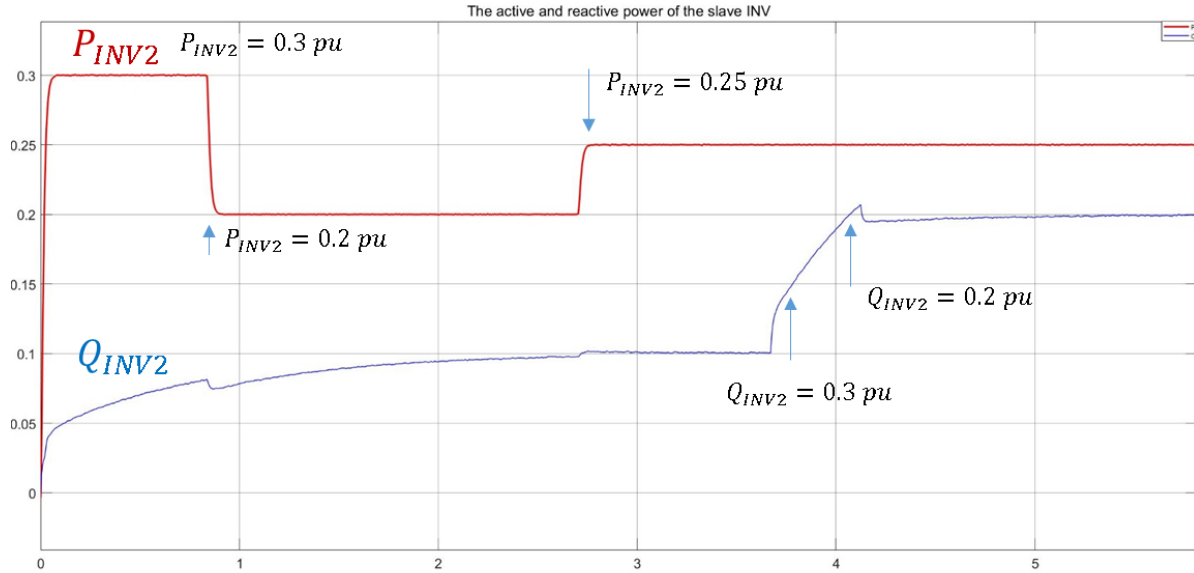


Figure 4-8 The Active and Reactive Power of the Slave INV

## 4.2 Simulation Results of the Proposed Microgrid with the Master Controller

Simulink, a dynamic simulation tool, was employed to simulate the entire system. Three different scenarios were designed to analyze the dynamic behavior of the system under different conditions. The simulation results were then analyzed to evaluate the performance of the proposed microgrid and the master controller. The simulation comprised three scenarios: transitioning from islanded mode (ISM) to grid-connected mode (GCM) with pulse load, operating in ISM with pulse load, and operating in ISM with communication delay in the presence of pulse load. All tasks of the master controller are depicted in Figure 4-9. As a result, for each scenario, the controller utilizes the corresponding unit to effectively manage the system. At the master controller level, several rules based on different cost functions can be defined to determine the power sharing coefficient for each unit. For instances, Machine learning techniques can also be utilized at this level to adjust the power sharing between sources. For the system under study, the primary objective is to minimize the contribution of energy storage in power generation. Therefore,  $K_{PSG}$  and  $K_{PINV}$

are calculated to support this goal. Table 4-1 provides the corresponding values for each source of the microgrid (MG) during simulation.

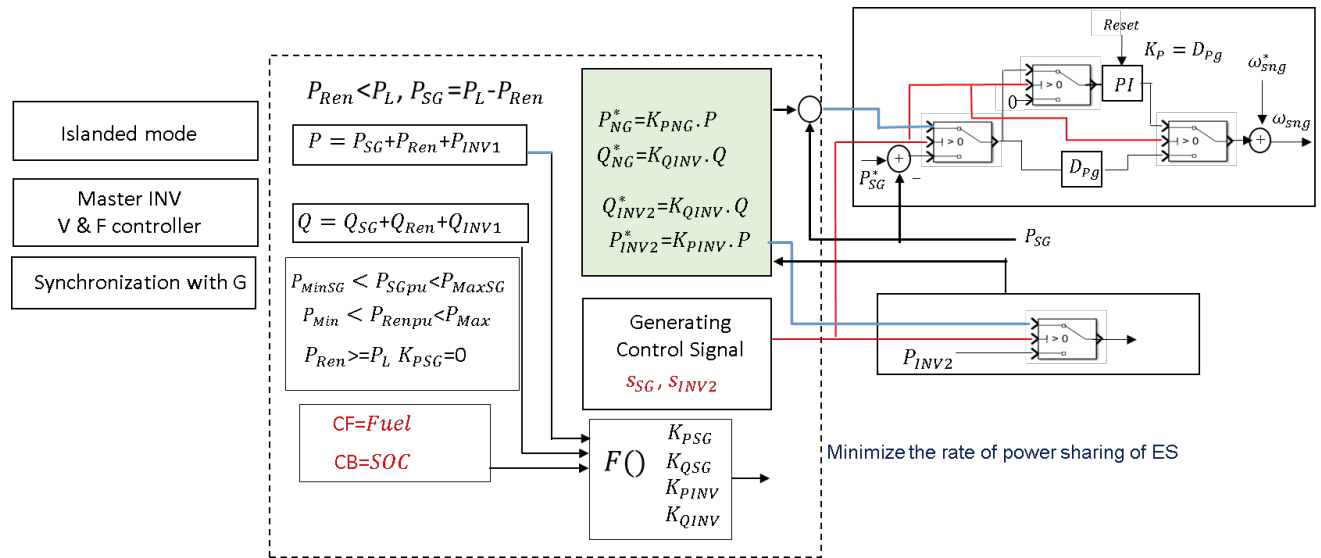


Figure 4-9 Block diagram of the master controller

Table 4-1 MG case study specification

DER	Rated Power
Synchronous Generator	200kW
Master Inverter	190 kW
Slave Inverter	190 kW

Case1: The model is operating in island mode, and in second 2, INV1 is going to be synchronized with the grid. Around second 5, the connection is established, and the system is operating in GCM. During GCM, the power changes due to the addition of a pulse load. At this moment, the grid-forming inverter is able to cover the transient response before having more contribution from the grid side. Around second 14, system is back to the ISM. The results show that the system is stable enough, and from a load perspective, there are no fluctuations during

different situations. Regarding UL 1741, the proposed system frequency is within the acceptable range, as demonstrated in Figure 4-11.

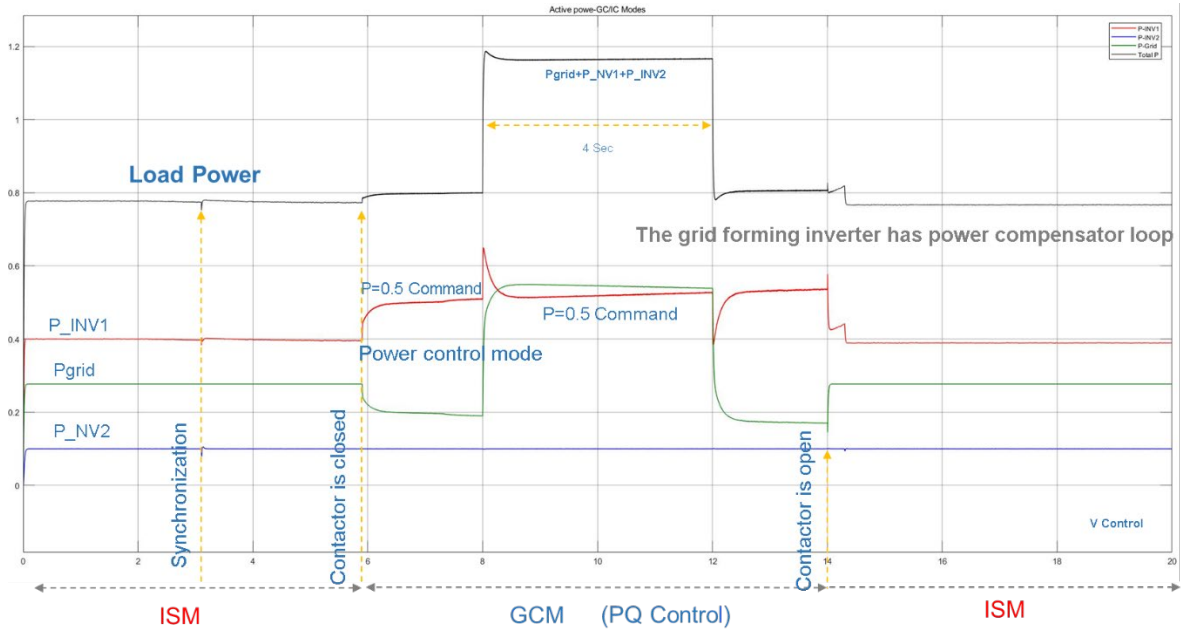


Figure 4-10 Active power plots of the proposed system during GMC

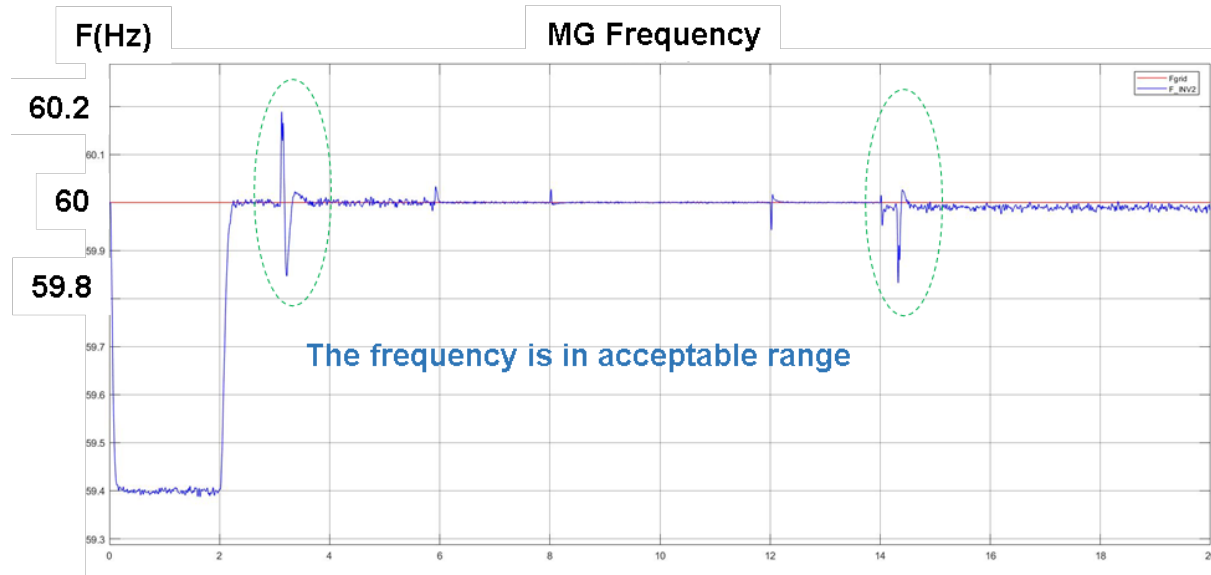


Figure 4-11 The frequency signal of the MG in GCM when Case 1 is applied

The process of synchronization begins with matching the frequency between the grid and MG, followed by voltage matching. The final step is to match the phase difference, as shown in Figure 4-12. The results demonstrate a smooth synchronization process.

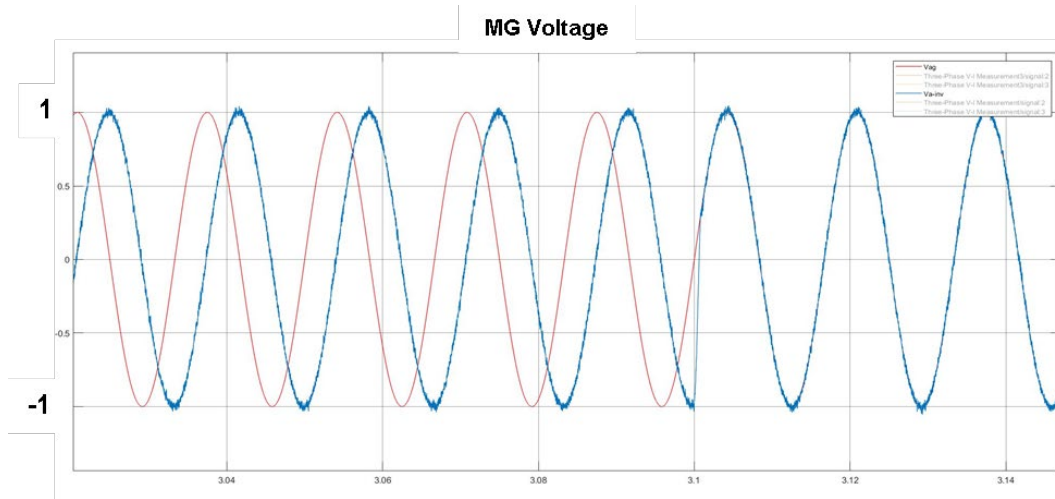


Figure 4-12 MG voltage signal during synchronization with grid

In Case 2, the same scenario was applied to the hybrid model in islanding mode. Simulation results showed that the microgrid (MG) was able to support a pulse load by utilizing the master inverter. The master controller generated contribution gain of each unit. Figure 4-13 illustrates all simulation details during islanding mode operation. The system maintained its stability while the master inverter regulated the voltage and frequency references for the system.

Case 3 aims to analyze the effect of communication delay on the stability of the MG. Two different communication delay values are applied to the communication line. For the first case, with  $T_d = 10$  ms, simulation results show that the controller is able to manage the load demand in the presence of the delay as depicted in Figure 4-14. On the other hand, the load power is not affected by the delay in the presence of the master control, because the MInv can compensate for the delay issue in the load side while keeping the system stable.

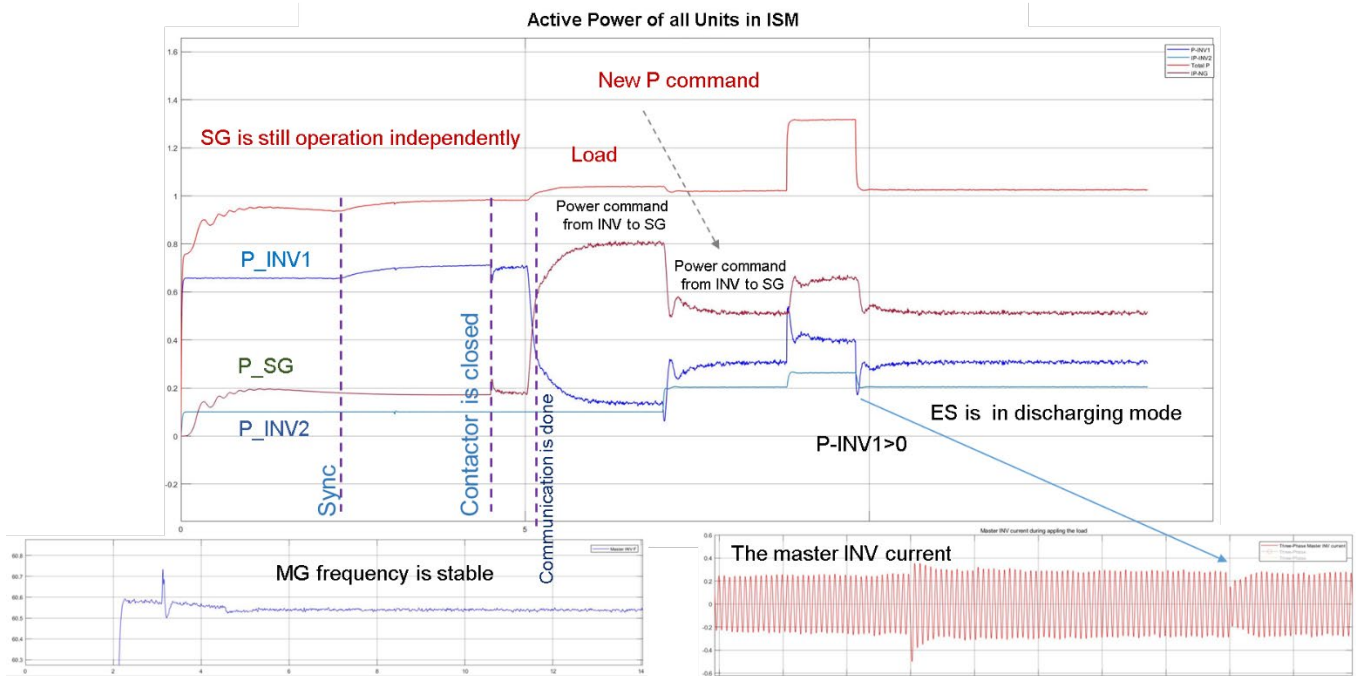


Figure 4-13 Active power plots of the proposed system during ISM

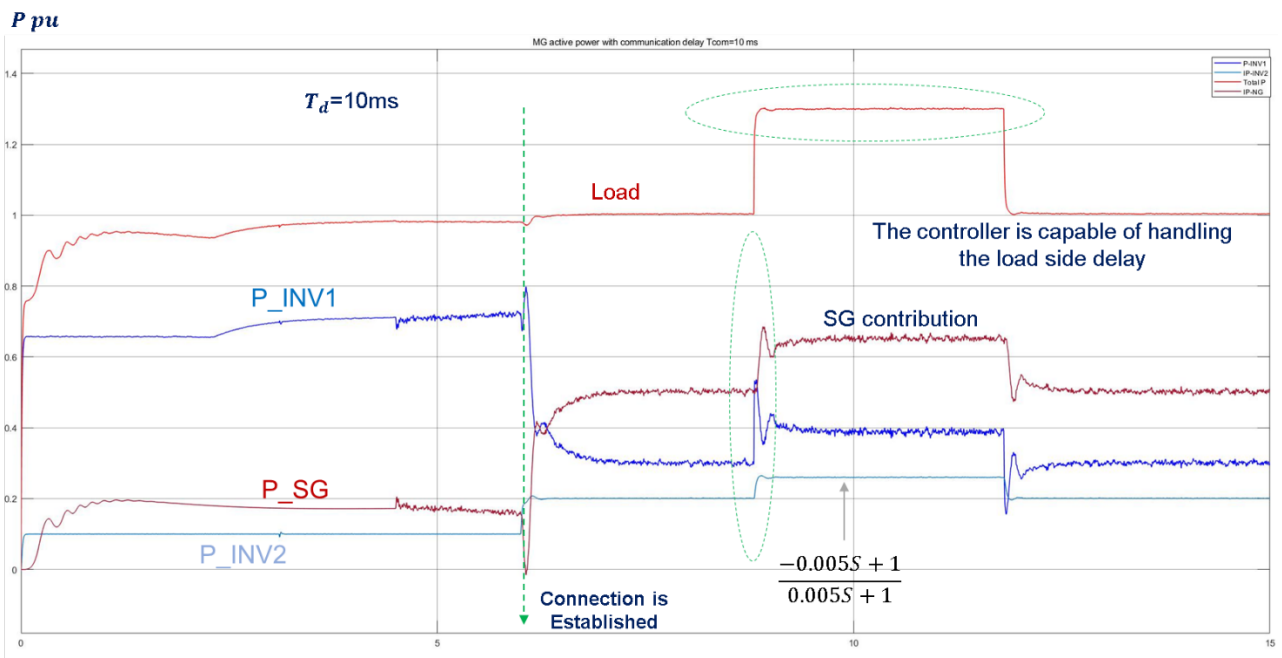


Figure 4-14 Adding communication delay (T<sub>d</sub>=10ms ) between SG and the master inverter in islanded mode

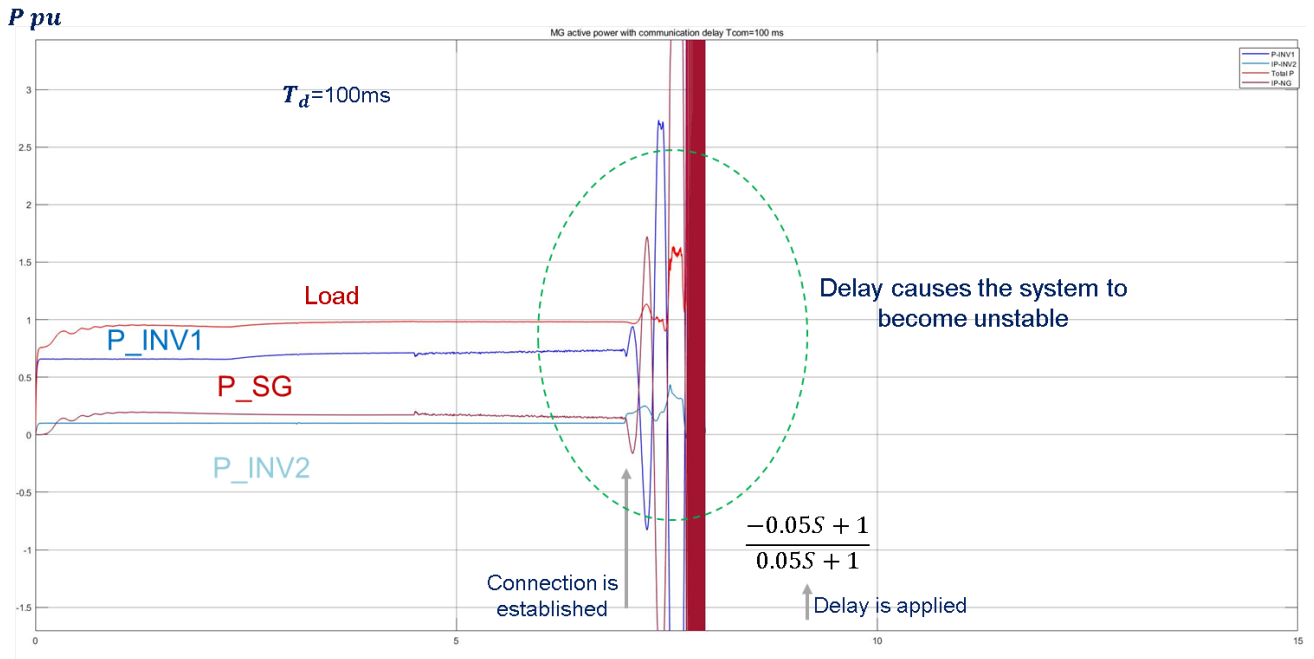


Figure 4-15 Adding communication delay ( $T_d=100\text{ms}$ ) between SG and the master inverter in islanded mode

Figure 4-15 depicts another simulation result with a different value of delay ( $T_d= 100\text{ms}$ ). As the latency increases, the system becomes unstable and eventually goes out of control.

## Chapter 3 Fault Classification based on Data Model to Support MG

### Resiliency

#### 5.1 Introduction

Microgrids are an emerging technology that have gained considerable attention in recent years due to their potential to improve the reliability and efficiency of the electricity grid. A microgrid is a small-scale, localized power system that can operate independently or in conjunction with the main grid. One of the key challenges in designing and operating microgrids is ensuring their resilience in the face of various disturbances and failures [45].

Resilience is the ability of a system to withstand and recover from disruptive events, such as natural disasters, cyber-attacks, and equipment failures. In the context of microgrids, resilience refers to the ability of the system to maintain its critical functions, such as power supply and distribution, in the event of a disturbance. Achieving resilience in microgrid systems requires a multi-disciplinary approach that incorporates advanced control algorithms, smart grid technologies, and backup power sources, among other measures. Additionally, ensuring the resilience of microgrids is a complex task that requires a thorough understanding of the various challenges and potential solutions [46].

Resilience is a multidisciplinary concept that has gained increasing attention in recent years due to its importance in understanding and managing complex systems. Researchers have focused on various aspects of resilience, including social, ecological, and technological resilience [47]. Another area of research has been the development of metrics and frameworks for resilience analysis of engineered and infrastructure systems. This is important for assessing the vulnerability of critical systems and identifying strategies for enhancing their resilience [48]. Adapting the theory of resilience to energy systems [49].

The concept of community resilience has also been the subject of significant research in recent years. This involves understanding how communities can prepare for, respond to, and recover from disasters and other disruptive events. Researchers have explored various factors that contribute to community resilience, including social capital, communication networks, and access to resources [50]. A metric and frameworks for resilience analysis of engineered and infrastructure systems is one of the areas that are currently being studied in the field of resilience analysis [51].

One of the main gaps in the literature is the lack of a physical metric to classify the level of resilience in the face of faults or disruptions. While there are various definitions and measures of resilience, there is still a need for a standardized and quantitative approach to assess and compare resilience across different systems and scenarios. This would enable more effective risk management and decision-making in the face of uncertainty and disruption.

The aim of this study is to propose a novel approach to classify resilience in the face of faults to support critical loads by considering control concepts. The proposed approach seeks to address the gap in the literature by developing a physical metric that incorporates control mechanisms to evaluate the resilience of a system.

## 5.2 Definitions of Resiliency

The ability of the system to continue to function against a disturbance, to maintain vital functions against a major disruption, and to minimize the duration and impact of a disruption [52]. One of the primary concerns is to ensure support for critical loads during disruptions. Figure 5-1 illustrates the different levels of microgrid operation and load priorities. The first level is grid-connected mode, which can support the load demand without any issues. The second

level is islanded mode with unlimited power supply, and the third level is standalone mode with limited power.

According to this definition, critical loads receive a higher priority when the microgrid is operating in the third level.

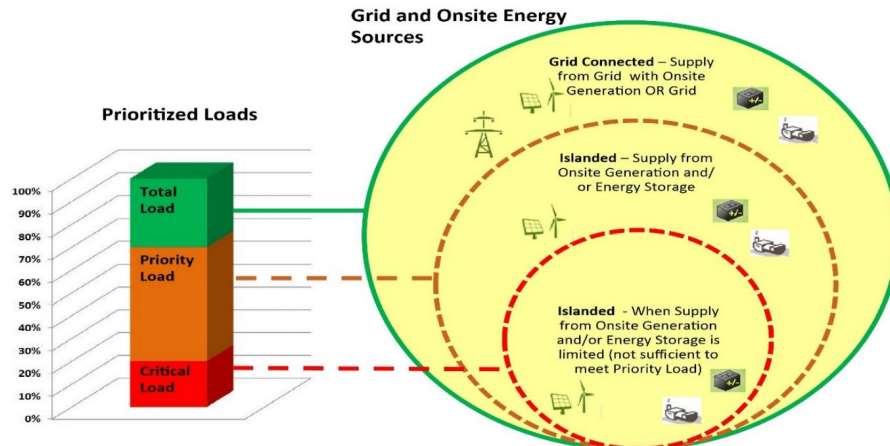


Figure 5-1 Load priority [53]

Figure 5-2 illustrates the three primary resilience layers with respect to time. The time period is divided into four states, which are: the robust state (before the event), the state shortly after the event (including the event occurrence state), the recovery state, and the post-recovery state. The size of the trapezoids, slopes, sequence, duration of temporal states, and the proportion of the presented resilience layers are primarily determined by the system's performance and the type of disruptive event. [54]. There are three layers, which include engineering resilience, operational resilience, and community resilience as depicted in figure 5-2.

The first layer of resilience is engineering-designed resilience, which involves designing energy system assets in a way that allows for the restoration of normal services after a short disruption. This layer is the focused area of this research. In other words, at this level, the focus is

on how to support critical loads and minimize recovery time based on the classification of resilience.

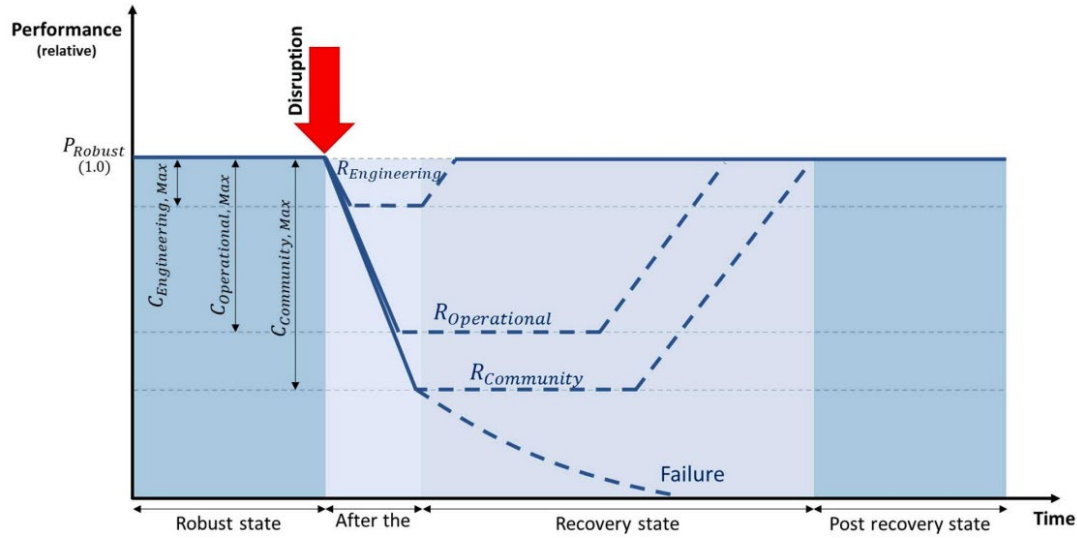


Figure 5-2 The three main resilience layers [55]

The focus of operational resilience is to improve system-level performance and operational characteristics that aim to mitigate the risk of failure and facilitate service recovery. Several measures can be taken to enhance operational resilience, including implementing demand response and demand-side management (DSM) strategies, prioritizing energy usage, using smart controls, and developing forecasting techniques.

Community-societal energy resilience accounts for the actions that should be done within the community by some or all of community users to maintain the minimum allowable community-societal services. Mass relocation, effective use of community resources during a disruption, and increasing the bonding, bridging, and linking the social capital [56], are examples of community-societal resilience enhancement measures.

As for the nature of defining operational and community levels, this research does not cover these two levels.

The next section defines different types of faults from a data analytics perspective. The faults are categorized based on controllability and observability concepts, and the system is analyzed using Kalman decomposition. Finally, based on the proposed data model, several categories of resilience have been identified.

### 5.3 Fault classification informed by data model

Three types of faults have been defined based on the variations of matrix A, B, and C in the system dynamic model. In the state space model of the system, as shown in Figure 5-3, matrix B serves as the interface between the input (actuator) and the states. Therefore, faults occurring in the control inputs correspond to variations of matrix B can be expressed as a control fault. On the other hand, matrix A represents the internal dynamics of the system. Faults affecting the internal dynamics of the system correspond to variations of matrix A is system fault. Lastly, matrix C represents the sensor data, and faults affecting the measurement (sensors) of states correspond to variations of matrix C, this fault can be classified as output faults. All detail are illustrated in Figure 5-3.

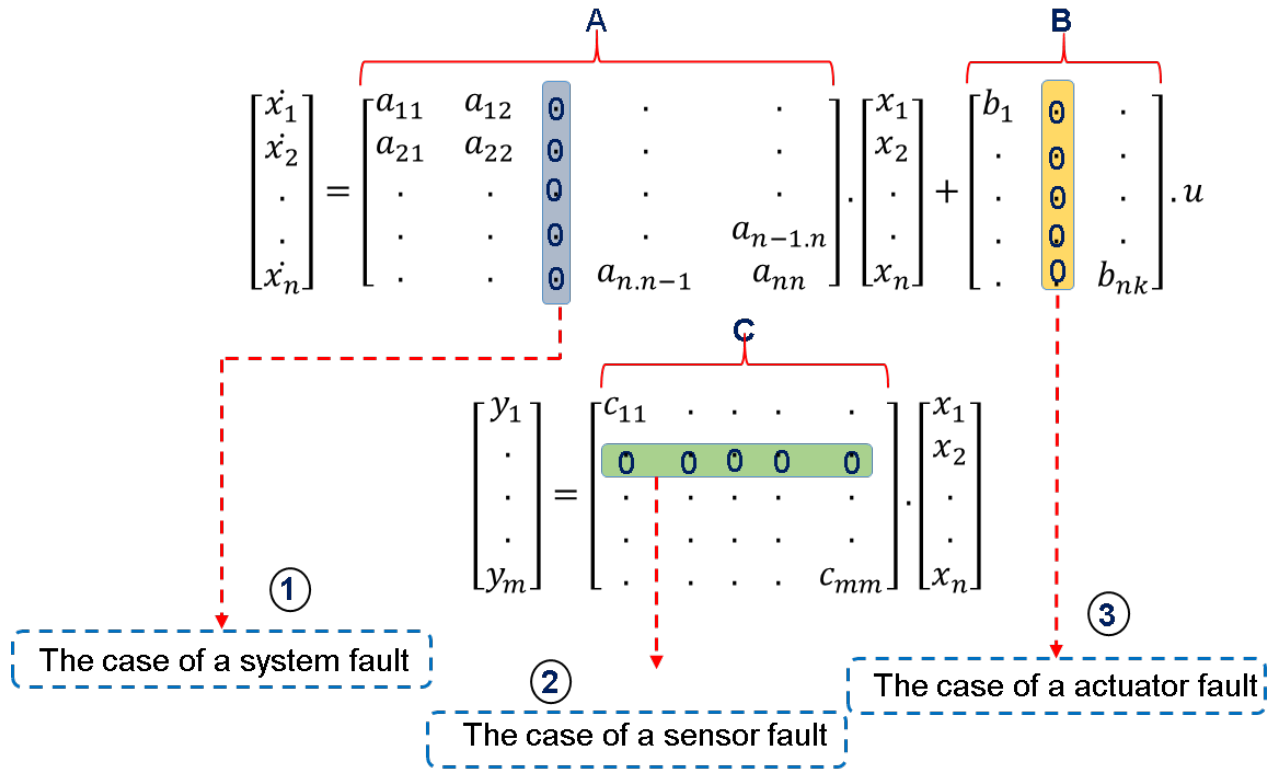


Figure 5-3 Fault classification informed by data model

Control Theory revolves around two core concepts - controllability and observability. In this study, we explore their role and influence on system safety.

A dynamical system is considered controllable if, with an appropriate selection of inputs, it can be driven from any initial state to a desired final state in a finite amount of time. This condition holds true only when the controllability matrix has full rank as expressed in equation (5-1).

$$rank[B \ AB \ \dots \ A^{n-1}B] = n \tag{5-1}$$

Where n is the number of states of the system.

The mathematical requirement for a system to be observable is that the observability matrix must have full rank as follows equation (5-2) [57].

$$\text{rank} \begin{bmatrix} C \\ CA \\ \vdots \\ CA^{n-1} \end{bmatrix} = n \quad (5-2)$$

In this work, controllability and observability are the two main tools used to analyze the data model and determine the system's ability to support critical loads. These tools help in understanding the situation of input controls and sensor data, enabling a thorough assessment of the system's capability. Additionally, Kalman decomposition (KD) is used to clarify the observable and controllable components of the system [58]. Hence, this method can be helpful in extracting the controllable and observable modes of a system as shown in Figure 5-4.

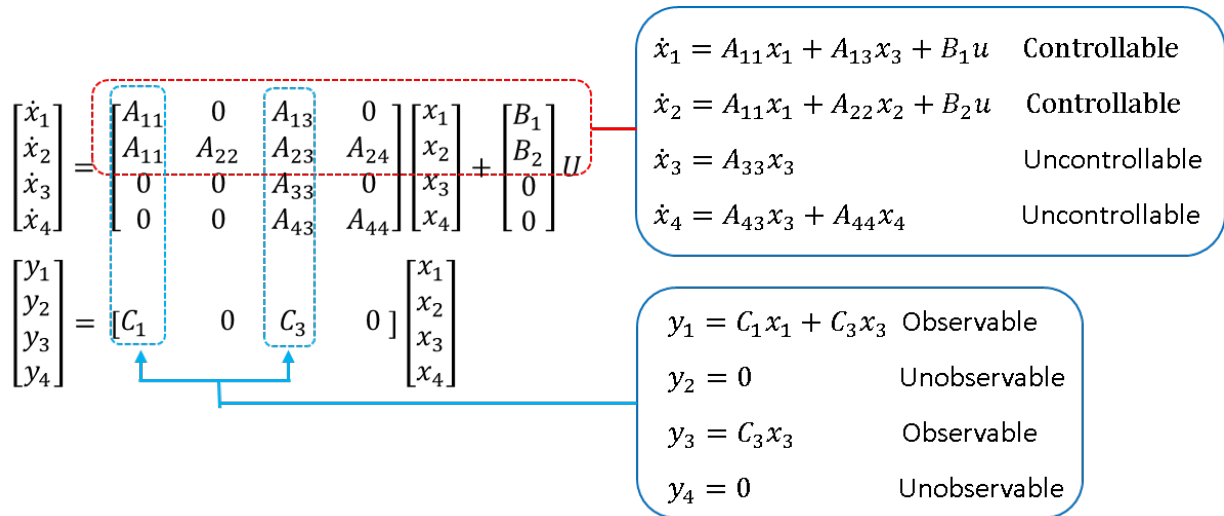


Figure 5-4 Kalman decomposition model

#### 5.4 A novel method for classifying data model under fault scenario

In this section, a new method will be proposed for classifying the resilience level of a system in the face of a fault. This method will enable the determination of the system's ability to withstand and recover from the fault scenario. The proposed method will take into account various

factors such as the type and severity of the fault, the system's design and components, and the availability of backup or redundancy measures. By using Resiliency Classification (ReC) method, it will be possible to accurately classify the system's resilience level and take appropriate measures to ensure its optimal functioning in fault scenarios.

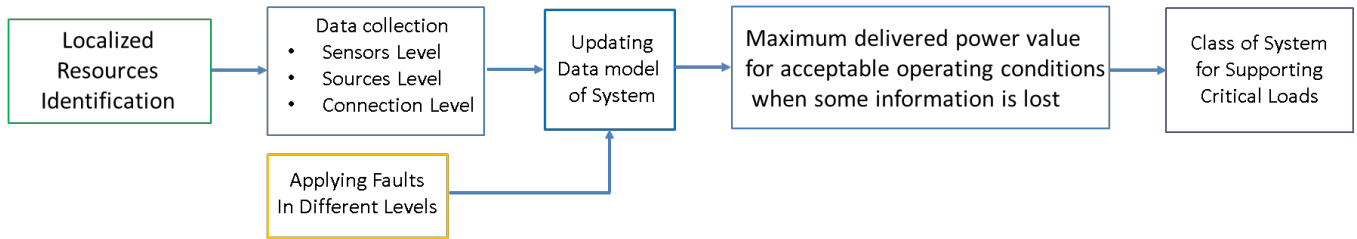


Figure 5-5 The block diagram of Resiliency Classification process

In accordance with the block diagram shown in Figure 5-5, the steps required to apply the ReC are presented. After obtaining the data model of the Microgrid (MG), which considers all resources, the data model is updated with new data obtained from the state of each source, sensor, and the dynamics of each data line.

#### 5.4.1.1 Model under study

The data model of a system is depicted in Figure 5-6. It consists of Natural gas generator (NG), Renewable source (Ren), energy storage (ES), load and grid.

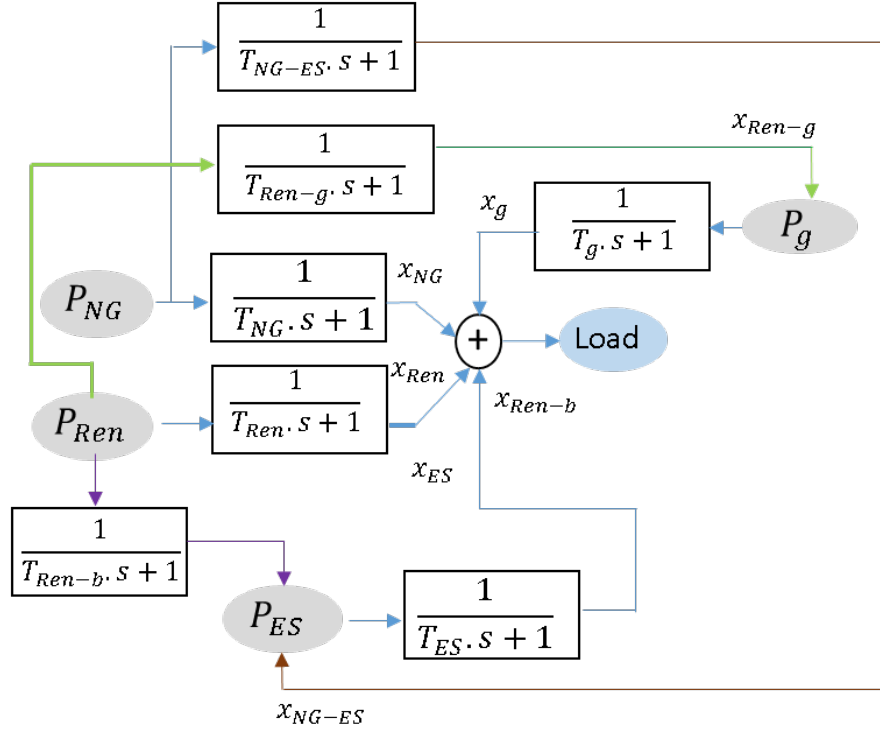


Figure 5-6 Data model of the system under study

The dynamic equation between the power generated in source and the sensor value in load side can be written as follows.

$$\dot{x}_{NG-ES} = -\frac{1}{T_{NG-ES}} x_{NG-ES} + \frac{K_{NG-ES}}{T_{NG-ES}} P_{NG-ES} \quad (5-3)$$

Where  $P_{NG-ES}$  is generated power from NG to meet ES demand,  $x_{NG-ES}$  is measured power in ES side and  $T_{NG-ES}$  is the delay for getting measured values.

$$\dot{x}_{NG} = -\frac{1}{T_{NG}} x_{NG} + \frac{K_{NG}}{T_{NG}} P_{NG} \quad (5-4)$$

Where  $P_{NG}$  is generated power from NG to meet the load demand.

$$\dot{x}_{Ren-g} = -\frac{1}{T_{Ren-g}} x_{Ren-g} + \frac{K_{Ren-g}}{T_{Ren-g}} P_{Ren-g} \quad (5-5)$$

Where  $P_{Ren-g}$  is generated power from Ren to supply the grid.

$$\dot{x}_g = -\frac{1}{T_g} x_g + \frac{K_g}{T_g} \cdot P_g + x_{Ren-g} \quad (5-6)$$

Where  $P_g$  is generated power from grid to meet the load demand.

$$\dot{x}_{Ren} = -\frac{1}{T_{Ren}} x_{Ren} + \frac{K_{Ren}}{T_{Ren}} \cdot P_{Ren} \quad (5-7)$$

Where  $P_{Ren}$  is generated power from Ren to meet the load demand.

$$\dot{x}_{soc} = -\frac{1}{T_{soc}} x_{soc} + x_{NG-ES} + x_{Ren-ES} - P_{ES} \quad (5-8)$$

Where  $x_{soc}$  is SOC value of ES

$$\dot{x}_{ES} = -\frac{1}{T_{ES}} x_{ES} + \frac{K_{ES}}{T_{ES}} \cdot P_{ES} \quad (5-9)$$

Where  $P_{ES}$  is generated power from ES to support the load demand.

$$\dot{x}_{Ren-ES} = -\frac{1}{T_{Ren-b}} x_{Ren-ES} + \frac{K_{Ren-b}}{T_{Ren-b}} \cdot P_{Ren-ES} \quad (5-10)$$

Where  $P_{Ren-ES}$  is generated power from Ren to support the ES

The data modeling of a system described by equations (5-3) to (5-10) is shown in Figure 5-7.

Most of the states in the system describe power propagation, and  $x_{soc}$  represents the state of charge level in the energy storage system. In order to evaluate the impact of different types of faults, as defined in the previous section, we need to introduce these faults into the system. For instance, a fault can be simulated by disconnecting the link between the renewable source and the grid. The resulting dynamic behavior can be observed in Figure 5-8.

After obtaining the new dynamic behavior, it is important to analyze the controllability and observability of the system. This can be achieved through the use of KD, which enables us to generate a new model of the system, as depicted in Figure 5-9.

$$\begin{bmatrix} \dot{x}_{NG} \\ \dot{x}_{NG-ES} \\ \dot{x}_{Ren-g} \\ \dot{x}_{Ren} \\ \dot{x}_{SOC} \\ \dot{x}_{ES} \\ \dot{x}_{Ren-ES} \\ \dot{x}_g \end{bmatrix} = \begin{bmatrix} -\frac{1}{2} & 0 & 0 & 0 & 0 & 0 & 0 & 0 \\ 0 & -\frac{1}{2} & 0 & 0 & 0 & 0 & 0 & 0 \\ 0 & 0 & -\frac{1}{2} & 0 & 0 & 0 & 0 & 0 \\ 0 & 0 & 0 & -\frac{1}{2} & 0 & 0 & 0 & 0 \\ 0 & 1 & 0 & 0 & -\frac{1}{4} & 0 & 1 & 0 \\ 0 & 0 & 0 & 0 & 0 & -\frac{1}{2} & 0 & 0 \\ 0 & 0 & 0 & 0 & 0 & 0 & -\frac{1}{2} & 0 \\ 0 & 0 & 1 & 0 & 0 & 0 & 0 & -\frac{1}{2} \end{bmatrix} \begin{bmatrix} x_{NG} \\ x_{NG-ES} \\ x_{Ren-g} \\ x_{Ren} \\ x_{SOC} \\ x_{ES} \\ x_{Ren-ES} \\ x_g \end{bmatrix} + \begin{bmatrix} 1 & 0 & 0 & 0 & 0 & 0 & 0 & 0 \\ 0 & 1 & 0 & 0 & 0 & 0 & 0 & 0 \\ 0 & 0 & 1 & 0 & 0 & 0 & 0 & 0 \\ 0 & 0 & 0 & 1 & 0 & 0 & 0 & 0 \\ 0 & 0 & 0 & 0 & -1 & 0 & 0 & 0 \\ 0 & 0 & 0 & 0 & .5 & 0 & 0 & 0 \\ 0 & 0 & 0 & 0 & 0 & 1 & 0 & 0 \\ 0 & 0 & 0 & 0 & 0 & 0 & 1 & 1 \end{bmatrix} \begin{bmatrix} P_{NG} \\ P_{NG-ES} \\ P_{Ren-g} \\ P_{Ren} \\ P_{ES} \\ P_{Ren-ES} \\ P_g \end{bmatrix}$$

$$\begin{bmatrix} y_{NG} \\ y_{Ren} \\ y_{SOC} \\ y_{ES} \\ y_{Ren-ES} \\ y_g \end{bmatrix} = \begin{bmatrix} 1 & 0 & 0 & 0 & 0 & 0 & 0 & 0 \\ 0 & 0 & 0 & 1 & 0 & 0 & 0 & 0 \\ 0 & 0 & 0 & 0 & 1 & 0 & 0 & 0 \\ 0 & 0 & 0 & 0 & 0 & 1 & 0 & 0 \\ 0 & 0 & 0 & 0 & 0 & 0 & 1 & 0 \\ 0 & 0 & 0 & 0 & 0 & 0 & 0 & 1 \end{bmatrix} \begin{bmatrix} x_{NG} \\ x_{NG-ES} \\ x_{Ren-g} \\ x_{Ren} \\ x_{SOC} \\ x_{ES} \\ x_{Ren-ES} \\ x_g \end{bmatrix} x_{SOC}$$

Figure 5-7 The Simplified Data Model Under Fault Scenario

$$A^f = \begin{bmatrix} -\frac{1}{2} & 0 & 0 & 0 & 0 & 0 & 0 & 0 \\ 0 & -\frac{1}{2} & 0 & 0 & 0 & 0 & 0 & 0 \\ 0 & 0 & -\frac{1}{2} & 0 & 0 & 0 & 0 & 0 \\ 0 & 0 & 0 & -\frac{1}{2} & 0 & 0 & 0 & 0 \\ 0 & 1 & 0 & 0 & -\frac{1}{4} & 0 & 1 & 0 \\ 0 & 0 & 0 & 0 & 0 & -\frac{1}{2} & 0 & 0 \\ 0 & 0 & 0 & 0 & 0 & 0 & -\frac{1}{2} & 0 \\ 0 & 0 & 0 & 0 & 0 & 0 & 0 & -\frac{1}{2} \end{bmatrix}$$

Figure 5-8 Matrix A after getting fault between Ren and grid

$$\dot{Z} = \begin{bmatrix} -\frac{1}{2} & 0 & 0 & 0 & 0 & 0 & 0 & 0 \\ 0 & -\frac{1}{2} & 0 & 0 & 0 & 0 & 0 & 0 \\ 0 & 0 & 0 & 0 & 0 & 0 & 0 & 0 \\ 0 & 1 & 0 & -\frac{1}{4} & 0 & \mathbf{1} & 0 & 0 \\ 0 & 0 & 0 & 0 & -\frac{1}{2} & 0 & 0 & 0 \\ 0 & 0 & 0 & 0 & 0 & -\frac{1}{2} & 0 & 0 \\ 0 & 0 & 0 & 0 & 0 & 0 & -\frac{1}{2} & \mathbf{0} \\ 0 & 0 & 0 & 0 & 0 & 0 & 0 & -\frac{1}{2} \end{bmatrix} \cdot Z + \begin{bmatrix} 1 & 0 & 0 & 0 & 0 & 0 & 0 & 0 \\ 0 & 0 & 1 & 0 & 0 & 0 & 0 & 0 \\ 0 & 0 & 0 & 1 & 0 & 0 & 0 & 0 \\ 0 & 0 & 0 & 0 & -1 & 0 & 0 & 0 \\ 0 & 0 & 0 & 0 & 0.5 & 0 & 0 & 0 \\ 0 & 0 & 0 & 0 & 0 & 1 & 0 & 0 \\ 0 & 0 & 0 & 0 & 0 & 0 & 1 & 0 \\ 0 & 1 & 0 & 0 & 0 & 0 & 0 & 0 \end{bmatrix} \begin{bmatrix} P_{NG} \\ P_{NG-ES} \\ P_{Ren-g} \\ P_{Ren} \\ P_{ES} \\ P_{Ren-ES} \\ P_g \end{bmatrix}$$

$$\begin{bmatrix} y_{NG} \\ y_{Ren} \\ y_{SOC} \\ y_{ES} \\ y_{Re-ES} \\ y_g \end{bmatrix} = \begin{bmatrix} 1 & 0 & 0 & 0 & 0 & 0 & 0 & \mathbf{0} \\ 0 & 0 & 1 & 0 & 0 & 0 & 0 & \mathbf{0} \\ 0 & 0 & 0 & 1 & 0 & 0 & 0 & \mathbf{0} \\ 0 & 0 & 0 & 0 & 1 & 0 & 0 & \mathbf{0} \\ 0 & 0 & 0 & 0 & 0 & 1 & 0 & \mathbf{0} \\ 0 & 0 & 0 & 0 & 0 & 0 & 1 & \mathbf{0} \end{bmatrix} \cdot Z$$

← Unobservable State Mode

Figure 5-9 Dynamic model after applying KD

The use of KD generates a new set of states, and it is important to establish a mapping between the original states and the new states. This mapping is shown in equation (5-11)

$$\begin{aligned} \dot{x} &= Ax + Bu \\ z &= Tx \\ \dot{z} &= TAT^{-1}z + T^{-1}Bu \end{aligned} \quad (5-11)$$

$$Z = \underbrace{\begin{bmatrix} 1 & 0 & 0 & 0 & 0 & 0 & 0 & 0 \\ 0 & 1 & 0 & 0 & 0 & 0 & 0 & 0 \\ 0 & 0 & 0 & 1 & 0 & 0 & 0 & 0 \\ 0 & 0 & 0 & 0 & 1 & 0 & 0 & 0 \\ 0 & 0 & 0 & 0 & 0 & 1 & 0 & 0 \\ 0 & 0 & 0 & 0 & 0 & 0 & 1 & 0 \\ 0 & 0 & 0 & 0 & 0 & 0 & 0 & 1 \\ 0 & 0 & 1 & 0 & 0 & 0 & 0 & 0 \end{bmatrix}}_T \begin{bmatrix} x_{NG} \\ x_{NG-ES} \\ x_{Ren-g} \\ x_{Ren} \\ x_{SOC} \\ x_{ES} \\ x_{Ren-ES} \\ x_g \end{bmatrix} = \begin{bmatrix} x_{NG} \\ x_{NG-ES} \\ x_{Ren} \\ x_{SOC} \\ x_{ES} \\ x_{Ren-ES} \\ x_g \\ x_{Ren-g} \end{bmatrix}$$

Figure 5-10 Mapping between two groups of states

Based on this mapping it can be inferred  $x_{\text{Ren-g}}$  is unobservable.

#### 5.4.1.2 Summary of ReC algorithm

Regarding the concepts mentioned above, the summary of the algorithm for classification can be written as follows.

- 1- Extracting the data model of the system
- 2- Applying three level of faults based on the profiles defined for the MG
- 3- Using KD to determine the controllability and observability states of the system
- 4- Mapping the states to identify Uncontrollable and Unobservable modes
- 5- Using the classification Table (5-1) to determine the level of resilience

Table 5-1 Table for resilience classification

State	Class
All sources are available	A
More than one sources	B
One source is available	C
Supporting for limited time	D
Information is not enough	D1
No acceptable information	O

#### 5.4.1.3 Analyze the system and simulation results

By applying all recommended ReC steps to the system being analyzed in four different cases, the obtained results are summarized in Table 5-2. In Case 1, the system was found to be operating normally, with no concerns regarding the support of energy for loads demand. According to the data model, the system is controllable and observable, and has been classified as having a resilience class A.

Table 5-2 The classification of resilience levels for supporting critical loads

Faulty case	Controllability	Observability	Critical load supporting	UC	UO	System state
Case1						
Fault-free functioning	1	1	1			
Case2 (Actuator)						
Grid-Load	1	1	A			
Ren to Grid	0	1	A	X Ren-g		
Gen to load	0	1	B	X Gen-L		
Gen to ES	0	1	B			
Ren to load	0	1	B			
ES to load	0	1	B			
Ren to ES	0	1	B			
Case 3 (Sensors)						
Grid-Load	1	0	D1		X Ren-g & Xg	
Gen to load	1	0	B			
Ren to load	1	0	B			
ES to load	1	0	B			
Ren to ES	1	0	B			
B SOC	1	0	D1		X SOC & X Gen-ES	
Case4 (Fault between two units)						
Grid-Load	1	1	A			P Ren + P ES + P Gen
Ren-Load	1	1	B			P ES + P Gen
Gen-Load	1	1	C			P ES
Ren-Grid	1	0	C		X Ren-g	P ES
Ren-ES	1	0	D			
Gen-ES	1	0	D		X Gen-ES	Limited time
Sensor :ES-Load	1	0	D		X ES	SOC can be helpful
Actuator:P_ES	0	0	O	X ES		Shut down

In Case 2, the objective is to analyze the impact of each source on the system from a load perspective. This is achieved by simulating the loss of power from each source, and then defining the class of resilience. When the first two sources are lost, the system remains in resilience class A since there are no issues from the perspective of other sources.

Although the system becomes uncontrollable in this scenario, this issue is on the grid side and not on the load side, thus allowing the system to maintain its level A resilience. For the remaining sources, the system shifts to resilience class B for a limited time upon the loss of each source.

$$\begin{aligned}
 \text{Load} &: P_{NG} + P_{ES} + P_g + P_{Ren} \\
 \text{ES} &: P_{NG-ES} + P_{Ren-ES} \\
 \text{Grid} &: P_{Ren-g}
 \end{aligned}
 \tag{ 5-12 }$$

In Case 3, the scenario is similar to Case 2, with the addition of considering the impact of sensors. As shown in Table 5-2, when the grid data is lost from the load side, the system becomes unobservable (UO). In addition, two groups of sensor data are lost, making it difficult to proceed without this information, which results in a classification of D1 according to Table 5-1. The state of charge (SOC) also experiences similar issues. For the remaining parts, the Resilience class is classified as B.

Case 4 is one of the important analyses to gather information from the system by sequentially removing each link of the source. The analysis starts from the grid side, and as the test continues, the value of Rec will be changed. Table 5-2 provides detailed information on the UC and UO data sources used to classify the resilience state.

The proposed technique can be useful for data analytics in assessing the resiliency of a system during its operation. The resilience class can help manage the state of the system in the face of different events and plan for minimizing recovery time and supporting critical loads

## Chapter 6 Conclusions

This thesis presents a comprehensive study on the modeling and control of a proposed microgrid (MG) system. Firstly, it provides an overview of the microgrid concept, its control hierarchy, and primary control techniques. The stability of microgrids is also discussed, and the problem statement that is aimed to be addressed in this thesis is identified.

The configuration of a hybrid system, comprising a natural gas generator, voltage source converter system, LCL filter and grid following convert is presented. It presents a detailed modeling of the natural gas generator, covering its mechanical and electrical models, along with the exciter state space modeling. Additionally, the state space modeling of the grid forming inverter and grid following inverter is included, which incorporates new details not covered in previous studies. The dynamic model of the hybrid MG system is presented, clarifying the role of each state, the number of inputs, and the interconnection between units. Importantly, the study also accounts for communication delay as part of the dynamic model, making it unique from other research conducted in this field.

The presented work discusses the control architecture of a proposed microgrid and provides simulation results. The results cover various scenarios, such as supporting pulse load during islanding mode and grid-connected mode of operation, and account for the impact of communication delay. The results are considered satisfactory as they demonstrate the effectiveness of the master controller in supporting the system with different dynamics, particularly in transient response.

The proposed work introduces a fault classification method based on a data model to support microgrid resiliency. Resiliency is defined, and a novel method for classifying the data

model under fault scenarios is presented. The proposed fault classification method provides a useful framework for analyzing the system's resilience to different types of faults.

In conclusion, this thesis presented a comprehensive study on the modeling and control of a proposed microgrid system. The proposed fault classification method provides a useful framework for analyzing the system's resilience to different types of faults, which can be used to improve the micro grid's overall performance and reliability. Our work can be extended to consider additional factors that may affect microgrid performance, such as hybrid electrical vehicle (EV) charger.

Further future considerations and analyses include evaluating the proposed control in real systems using hardware in the loop (HIL) method. Additionally, the study's results could be applied to evaluate the performance of EV hybrid charger.

## References

- [1] F. Katiraei, "Low Dynamic analysis and control of distributed energy resources in a".
- [2] Caldon, R., Coppo, M., Raciti, A. and Turri, R., "Dynamic control of inverter-connected generators for intentionally islanded MV distribution networks," in *International Universities' Power Engineering Conference (UPEC)*, 2013.
- [3] C. Marnay, H. Asano, S. Papathanassiou and G. Strbac, "Policymaking for," *Power and Energy Magazine*, Vols. vol. 6,, pp. 66-77, 2008.
- [4] H. Jiayi, J. Chuanwen and X. Rong,, "A review on distributed energy resources," *Renewable and Sustainable Energy Reviews*, vol. 12, p. 2472, 2008.
- [5] C. Bayliss, C.R. Bayliss and B.J. Hardy, "Transmission and distribution electrical," *Elsevier*, 2012.
- [6] Lasseter, R.H., "Microgrids," in *Power Engineering Society Winter Meeting*," *IEEE*, pp. 305-308, 2002.
- [7] Paigi, R.H. Lasseter and P., "Microgrid: a conceptual solution," *Power*, vol. 6, pp. 4285-4290, 2004.
- [8] Strachinescu, A., "<https://www.europeanenergyinnovation.eu/Articles/Spring-2017/The-role-of-the-storage-in-the-future-European-energy-system>," 2017. [Online].
- [9] S Narasimalu, B Chelliah, "Integration of Energy Storage System with Renewable Energy Source," in *Asian Conference on Energy*, 2018.
- [10] Anonymous, "DOE Microgrid workshop report," US Department of Energy, 2011.
- [11] "<https://www.tcpowertec.com/micro-grid-solutions>," 2022. [Online].
- [12] Sub-domains, IEEE Smart Grid Domains &, "<http://smartgrid.ieee.org/domains>," IEEE Smart Grid Society, 2016. [Online].
- [13] Zhang, X., Fu, L., Ma, F. and Wang, Y, "An emergency control strategy for isolated power system of three-phase inverter and diesel-engine generator operating in parallel," *IEEE Access*, vol. 6, pp. 66223-66234, 2018.
- [14] Lasseter, ] P. Piagi and R.H., "Autonomous control of microgrids,," *Power Engineering Society General Meeting,IEEE*, 20069.
- [15] S. Bhaskara, "Control and operation of multiple distributed generators in a microgrid," 2012.
- [16] Bahrani, B., Karimi, H. and Iravani, R, "Decentralized control of parallel connection of two distributed generation units," In *2009 35th Annual Conference of IEEE Industrial Electronics*, pp.

358-362, 2009.

- [17] J. M. Guerrero, M. Chandorkar, T. L. Lee and P. C. Loh, "Advanced Control Architectures for Intelligent Microgrids—Part I: Decentralized and Hierarchical Control," *IEEE Transactions on Industrial Electronics*, pp. 1254-1262, 2013.
- [18] Prajof Prabhakaran, Umashankar Subramaniam, J. L. Febin Daya, *Smart Grids and Microgrids*, Wiley, 2022.
- [19] Che, Y. and Chen, J., "Research on design and control of microgrid system," *Electrical Review ISSN*, pp. 83-86, 2012.
- [20] Duan, J., Wang, C., Xu, H., Liu, W., Xue, Y., Peng, J.C. and Jiang, H., "Distributed control of inverter-interfaced microgrids based on consensus algorithm with improved transient performance," *IEEE Transactions on Smart Grid*, vol. 10, pp. 1303-1312, 2017.
- [21] Kroutikova, N., Hernandez-Aramburo, C.A. and Green, T.C., "State-space model of grid-connected inverters under current control mode," *IET Electric Power Applications*, vol. 3, pp. 329-338, 2007.
- [22] F. Katiraei, M. Iravani and P. Lehn, "Small-signal dynamic model of a microgrid including conventional and electronically interfaced distributed resources," *IET Generation, Transmission & Distribution*, vol. 1, pp. 369-378, 2007.
- [23] N. P. M. a. G. T. Pogaku, "Modeling, analysis and testing of autonomous operation of an inverter-based microgrid," *IEEE Transactions on power electronics*, vol. 22, pp. 613-625., 2007.
- [24] Yoash Levron, Juri Belikov, "The Synchronous Machine," Control Lab, 2019. [Online]. Available: <https://a-lab.ee/projects/dq0-dynamics>.
- [25] I. Canay, "Causes of discrepancies on calculation of rotor quantities and exact equivalent diagrams of the synchronous machine," *Power Apparatus and Systems, IEEE Transactions*, pp. 1114-1112, 1969.
- [26] Willis, K. Yeager and J., "Modeling of emergency natural gas generators in an 800 megawatt nuclear power plant," *Energy Conversion, IEEE Transactions*, vol. 8, pp. 433-441, 1993.
- [27] Du, W., Tuffner, F.K., Schneider, K.P., Lasseter, R.H., Xie, J., Chen, Z. and Bhattarai, B., "Modeling of Grid-Forming and Grid-Following," *IEEE TRANSACTIONS ON POWER DELIVERY*, vol. 36, pp. 2035-2045, 2021.
- [28] Rosso, R., Wang, X., Liserre, M., Lu, X. and Engelken, S., "Grid-forming converters: Control approaches, grid-synchronization, and future trends," *EEE Open Journal of Industry Applications*, vol. 2, no. 93-109, 2021.
- [29] Aleksandr Reznik, Marcelo Godoy Simões, Ahmed Al-Durra, "LCL Filter Design and Performance

- Analysis for," *IEEE TRANSACTIONS ON INDUSTRY APPLICATIONS*, vol. 50, no. 1225-1231, 2014.
- [30] Alimeling, J., and Hammer, W, "Plecs-piece-wise linear electrical circuit simulation for simulink," *IEEE Conf. on Power Electronics and Drive Systems*, vol. 1, pp. 355-360, 1999.
- [31] A. E. Fitzgerald, C. Kingsley, and S. D. Uman, *Electric Machinery*, . New Yor: McGraw-Hill, 2003.
- [32] P. Kundu, *Power system stability and contro*, McGraw-Hil, 2020.
- [33] A. Perera, "Virtual synchronous machine based power control in active rectifiers in," Norwegian university of Science and Technology, 2012.
- [34] M. Rasheduzzaman, J. A. Mueller, and J. W. Kimball,, "An accurate small-signal model of inverter-dominated islanded microgrids using dq reference frame,," *IEEE Journal on Emerging and Selected Topics in Power Electronics*, 2014.
- [35] Miao, Z., Domijan, A. and Fan, L, "Investigation of microgrids with both inverter interfaced and direct AC-connected distributed energy resources," *IEEE Transactions on Power Delivery*, pp. pp.1634-1642, 2011.
- [36] Pogaku, N., Prodanovic, M. and Green, T.C, "Modeling, analysis and testing of autonomous operation of an inverter-based microgrid," *IEEE Transactions on power electronics*, pp. 613-625, 2017.
- [37] Pournazarian, Bahram, Maysam Saeedian, Bahman Eskandari, Matti Lehtonen, and Edris Pouresmaeil., "Feasible ranges of microgrid parameters based on small-signal stability analysis.,," *IEEE 21st Workshop on Control and Modeling for Power Electronics*, pp. 1-6, 2020.
- [38] Q. Shafiee, J. M. Guerrero, and J. C. Vasquez,, "Distributed secondary control for islanded microgrids—A novel approach," *IEEE Trans. PowerElectronics*, vol. 29, pp. 1018-1031, 2014.
- [39] H. Xin, L. Zhang, Z. Wang, D. Gan, and K. P. Wong,, "Control of island AC microgrids using a fully distributed approach," *IEEE Trans. Smart Grid*, vol. 6, p. 943–945, 2015.
- [40] M. Rasheduzzaman, J. A. Mueller, and J. W. Kimball, "An accurate small-signal model of inverter-dominated islanded microgrids using dq reference frame,," *IEEE J. Emerg. Sel. Topics Power Electron*, vol. 2, p. 1070–1080, 2014.
- [41] X. Wang, F. Blaabjerg, and Z. Chen,, "Autonomous control of inverterinterfaced distributed generation units for harmonic current filtering and resonance damping in an islanded microgrid," *IEEE Trans. Ind. Appl.*, vol. 50, p. 452–461, Jan./Feb. 2014..
- [42] J. C. Vasquez, J. M. Guerrero, M. Savaghebi, J. Eloy-Garcia, and R. Teodorescu, "Modeling, analysis, and design of stationary reference frame droop controlled parallel three-phase voltage

- source inverters," *IEEE Trans. Ind. Electron*, vol. 60, p. 1271–1280, 2013.
- [43] Weber, L.G., Nasiri, A. and Akbari Haghghat, H, "Dynamic modeling and control of a synchronous generator in an AC microgrid environment. *IEEE Transactions on Industry Applications*, 54(5), pp.4833," *IEEE Transactions on Industry Applications*, vol. 54, pp. 4833-4841, 2018.
- [44] Akbari Haghghat, H., ALTIN, N. and Nasiri, A., "Mitigating Communication Delay Impact on Microgrid Stability Using a Compensator Based on Smith Predictor.," *IEEE Energy Conversion Congress and Exposition (ECCE)*, pp. 6309-6313, 2019.
- [45] Vugrin, E.D., Castillo, A.R. and Silva-Monroy, C.A, "Resilience Metrics for the Electric Power System: A Performance-Based Approach," Sandia National Lab.(SNL-NM), Albuquerque, NM (United States), 2017.
- [46] Mishra, S., Anderson, K., Miller, B., Boyer, K. and Warren, A., "Microgrid resilience: A holistic approach for assessing threats, identifying vulnerabilities, and designing corresponding mitigation strategies," *Applied Energy*, vol. 264, p. 114726, 2020.
- [47] "Electric Grid Resilience to Weather Outages," 30 september 2016. [Online]. Available: [http://energy.gov/sites/prod/files/2013/08/f2/Grid%20Resiliency%20Report\\_FINAL.pdf](http://energy.gov/sites/prod/files/2013/08/f2/Grid%20Resiliency%20Report_FINAL.pdf).
- [48] Hosseini S, Barker K, Ramirez-Marquez JE, "A review of definitions and measures of system resilience," in *Reliability Engineering & System Safety*, 2016.
- [49] Jesse B-J, Heinrichs HU, Kuckshinrichs W., "Adapting the theory of resilience to energy system," in *Energy, Sustainability and Society.*, 2019.
- [50] Koliou M, van de Lindt JW, McAllister TP, Ellingwood BR, Dillard M, Cutler H., "State of the research in community resilience: progress and challenges," in *Sustain Resilient Infrastruct*, 2018.
- [51] Francis R, Bekera B, "A metric and frameworks for resilience analysis of engineered and infrastructure systems.," *Reliability Engineering & System Safety*, vol. 121, pp. 90-103, 2014.
- [52] Shandiz, S.C., Foliente, G., Rismanchi, B., Wachtel, A. and Jeffers, R.F., "Resilience framework and metrics for energy master planning of communities," *Energy*, vol. 203, p. 117856, 2020.
- [53] C. Peterson, "Systems architecture design and validation methods for microgrid systems," (Doctoral dissertation, Monterey, CA; Naval Postgraduate School, 2019.
- [54] Shinozuka M, Chang SE, Cheng TC, Feng M, O'Rourke TD, Saadeghvaziri MA., "Resilience of integrated power and water systems," *MCEER Research Progress and Accomplishments*, pp. 65-86, 2004.
- [55] Panteli M, Mancarella P, N. Trakas D, Kyriakides E, D. Hatziaargyiou N., "Metrics and

Quantification of Operational and Infrastructure Resilience in Power Systems., " *IEEE Transactions on Power Systems.*, vol. 32, pp. 4732-42, 2017.

[56] Aldrich DP., " Black Wave," University of Chicago Press, 2019, 2019.

[57] M. C. Andriulli, "OBSERVABILITY ANALYSIS FOR THE," Naval Postgraduate School, Monterey, CA, 2019.

[58] I. Petersen, "A Kalman decomposition for possibly controllable uncertain linear systems," *IFAC Proceedings*, vol. 4, pp. 6389-6395., 2008.

## Appendix: System parameters for simulation

<i>C<sub>f</sub></i>	<i>1.30E-04</i>
<i>F</i>	<i>60</i>
<i>F<sub>s</sub></i>	<i>15000</i>
<i>J</i>	<i>33.536</i>
<i>L1</i>	<i>4.50E-04</i>
<i>L2</i>	<i>1.60E-04</i>
<i>L<sub>g</sub></i>	<i>5.00E-02</i>
<i>R</i>	<i>0.05</i>
<i>R<sub>c</sub></i>	<i>1</i>
<i>R<sub>g</sub></i>	<i>0.0001</i>
<i>S<sub>b</sub></i>	<i>2.00E+05</i>
<i>S<sub>g</sub></i>	<i>190000</i>
<i>SG</i>	<i>250000</i>
<i>T<sub>s</sub></i>	<i>1.00E-05</i>
<i>V<sub>b</sub></i>	<i>208</i>
<i>V<sub>dc</sub></i>	<i>1000</i>